Empirical models of the incidence and spread of tropical fires.

Submitted by

Imogen Nancy Fletcher

to the University of Exeter as a thesis for the degree of

Doctor of Philosophy in Mathematics

in September 2014

I certify that all material in this thesis which is not my own work has been identified and that no material has previously been submitted and approved for the award of a degree by this or any other University.

Signature: .....

Abstract

Tropical wildfires account for up to 93% of global burnt area and approximately 85% of the resulting carbon emissions, yet are significantly under-represented in existing fire models. These models are predominantly process-based, require a multitude of input datasets, parameters and calculations, and are difficult to reproduce or use independently from a dynamic global vegetation model (DGVM). The aim of this thesis is to develop empirical parameterisations of tropical fire occurrence and spread that represent an improvement in accuracy over existing models and that can be easily implemented both as standalone models or within a DGVM. These models are based on well-documented relationships from the literature. An index of potential fire is produced based on the observed peak of fire activity at intermediate levels of productivity and aridity. This can be converted into expected fire counts using a simple, observation-derived parameter map. Fire sizes have been shown to follow an approximately fractal distribution in a range of ecosystems, which is used to develop a new burnt area model.

Replacing the fire count and burnt area calculations of existing fire models with these new parameterisations improves the spatial distribution of the resulting estimates, while giving temporally comparable predictions to the original models. The magnitude of the resulting burnt area estimates is also improved. The use of empirical fire modelling is therefore a viable alternative to current process-based methods, and makes practical use of theories that are well-documented in the literature. These models require few input variables and

can be easily incorporated into a DGVM. However, further work to improve the temporal accuracy and dynamicity of these models would be beneficial, as would a method to link these models to parameterisations of combustion and trace gas emissions.

Acknowledgements

I am indebted to my supervisors, Prof. Pierre Friedlingstein and Dr. Luiz Aragão, for their invaluable guidance and support. I would like to extend my deepest thanks to them for giving me the opportunity to do this research, and for their perpetual encouragement along the way.

I would not have been able to embark on this project without the funding from the Climate Change and Sustainable Futures research project at the University of Exeter, and am grateful for the additional funding from the EMBRACE project.

I would like to thank my friends in the many offices I have occupied, for their humour, companionship and support. My fellow PhD students have shared the highs and lows of the process with me, and my post-doc friends have offered me invaluable advice and reassurance along the way.

Finally, I offer all my love and gratitude to Matt, who has kept me sane.

Table of contents

List of figures

List of tables

Abbreviations

The abbreviations used in this thesis are listed below for reference purposes. Model and dataset names are excluded from this list.

AOGCM: Atmosphere-ocean global circulation model

BA: Burnt area

DGVM: Dynamic global vegetation model

DSI: Dry season intensity

E: Evapotranspiration

ESM: Earth system model

FDI: Fire danger index

FFDI: Forest fire danger index (specifically refers to the McArthur index)

FWI: Fire weather index (specifically refers to the Canadian index)

GCM: General circulation model

GPP: Gross primary productivity

IAV: Interannual variability

LCT: Land cover type

LSM: Land surface model

LSMM: Linear spectral mixing model

MCWD: Maximum cumulative water deficit

NI: Nesterov index

NPP: Net primary productivity

P: Precipitation

PD: Population density

PFI: Potential fire index

PFT: Plant functional type

PWL: Percentage water-limited

RMSE: Root mean square error

WSI: Wet season intensity

1. Introduction

1.1 THE GLOBAL FIRE REGIME

Fire affects large areas of the land surface. Estimates of total global annual burnt area range from anywhere between 200 and 608 Mha (Table 1.1), with the average literature value close to approximately 350 Mha. There is a large amount of interannual variability, with estimates varying by up to 300 Mha between years (Schultz et al., 2008).

Such widespread burning has significant impacts on the earth system (Fig. 1.1). It affects not only the land surface, but also the global carbon cycle and hence the climate. In addition, wildfire also has considerable effects on humans and society.

1.1.1 Impacts of fire on the land surface

One of the main historical impacts of the global fire regime is the distribution of ecosystems (Pausas & Keeley, 2009). It has been suggested that if fire were not a component of the earth system, the proportion of land covered by closed forests would be twice as large, and C3 and C4 grasses and shrubs would be considerably less abundant (Bond et al., 2005). Grasses dry and recover rapidly, and favourable fire conditions are much more prevalent in grasslands than in forests (D'Antonio & Vitousek, 1992). Repeated burning prevents tree and shrub species from taking hold if they have not yet grown sufficiently large to withstand fire damage. Grasses will reappear quickly, providing fuel to encourage further fire activity. Hence, the relationship between fire activity and

the spread of grasslands is somewhat symbiotic.

Forests contain an abundance of fuel, but the closed canopies prevent rapid drying, making them significantly less flammable than grasslands or other ecosystems. Tropical forests are particularly affected by this, due to extended wet seasons and the high humidity at tropical latitudes. If fire does occur, however, it can have one of two contradictory long-term effects: it can either increase or decrease the likelihood of subsequent fires (Alencar et al., 2011). Increases in flammability are caused by the mortality of large trees, their subsequent degradation and the resulting growth in the fuel load, the increase in light-demanding species, and faster drying rates resulting from gaps in the forest canopy (Cochrane et al., 1999; Cochrane, 2001; Barlow et al., 2003; Haugaasen et al., 2003; Blate, 2005). Hence, a forest becomes more fire prone after an initial burn: in the north-eastern US it was found that the average fire return interval was 200 years, but in stands that actually burned, this value was only 5 years (Houghton et al., 2000b). However, repeated burning in a stand can also cause the aforementioned decrease in forest flammability, since it may ultimately reduce the tree density to such an extent that the limited fuel availability lowers the likelihood of high-intensity fires (Balch et al., 2008; Yocom & Fulé, 2012). The frequency of fire in forests influences whether savannah or forest tree species will dominate during post-burning regrowth, and hence is responsible for transitions between these two ecosystem types (Hoffman et al., 2012).

Forest and savannah ecosystems have been shown to be stable states with very distinct levels of tree cover, suggesting that transitions between the two can be considered “tipping points”, which are difficult to reverse (Hirota et

al., 2011; Staver et al., 2011). While tree cover is generally controlled by rainfall, these transitions, which occur in regions with intermediate levels of precipitation and mild seasonality (Staver et al., 2011), are controlled by fire and the positive feedbacks discussed above, of repeated burning increasing the likelihood of fire (Hirota et al., 2011).

Forest fires cause approximately 10% of the total global burnt area, whereas savannahs and shrublands account for the significant majority (Table 1.1) due to an abundance of fuel that dries relatively quickly. Shifts between the two types will therefore greatly alter the fire regime and further contribute to the changing distribution of ecosystems across the globe.

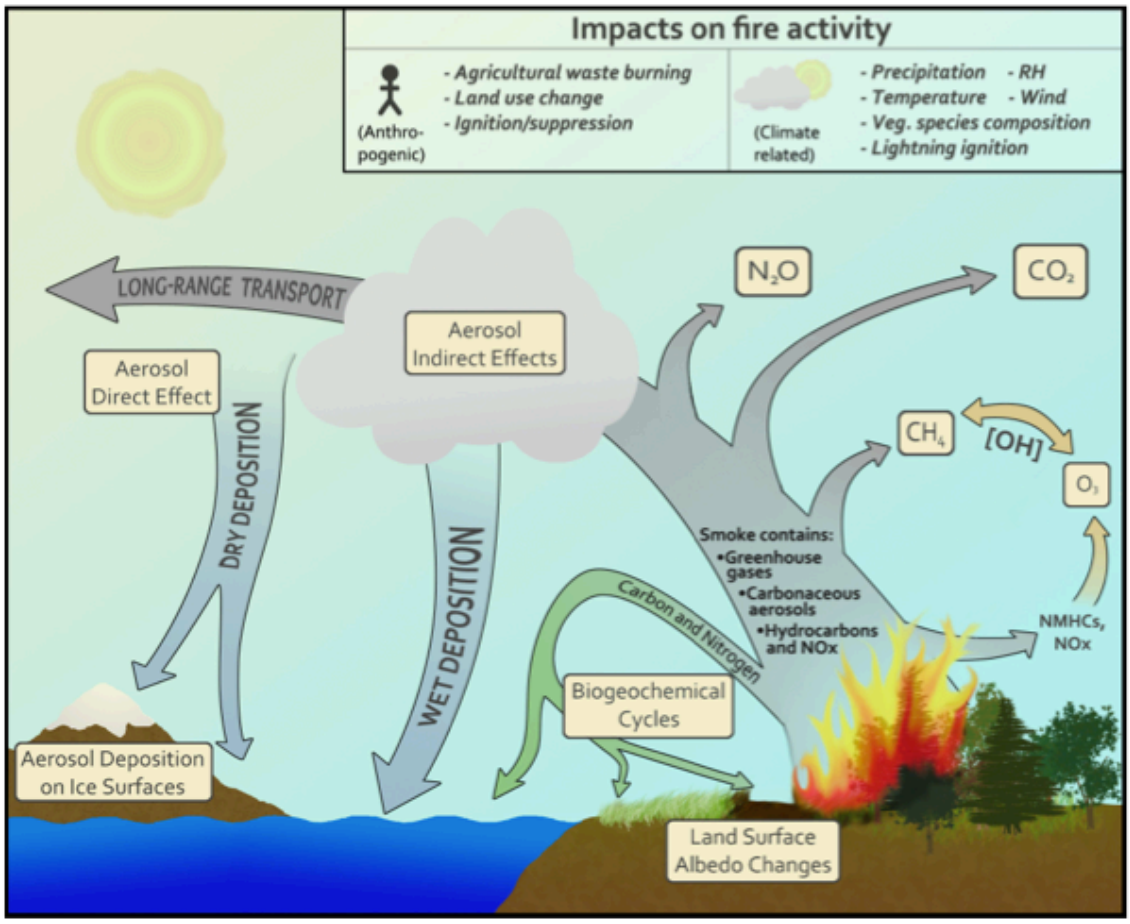

Figure 1.1: From Ward et al. (2012): A schematic illustrating the various impacts of fire on the atmosphere, land surface, ice surfaces and the ocean.

In the present day, the addition of intentional, anthropogenic fire regimes, such as deforestation to transform forests into pasture for livestock grazing or agriculture, further affects the distribution of ecosystems (Marlon et al., 2008), and future changes to global land cover can be expected if the fire regime is altered.

1.1.2 Fire in the global carbon cycle

Fire is an important component of the global carbon cycle, with multiple interactions present between the two. Fire contributes to the carbon fluxes to the atmosphere both directly and indirectly, post-fire recovery of an ecosystem fixes atmospheric carbon into the land sink, and changes in climate resulting from the atmospheric CO_2 concentration indirectly influence the fire regime by affecting fuel availability and burning conditions (Flannigan et al., 2000). The main interactions between fire and the atmosphere are summarised in Fig. 1.1, from Ward et al. (2012).

The most direct contribution of fire to the global carbon cycle is the release of considerable quantities of carbon into the atmosphere, as a result of biomass combustion. The magnitude of this flux at any given time or from a particular region is difficult to determine, and estimates of total global carbon fluxes resulting from wildfires vary considerably in the literature (Table 1.2). There are some studies that estimate this flux to be less than 2 Pg C annually, but these are recognised as being exceptionally low: Hoelzemann et al. (2004), for instance, emphasise that their estimate of the CO_2 flux (1.56 Pg C) is lower

Table 1.1: Summary of key burnt area (BA) estimates given in the literature. The relative contribution of each continent or vegetation type are given where available.

Source	Global BA estimate Mha yr^{-1}	BA per continent	BA per vegetation type	Time period	Estimation method
GBA-2000 Tansey et al. (2004)	> 350	64% Africa 16% Australia 14% Asia 3% S. America 2% N. America 1% Europe	80% wood/ shrubland 17% grass/ cropland 3% forest	2000	Satellite products (SPOT VGT-S1[1,2] & ERS ATSR-2: GLOBSCAR[3])
GLOBSCAR Simon et al. (2004)	~ 200	59% Africa 9% Australia 11% Asia 7% S. America 6% N. America 8% Europe		2000	Satellite product (ERS ATSR-2[4])
Mouillot & Field (2005)	608		86% savannah 9% tropical forest 3% temperate grassland 2% boreal/ temperate forest	1990 - 2000	Satellite (ATSR[5]) + literature values + interpolation
MODIS BA: MCD45 Roy et al. (2008)	366	68% Africa 17% Australia 9% Eurasia 5% S. America 1% N. America	64% savannah 17% grass/ cropland 12% shrubland 5% forest	July 2001 - June 2002	Satellite product (MODIS, Terra & Aqua[6])
MODIS active fire: MOD14 Roy et al. (2008)	278	49% Africa 14% Australia 18% Eurasia 14% S. America 5% N. America	55% savannah 20% grass/ cropland 13% shrubland 12% forest	July 2001 - June 2002	Satellite product (MODIS, Terra & Aqua[6])
Schultz et al. (2008)	383 (273 - 567)	70% Africa 15% Australia 7% S. America 5% Asia 1% N. America 1% Europe		1960 - 2000	Literature review
GFED3 Giglio et al. (2010)	330 - 431	69% Africa 15% Australia 8% Asia 6% S. America 1% N. America <1% Europe		1997-2008	Satellite product (MODIS, Terra[7,8,9])
LPX: Prentice et al. (2011)	309			1997 - 2005	Fire model
Li et al. (2012a)	330	55% Africa		1997 - 2004	Fire model
Li et al. (2013)	337	59% Africa		1997 - 2004	Fire model

[1]Eastwood et al. (1998); [2]Fraser & Li (2002); [3]Kempeneers et al. (2002); [4]Bailey (1995); [5]Arino et al. (2001); [6]Roy et al. (2005); [7]Vermote & Justice (2002); [8]Justice et al. (2002); [9]Friedl et al. (2002)

Table 1.2: Literature estimates of global annual carbon emissions from wildfire, and the corresponding quantities of CO_2, CO and CH_4, where available. These values are gross fluxes resulting from the combustion of biomass – they do not account for post-fire regrowth or the decomposition of vegetation killed by fire.

Source	Gross fluxes from biomass burning			Time period	Estimation method
	CO_2 (Pg C yr^{-1})	CO (Pg CO yr^{-1})	CH_4 (Pg CH_4 yr^{-1})		
Andreae & Merlet (2001)	2.24	0.41	0.019	Late 1990s	Biomass burning data (unpublished, emission factors.
van der Werf et al. (2004)	3.53	n/a	n/a	1997 - 2001	CASA model[1]
Ito & Penner (2004)	2.29	0.50	0.03	2000	GBA-2000 BA satellite product[2,3], biomass density[4,5], emission factors.
Hoelzemann et al. (2004)	1.56	0.27	0.013	2000	GWEM using GLOBSCAR BA[6,7], LPJ-DGVM[8], emission factors[9]
van der Werf et al. (2006)	2.43	0.43	0.021	1997 - 2004	CASA biogeochemical model[1], satellite BA[10]
Schultz et al. (2008)	1.93 (1.56-2.36)	0.33 (0.25-0.42)	0.015 (0.01-0.02)	1960 - 2000	Literature review
Thonicke et al. (2010)	2.24	0.45	0.019	1982 - 2002	SPITFIRE model within LPJ-DGVM[8]
Kloster et al. (2010)	2.0-2.4 1.7-2.2	n/a	n/a	1997 - 2004 1960 - 2000	CLM v3.5[11,12] with CLM-CN biogeochemical model[13,14,15]
van der Werf et al. (2010)	2.01 (1.52-2.78)	n/a	n/a	1997 - 2009	CASA biogeochemical model[1] with MODIS BA[16]
Prentice et al. (2011)	3.81	n/a	n/a	1997 - 2005	Fire model in LPX-DGVM
Ward et al. (2012)	1.3 2.4	n/a	n/a	Present Future	CLM v3.5[11,12,17]

[1]van der Werf et al. (2003); [c]Tansey (2002); [3]Grégoire et al. (2003); [4]Myeni et al. (2001); [5]Potter et al. (2001); [6]Simon (2002); [7]Simon et al. (2004); [8]Sitch et al. (2003); [9]Andreae & Merlet (2001); [10]Giglio et al. (2006); [11]Oleson et al. (2008); [12]Stoeckli et al. (2008); [13]Thornton et al. (2007); [14]Thornton et al. (2009); [15]Randerson et al. (2009); [16]Giglio et al. (2010); [17]Kloster et al. (2010).

than other literature estimates. Other authors produce estimates that significantly exceed 3 Pg C yr^{-1}, but also concede that these values are inconsistent with the average literature estimate. Prentice et al. (2011) state that their value of 3.81 Pg C "*exceeds a number of published estimates for various periods*", and that although a similarly high value is given by van der Werf et al. (2004), this value was "*downgraded in later work*".

Regardless of the exact magnitude of the total global carbon fluxes from wildfires, they contribute considerably to total carbon emissions. For comparison, global CO_2 fluxes from fossil fuel burning were on average 8.3 Pg C annually between 2002 and 2011 (Boden et al., 2011; Ciais et al., 2013), only three times larger than wildfire emissions. Based on approximate CO_2 emissions resulting from the combustion of fossil fuels given by Raupach et al. (2007), Flannigan et al. (2009) estimate that gross emissions from wildfires are equivalent to somewhere between 26% and 31% of fossil fuel emissions. However, net emissions from wildfires are significantly less, since these emissions are partially counteracted by post-fire vegetation regrowth.

CO_2 fluxes from biomass burning are highly variable from year to year. For instance, the RETRO study gives the range as 1.56 to 2.36 Pg C yr^{-1} between 1960 to 2000 (Schultz et al., 2008), Kloster et al. (2010) gives estimates that range from 1.7 to 2.2 Pg C yr^{-1} over the same period, and from 1997 to 2009, between 1.5 and 2.8 Pg C are estimated as released through biomass burning each year (van der Werf et al., 2010). In other words, emissions in extreme fire years are up to 80% higher than the lowest annual emissions. Despite being responsible for only a small proportion of global burnt area, fires in forests are believed to cause the majority of the interannual

variability (IAV) of global burning (van der Werf et al., 2006) due to their high fuel loads.

This IAV is particularly high in comparison to other sources of carbon emissions to the atmosphere. Evidence suggests that wildfires are a major contributor to the IAV in total carbon fluxes (Peylin et al., 2005). Even increases in fire activity in small regions can have a large effect on global emissions. For instance, exceptionally large and long-lasting wildfires in Indonesia were largely responsible for the observed doubling of the atmospheric carbon dioxide growth rate in 1997-1998 (Schimel and Baker, 2002; Page et al., 2002).

Direct emissions from combustion are not the only carbon fluxes to result from wildfire. A single fire can affect the carbon cycle for years, due to the subsequent decomposition of dead biomass, and recovery processes of the area (e.g. Mouillot and Field, 2005; Phillips et al., 2009) In some cases, the magnitude of fluxes resulting from the long-term decomposition of species killed by fire is equivalent to nearly half of the immediate flux from burning (van der Werf et al., 2003). The regrowth of vegetation in fire-affected regions results in the reabsorption of some of this carbon from the atmosphere back into the land, and therefore counteracts some of these fluxes. However, an increase in carbon stored in above ground biomass does not necessarily mean an increase in carbon stored in the ecosystem: Kasischke et al. (1995) found that the fire regime in boreal forests results in a net loss of carbon from the ecosystem, as a result of the combination of an increase in carbon in living biomass resulting from vegetation reestablishment, and a decrease in carbon in the ground layer.

There is a delicate balance between a biome being a source or a sink of carbon, and changes in the fire regime can tip the balance either way. In

Amazonia, for instance, the carbon sink was shown to be approximately equal to the combined fluxes from deforestation, abandonment, logging and fire, based on measurements taken between 1989 and 1998, although the IAV of the carbon sources was greater than for the sink (Houghton et al., 2000a). Increases in fire could tip this balance in favour of the region being a net source of carbon to the atmosphere.

Such changes in the carbon cycle will affect the climate, which in turn will further affect the fire regime, so it is important to understand the potential implications of changes in climate on fire occurrence and spread. Although the exact relationships are not fully understood, much work has been done to explore the links between the atmosphere and fire (Flannigan et al., 2009). Climate affects fuel availability, flammability, fire spread and lightning ignition frequency (Lavorel et al., 2007). Temperature is one of the most important indicators of fire activity, both in the present day and historically (Daniau et al., 2012). Precipitation patterns are also highly influential: droughts increase flammability, but can also reduce the quantity of aboveground biomass that can be burnt (e.g. Westerling et al., 2006; Krawchuk et al., 2009; Chen et al., 2013; Bradstock, 2010; Krawchuk & Mortiz, 2011). Climate can also affect land cover, fuel loads and fuel type, which are key influences on fire occurrence (Pausas & Paula, 2012; Archibald et al., 2013). Various studies suggest lengthening growing seasons in recent decades. Piao et al. (2007) found that this correlated with increases in gross and net primary productivity (GPP and NPP), thus providing more fuel for fires. Conversely, the Amazon rainforest may experience a climate-change induced dieback (the likelihood of which is discussed in Malhi et al., 2009), which would increase the fragmentation of the canopy layer, thus

speeding up the drying of fuel and also increasing the likelihood of further fire. Based on future climate predictions, decreases in fire risk are expected in some boreal forests and tropical Africa, in contrast to most semi-arid regions and South America, where increases in fire activity are predicted (Scholze et al., 2006).

Regional changes in the global fire regime may balance each other out (e.g. Krawchuk et al., 2009) in terms of overall carbon emissions, but may also further contribute to rising atmospheric CO_2 concentrations.

1.2 TROPICAL FIRE

1.2.1 Contribution of tropical fires to global fire activity

Fire in the tropics are responsible for the majority of global burning in terms of surface area. Approximately 65% of global burnt area can be attributed to tropical Africa alone (Giglio et al., 2006), due to the abundance of savannahs on this continent, which account for between an estimated 55% and 86% of global burning (Table 1.1). Even allowing for error within fire estimates, the overwhelming consensus in the literature is that the majority of global fire activity can be found in tropical ecosystems (Dwyer et al., 2000). In contrast, only a small percentage (< 10%) of fire-affected regions are found in extra-tropical latitudes.

Carbon emissions from tropical fires are therefore considerably larger than those from fires in boreal or temperate regions. However, the emissions are prone to significant variation and are difficult to quantify (Cochrane, 2003). On average, approximately 85% of annual fire emissions are attributable to the tropical latitudes (Andreae, 1991; van der Werf et al., 2010). In the 1997-1998

El Niño period, tropical fires accounted for an approximate 90% of total C emissions from wildfire (van der Werf et al., 2004). From 1998 to 2001, tropical fires were estimated to emit 3.8 Pg C yr^{-1} in total from both combustion and the subsequent decomposition of dead matter (van der Werf et al., 2003). All of these estimates are gross fluxes, since they do not include the post-fire recovery of vegetation and the resulting carbon sequestration.

Changes in the tropical fire regime therefore have the potential to impact the global carbon cycle majorly, particularly due to the vast quantities of carbon stored in tropical vegetation. Amazonian forests contain an estimated 93 ± 23 Pg C in their aboveground biomass, with an additional 10% of this quantity in dead fuel, and 21% in belowground biomass (Malhi et al., 2006). A total of 247 Pg C is believed to be stored across all tropical forests, with nearly half of this found in Latin America, and the remainder split relatively evenly between Africa and S.E. Asia (Saatchi et al., 2011). Lewis et al. (2009) shows that many DGVMs forecast an increase in the carbon stored in tropical forests as the CO_2 concentration in the atmosphere rises, which may partially offset the carbon emitted as a result of fire. However, this simultaneously increases the potential carbon emissions from future forest fires. Sitch et al. (2008) predicts large increases in carbon emissions from wildfires by 2100, and most of this increase is attributed to more fuel and fires in Amazonia.

Fire is a rare natural occurrence in tropical forests (Aragão et al., 2010, Cochrane, 2003; Mouillot and Field., 2005), due to the high levels of moisture. Severe droughts such as those in 1998, 2005 and 2010 increase forest mortality and the risk of fire (Aragão et al., 2007, Aragão et al., 2010). As the risk of drought increases as a result of a changing climate (e.g. Cox et al., 2008;

Fu et al., 2013), so does the potential for exceptionally severe fire seasons in these ecosystems. Since the 1960s, the expansion of agriculture has required the use of deforestation fires in tropical forests, and as a result, burned areas in tropical forests have increased exponentially, in contrast to the general decrease in burned area observed at higher latitudes (Mouillot and Field, 2005). Deforestation fires differ from other fires in that the same area will typically be burned multiple times before it is suitable for agriculture, since the tree canopy cover must be reduced to below 10 – 30% (van der Werf et al., 2009) and burning efficiency is relatively low (Mouillot and Field, 2005). Approximately 60% of total global fire carbon emissions can be attributed to naturally occurring forest, grassland or savannah fires (van der Werf et al., 2010), with the remainder coming from deforestation and other anthropogenic fires. In the tropics, the majority of fires are caused by humans rather than lightning, though the exact proportions are difficult to quantify and vary between ecosystems (Frost, 1999).

1.2.2 Differences between tropical and non-tropical wildfires

A single fire in the tropics may have a vastly different effect on the vegetation and local carbon fluxes than a fire event outside the tropics. As Cochrane (2003) states so succinctly, "*while the chemistry of fire may be universal, its effects are not*".

Tropical fires are generally small in size and intensity but frequent, in contrast to boreal or mid-latitude fires that tend to affect much larger areas but are relatively infrequent (Schultz et al., 2008). The return intervals of fire affect the susceptibility of an ecosystem to fire damage. Most tree species in boreal

forests are relatively fire-intolerant due to the low fire frequencies: if the fire is of sufficiently high intensity, or if the crown is affected, the likelihood of mortality is high (Kasischke et al., 1995). There are a few exceptions: some boreal species have thicker bark and are therefore more resistant to fire damage (Nikolov and Helmisaari, 1993), while some species depend on fire to release seeds and promote the spread of the species (Rowe and Scotter, 1973). Tropical savannah species, which burn frequently, tend to have thick bark, and are therefore less likely to be killed by fire (Hoffmann et al., 2003), whereas in tropical forests, fire is considerably less frequent, resulting in vegetation that is less fire-adapted, with thinner bark than boreal tree or tropical savannah species, hence higher post-fire mortality rates (Cochrane, 2003).

The surface area of tropical forests is changing considerably as a result of deforestation and other human disturbances, whereas non-tropical forests are not changing in extent so much as in density, because they are, for the most part, recovering from previous disturbances (Houghton, 2005). These changes will impact various aspects of the respective fire regimes in different ways, from the probability of fire occurring, to the subsequent fire spread and fuel combustion.

Fires in tropical regions are not only affected by different vegetation cover to boreal fires, but are also subject to different climatic conditions. The tropics experience distinct wet and dry seasons that promote fuel growth and fuel drying, respectively, in vegetated regions, which in turn increases flammability (Westerling et al., 2006), especially in sparsely-vegetated areas such as savannahs. In boreal forests, there is much less seasonality in precipitation patterns, and the overall rainfall levels are of more importance than

the timing. In addition, the tropics experience higher temperatures than the higher latitudes, further encouraging fuel drying.

1.3 LAND SURFACE MODELLING FOR CLIMATE PROJECTIONS

Processes that occur on the land surface have a considerable and growing impact on the atmosphere. Currently used Earth System Models (ESMs) are replacing Atmosphere-Ocean General Circulation Models (AOGCMs) for predicting future atmospheric conditions and changes in the climate (Flato et al., 2013). Both of these model structures include the main components of the earth system – atmosphere, ocean, land and sea ice – but ESMs go further than their precursors and attempt to model biogeochemical cycles, particularly the oceanic and terrestrial carbon dioxide cycles. The terrestrial component of an ESM is known as a Dynamic Global Vegetation Model (DGVM) or a Land Surface Models (LSM).

The typical structure of a DGVM is shown in Fig. 1.2. The parameterisations for each process may vary between models, but the components are generally the same. Significant modelling advances have been made in the past couple of decades regarding soil hydrology, vegetation growth, and many other processes (e.g. Chen & Dudhia, 2001; Ek et al., 2003; Han et al., 2014). However, many DGVMs still do not contain a wildfire component (Le Quéré et al., 2009; Fig. 1.2), despite the significant impacts of fire on the global carbon cycle. In addition to this, many existing fire parameterisations produce inadequate estimates of fire activity in tropical latitudes, particularly in moist tropical forests (Prentice et al., 2011).

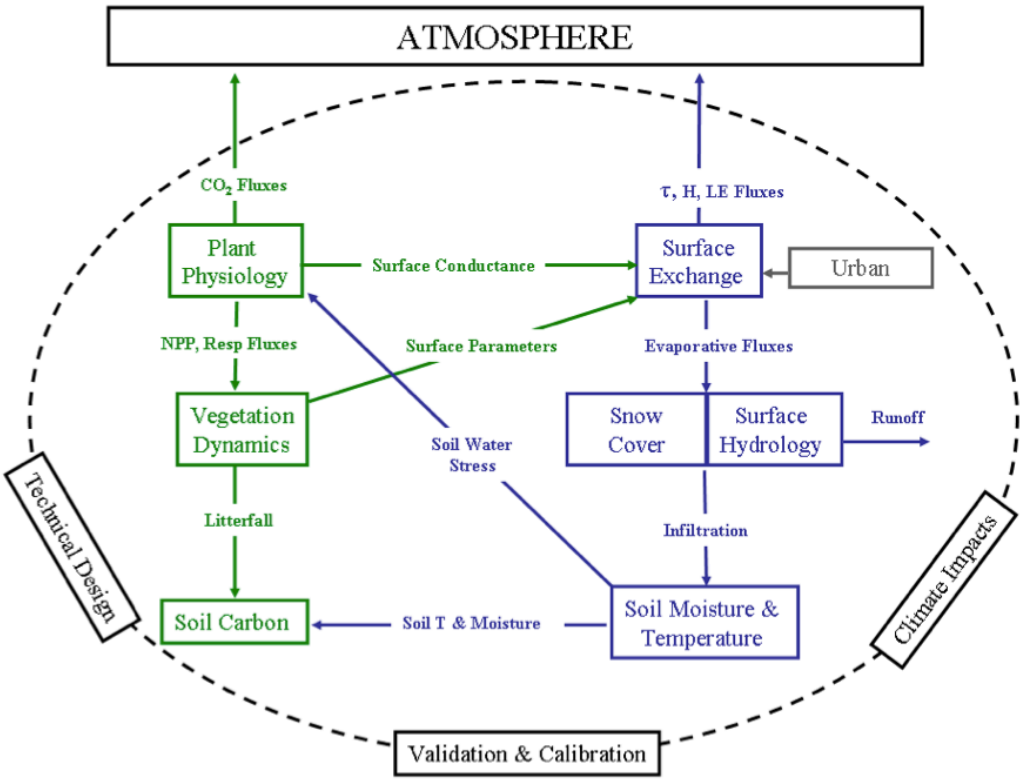

Figure 1.2: From Best et al. (2011): The structure of the JULES model, where the boxes represent the individual modules, and the arrows show the interactions between the modules.

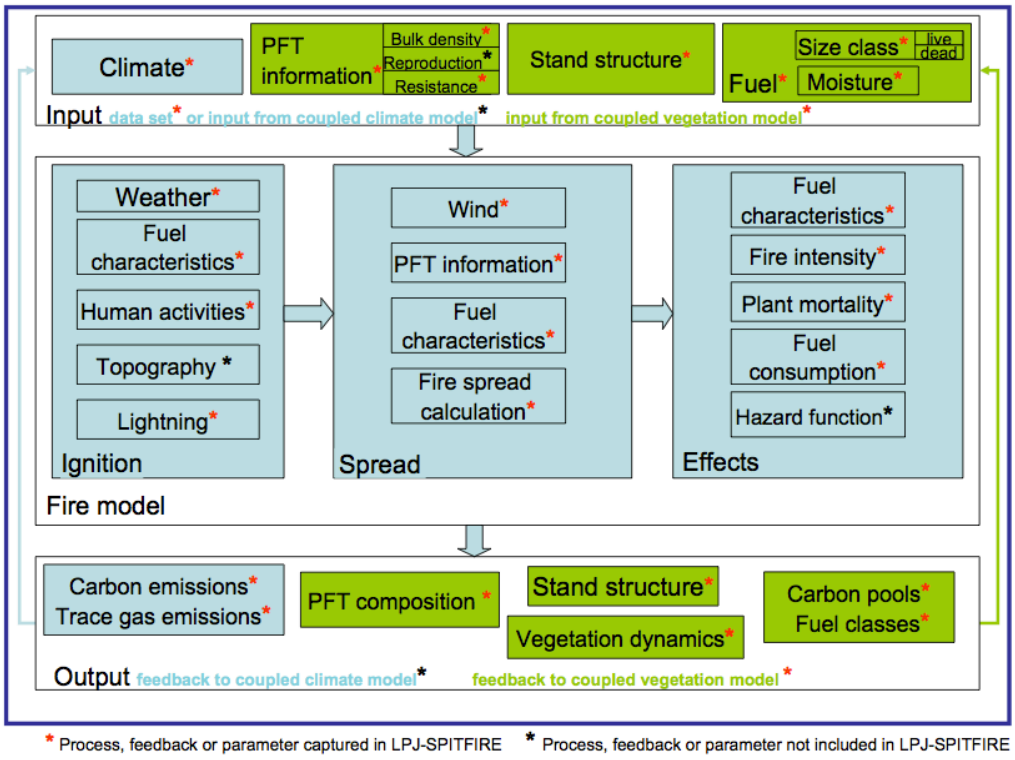

Figure 1.3: From Thonicke et al. (2010): Suggested key components and processes that should be considered in a fire model.

The incorporation of a fire module into a DGVM requires interactions with several existing modules. Fig. 1.3 shows the main processes that should be included within a fire model, and how these link to a DGVM and climate model.

1.4 FIRE DANGER INDICES

Multiple fire danger indices (FDIs) have been developed to provide an indication of the likelihood of fire occurrence, fire spread and potential damage based on local fuel and climatic conditions. These indices were designed for specific regions with the intention of providing early warnings of possible extreme fire seasons for fire management purposes. The main components of each of the most commonly-used FDIs are summarised in Table 1.3.

These FDIs are generally unsuitable for use for land surface modelling purposes. They were all designed for specific regions and vegetation types: the McArthur FFDI, for instance, is calibrated for eucalypt forests in Australia, and hence it cannot be assumed that it is valid in any other forest type. Extrapolation of these indices to other regions is generally ineffective: even the Canadian FWI, the most commonly-used FDI which has been adapted to a large number of ecosystems, is unreliable on a global scale (Planas and Pastor, 2013). Additionally, despite their relative simplicity which makes them easy to implement within a land surface model, the information they provide is not necessarily suitable for modelling purposes, since fire danger is not equivalent to actual predictions of fire occurrence or spread. Indeed, the values produced by the indices have no physical meaning, but are instead interpreted relative to one another. Despite these issues, however, they are often used within existing

fire models.

Further details of the indices and their suitability for use within land surface models are given in Chapter 2, Section 2.1.2.

Table 1.3: Summary of the inputs and intermediate calculations required for each of the main fire danger indices.

Fire Danger Index	Reference	Calibration region	Inputs	Intermediate calculations
Canadian Fire Weather Index (FWI)	Van Wagner & Pickett, 1985	Canada	Air temp. Relative air humidity Wind Rainfall	Fuel and fine fuel moisture - fire spread Duff moisture Drought - fuel build-up
McArthur Forest Fire Danger Index (FFDI)	McArthur, 1967	Australia - eucalyptus forests	Fuel load Wind Air temp. Relative humidity Rainfall Cloudiness	Keetch-Bryam drought index (KBDI)
American National Fire Danger Rating System (NFDRS)	Deeming et al., 1977	USA	Fuel Latitude Slope Temperature Wind speed Relative humidity Cloudiness	Keetch-Bryam drought index (KBDI) - Fuel moisture content - Ignitions, spread, energy release

1.5 PROCESS-BASED FIRE MODELS

The majority of existing fire models developed for use within DGVMs are process-based. This means that the key physical processes behind every stage of fire ignition, spread, and fuel combustion are modelled. Although there is a general agreement amongst existing models about which processes are important and how they are driven, there are also considerable differences.

There are four main modelling stages: fire occurrence, fire spread and burnt area, combustion and mortality, and the resulting emissions of carbon and other trace gases. A breakdown of how each stage is modelled in each of the major fire models is given in Table 1.4 and discussed in more detail below.

1.5.1 Fire occurrence

The occurrence of fire is dependent on the presence of an ignition source, either natural (e.g. lightning) or anthropogenic, and the flammability of the fuel. Approaches to modelling ignitions range from very simple, considering only lightning ignitions and excluding human-caused fires (MCFIRE, Glob-FIRM, and the LPX fire model), to highly complex in the case of the CESM1 parameterisation, where anthropogenic ignitions for a range of purposes (e.g. deforestation or agricultural clearing) are considered in turn.

The flammability of a region is influenced by the quantity and structure of available fuel, how wet the fuel is as a result of precipitation, and how fast it dries as a result of evapotranspiration, wind, and temperature. In existing fire models, fuel availability is often only included as a threshold value, i.e. fire is modelled providing there is some minimum quantity of biomass available to burn. The CTEM, CSM and CESM1 fire parameterisations (Arora & Boer, 2005; Li et al., 2012a,b; Li et al., 2013) let fire occurrence increase linearly as fuel load increases, between lower and upper thresholds. However, the assumption of a linear relationship between fuel and fire activity may be too simple.

The effect of fuel moisture on fire is modelled in a more complex manner. The likelihood of fire decreases as moisture levels increase towards some

Table 1.4: Summary of the key features of existing fire models

DGVM/ LSM	MC1 *(Bachelet et al., 2000)*	LPJ *(Sitch et al., 2003; Gerten et al., 2004)*			LPX	CTEM	CSM	CESM1
Fire model	**MCFIRE** *Lenihan et al., 1998)*	**Glob-FIRM** *(Thonicke et al., 2001)*	**Reg-FIRM** *(Venevsky et al., 2002))*	**SPITFIRE** *(Thonicke et al., 2010)*	unnamed *(Prentice et al., 2011)*	unnamed *(Arora & Boer, 2005)*	unnamed *(Li et al., 2012a,b)*	unnamed *(Li et al., 2013)*
Fire occurrence	Drought index - 1000hr fuel moisture content Probability of ignition and spread - lightning - fuel flammability - rate of spread	- temperature - fuel load - fuel moisture Ignitions (assumed to always be present)	Fire danger index (based on Nesterov Index) - temperature Ignitions - lightning - population density	Fire danger index (based on simplified Nesterov Index) - temperature - fuel moisture - fuel load Ignitions - lightning - population density	Fire danger index (based on simplified Nesterov Index) - temperature - fuel moisture - fuel load Ignitions - lightning	- aboveground biomass - soil moisture content Ignitions - lightning - regional probability of human ignitions	- aboveground biomass - relative humidity - soil moisture Ignitions - lightning - latitude - population density	Agricultural, deforestation, non-peat and peat fires - land cover - precipitation - soil moisture - soil temperature - temperature - population - GDP
Fire spread & burnt area	Surface fires - Rothermel equations Crown fires - van Wagner (1993) equations	Fractional area burnt - length of fire season - fuel conditions	Fractional area burnt - wind - fuel moisture - fuel bulk density - temperatur e	Mean fire area (Rothermel equations) - wind - fuel moisture - fuel bulk density	Mean fire area (Rothermel equations) - wind - fuel moisture - fuel bulk density	Mean fire area - wind speed - soil moisture - fire duration - fire extinguish probability	Mean fire area - wind speed - soil moisture - relative humidity	Mean fire area - wind speed - soil moisture - relative humidity

Combustion & mortality	Live and dead fuel consumption - fuel moisture content	Grasses and litter fully consumed.		Live and dead fuel consumption - fuel moisture content	Live and dead fuel consumption - fuel moisture content	Combustion - constant per PFT and per fuel class	Combustion - constant per PFT and per fuel class	Combustion - constant per PFT and per fuel class
	Crown mortality - fire duration - bark thickness Live root mortality - Duration of flaming and smouldering combustion	Mortality - prescribed fire resistance per PFT	Mortality - proportional to area burnt, relationship defined per PFT	Probability of mortality - surface fire intensity - fire duration - bark thickness	Probability of mortality - surface fire intensity - fire duration - bark thickness	Mortality - prescribed per PFT and per fuel class	Mortality - prescribed per PFT and per fuel class	Mortality - prescribed per PFT and per fuel class
Emissions	Constant per LCT	–	–	Constant emission factors per PFT.	Constant emission factors per PFT.	Constant emission factors per PFT.	Constant emission factors per PFT.	Constant emission factors per PFT.

moisture of extinction, above which fire is assumed impossible, though the exact relationship varies between models. Additionally, there is no consensus on the best way to model fuel moisture. A common approach is to model fuel drying as a function of temperature, using the Nesterov Index (Venevsky et al., 2002; Thonicke et al., 2010; Prentice et al, 2011), but it is also not unusual for models to use soil moisture as a proxy for fuel moisture (Arora & Boer, 2005; Li et al., 2012a,b; Li et al., 2013).

The majority of the existing models treat ignitions as independent from flammability. The exceptions to this are the MCFIRE model (Lenihan et al., 1998), in which fine fuel flammability and modelled rate of fire spread are combined with lightning data to produce a joint probability of fire ignition and spread, and the fire parameterisation designed by Li et al. (2013) for use in the Community Earth System Model (CESM1), where the interactions between climate and ignitions are considered. For instance, in this latter model precipitation is used not only to model soil moisture, but also to account for the reduced likelihood of humans setting fires for deforestation purposes if it is raining or has recently rained.

1.5.2 Fire spread and burnt area

The spread of wildfire is dependent on the continued presence of sufficiently flammable fuel, the current climatic conditions, and the absence of intentional human suppression tactics. No two fires will spread in the same way, and hence many assumptions need to be made to model how much area fire will burn.

Methods for modelling the spread of fires are generally quite similar across the existing models. The use of the Rothermel fire spread equations is

common (Venevsky et al., 2002; Thonicke et al., 2010; Prentice et al., 2011). The CTEM fire parameterisation (Arora & Boer, 2005) use a similar burnt area calculation to the Rothermel equations, in that the fire is assumed to be elliptical in shape, and a length-to-breath ratio of this ellipse is calculated as a function of wind speed, though there are slight differences.

Most of the models do not distinguish between crown and surface fires. MCFIRE (Lenihan et al., 1998) is the only one considered here that explicitly provides separate calculations for each of these fire types.

The models generally assume that fires will continue to burn until there is no fuel left or they are extinguished by an increase in moisture. The CTEM fire model contains an additional term to account for the probability that a fire will be extinguished by human intervention or by natural barriers such as water bodies or rocky terrain, thus restricting burnt area.

1.5.3 Combustion and mortality

Combustion refers to the chemical change in biomass when it is burnt, and can occur within both dead and live fuels. Mortality, on the other hand, is simply the process of vegetation being damaged beyond recovery. Despite this, these two processes are used somewhat interchangeably within models, making it difficult to compare the parameterisations directly to one another.

The combustion of fuel during a fire is dependent on a host of factors, including the type and characteristics of the vegetation, the proportion of live to dead fuel, the intensity of the fire as a result of local conditions and the moisture of the fuel (Tansey et al., 2004). This is dealt with in existing fire models in a range of approaches, ranging from the very simple to the reasonably complex.

Fuel consumption is not considered within Reg-FIRM (Venevsky et al., 2002), presumably since this information is not necessary if, as is the case here, estimates of emissions resulting from fire are not of interest. In the majority of other models, empirical relationships between burnt area and both combustion and mortality are used. Combustion and mortality rates are prescribed per plant functional type and, in most cases, also per fuel class. MCFIRE, SPITFIRE and the LPX fire models are exceptions to this, modelling combustion as a function of fuel moisture content, and mortality as a function of bark thickness, fire duration, and fire intensity. MCFIRE additionally estimates root mortality based on the duration of both flaming and smouldering combustion.

1.5.4 Emissions

The emissions resulting from wildfires are of particular interest to climate scientists, and, as discussed previously, can have a cyclical effect on fires as a result of a changing climate. They are influenced by the nature of the combustion and the type and conditions of fuel (Tansey et al., 2004), but fire models tend to take a relatively simplistic approach to their representation. Apart from Glob-FIRM and Reg-FIRM, which do not attempt to predict emissions from fires, all of the existing models use the same approach to model these fluxes. It is assumed that for each PFT, a constant amount of each trace gas is emitted for every unit of biomass burnt. These values are obtained empirically, and there is no evidence to suggest that this is not a reasonable approximation to make.

1.5.5 Advantages of process-based fire modelling

Theoretically, process-based models have the potential to produce highly accurate estimates of fire activity. They account for subtle changes in a wide range of drivers, and hence are fully dynamic, providing the input variables are as well, though this is not always the case: mean lightning flashes per month are sometimes used to model ignitions, for instance, for want of accurate lightning datasets over a long time period. The dynamicity of the models theoretically allows them to be used in any ecosystem with any conditions, and they can be extended far into the future or used to recreate historical fire regimes. Their accuracy in such cases is dependent on the accuracy of their constituent parameterisations of each process.

Process-based models also provide an in-depth insight into what is happening within a burning ecosystem. The effects of single variables on the fire regime can be isolated and analysed, and therefore the relative importance of various drivers can be determined.

1.5.6 Drawbacks of process-based fire modelling

Process-based fire models have the capacity to become very complicated, due to the sheer number of factors that influence each component of wildfire. To model fire occurrence alone, data about the distribution of fuel for each plant functional type (PFT) and fuel class is generally required, as well as maximum and minimum daily temperature, precipitation, lightning flashes and population density, and a range of prescribed parameters. The fact that no two models considered here model fire occurrence in the same way shows the complexity of the process and the difficulty in determining the exact relationship between

variables. This difficulty occurs in part due to the problem of isolating the effects of individual drivers from one another. However, it is also difficult to calibrate an ignitions model, for example, when ignition data is not available, since ignitions are not the same as fire events: an ignition does not necessarily become a fire event if the local conditions are unfavourable to fire, and hence is not recorded.

To produce accurate predictions of fire activity, a high level of detail is required at every stage of the model, and it is impossible to include every possible process in the model. Process-based modelling is a huge undertaking that requires constant revision and improvements, and a vast array of input variables and estimated parameters, each of which adds to the uncertainty of the model. The complexity of the models also makes them difficult to recreate or implement within a DGVM other than the one for which they were designed, since not all of the required input variables will necessarily be available.

While process-based models are highly useful in many situations, and are capable of producing highly accurate estimates of a range of climatic and ecological variables, existing fire models are not yet at this stage. They have been shown to produce estimates of burnt area and emissions from combustion that do not agree closely with one another or with data from satellite observations (Kantzas et al., 2013). In addition, many produce inadequate estimates of fire activity in the tropics, due in part to an incomplete understanding of the effect of human behaviour on the fire regime.

A further consideration is the suitability of these models on a large scale. Process-based models are often developed based on data from individual fires or regions. For instance, the rate at which a fire spreads is generally parameterised for local conditions, i.e. for an individual fire. This assumes

homogeneity of the vegetation structure and climate for the full extent and duration of a fire, which is often not an accurate representation of reality, making these models unsuitable for extrapolation to larger scales (McKenzie et al., 1996). Anderson et al. (2003) suggest that “the cumulative effects of any fire regime cannot be described as simply the sum of the effects of individual fires”.

Although it would be possible to add further processes and details into existing fire parameterisations, and ensure that these are properly calibrated to tropical forests as well as boreal ecosystems, this would exacerbate some of the problems mentioned above. An alternative option is to find an approach to fire modelling that is not process-based, but still works within a DGVM framework. This can be done by considering relationships that have been observed between climate and fire variables, and representing these statistically. The processes that drive these relationships would therefore be dealt with implicitly, rather than explicitly.

1.6 EMPIRICAL MODELLING

1.6.1 Observed climate/fire relationships

Independently from the land surface modelling field, much work has been done to identify the relationships between climate and fire at a regional level. However, these are not necessarily applicable to a larger study area without recalibration or considerable development, since the relationships between variables are likely to vary significantly between regions (Lehmann et al., 2014). In addition, some of these would not easily fit into an existing fire modelling framework. For instance, the relationship between sea surface temperature anomalies and fire season severity (Chen et al., 2011) has no practical

modelling applications since sea surface temperatures are not modelled within a DGVM, and fire season severity is not a common variable used in existing fire models, so new methods for converting fire season severity into fire counts or burnt area would need to be developed.

A few interesting relationships in particular reappear repeatedly in the literature, for a range of ecosystems. The first of these is a peak in fire activity at intermediate levels of precipitation, suggesting that increased moisture in normally arid regions results in an increase in fuel to burn, whereas a wetter climate in densely vegetated areas makes the available fuel less flammable. Additionally, if there are no storms (i.e. no precipitation), there will also be no lightning and hence no natural ignitions. This relationship has been demonstrated using a range of fire and precipitation variables: annual precipitation, wet season precipitation, current and antecedent soil moisture, active fire detections and burnt area products, among others (Spessa et al., 2005; Westerling et al., 2006; Krawchuk et al., 2009; Krawchuk et al., 2011; van der Werf et al., 2008; Prentice et al.; 2011). However, despite being an often-observed and widely-accepted pattern, it has not, to my knowledge, been parameterised for global use or developed for modelling purposes, despite its potential for minimising the required number of input variables.

A second relationship that appears frequently in the literature but that shows slightly more variability relates to the apparently scale-invariant fractal distribution of fire sizes within any group of fires. This means that theoretically, regardless of the study region, grid cell size or time period, the probability that a fire is a certain size consistently decreases as larger sizes are considered. The exact nature of this distribution is debated in the literature, and appears slightly

different for different ecosystems: some studies show simple power-law distributions (Malamud et al., 1998; Moreno et al., 2011), while others suggest that this is only true within certain size boundaries, and that truncated, piecewise or tapered distributions may be more suitable (Ricotta et al., 1999; Cumming, 2001; Schoenberg et al, 2003; Holmes et al., 2004; Cui and Perera, 2008; Pueyo et al., 2010). Although attempts have been made to estimate parameters for these distributions for the study regions of interest, no general method of predicting these parameters has been developed. If this can be done, it could drastically simplify fire modelling by providing a simple link between fire counts and burnt area, rather than the current complex calculations of fire spread. However, the relationships between variables are likely to vary significantly between regions (Lehmann et al., 2014), and this must be taken into consideration when developing the models.

While there are undoubtedly many other established connections between climate and fire variables, these are two that appear frequently in the literature, and have significant potential for development into working models. In addition, the resulting models would cover the first two main processes of fire modelling: fire occurrence and burnt area. It is critical to get these right before attempting to improve the later steps, such as combustion of fuel and carbon emissions, since these are the foundations on which the later estimates are based. Even if the ultimate aim is to improve combustion and emission estimates, there is a limit to how accurate these predictions can be if estimates of fire occurrence or burnt area are sub-optimal. Also, the existing models already use some empirical relationships to estimate combustion, mortality and emissions, hence it is possible that these could be used as they are.

More detailed reviews of the literature concerning each of these relationships are given at the relevant points throughout this thesis: the fire activity peak at intermediate precipitation levels is discussed further in Chapter 2, and the fractal distributions of fire sizes shown in a range of studies are compared in Chapter 3.

1.6.2 Potential advantages and limitations to empirical fire modelling

Empirical fire models have several potential advantages of process-based models. They will be designed to be considerably less complex, with fewer input variables required, and therefore should be easy to use on their own, or to implement within a DGVM. They are based on observable relationships, whereas process-based models often estimate unobservable variables, such as ignitions (as opposed to fire events, which are ignitions that actually take hold). With fewer parameters and calculations, the errors associated with each of these will be minimised.

However, the main potential limitation to empirical fire modelling is its suitability in ecosystems or time periods that vary significantly from those for which the models are calibrated, since there are no dynamic elements to the model. However, providing they are driven by dynamic variables, this should not be a problem. This is discussed in more detail in Chapter 5.

1.7 RESEARCH AIMS AND OBJECTIVES

The research presented in this thesis address the issue of modelling tropical fires. It seeks to improve the way that fires can be modelled within a dynamic global vegetation model (DGVM). Existing fire models are predominantly

process-based, and hence better suited to small regions or individual fires than to large-scale fire modelling within a DGVM. They perform particularly poorly in the tropics, despite the large contribution of tropical fires to the global fire regime, and the importance of wildfire on a range of land and atmospheric processes.

Several interesting relationships between climate variables and fire activity have been found repeatedly in the literature for a range of study regions and time periods, and yet have not been used for modelling purposes. The aim of the research presented in this thesis is to parameterise these relationships to produce models of fire occurrence and spread that can be used on their own, or implemented within an existing fire model framework, coupled to a DGVM. This has the potential to reduce the uncertainty and error associated with large numbers of input variables and parameters, and increase the accuracy of tropical fire predictions.

Specifically, the aims of this thesis are:

(1) To develop empirical models that predict the likelihood of fires occurring as a result of the local climate and vegetation; the number of fires that are expected to actually occur; and the subsequent spread of these fires. This will be done by:
    a. using previously-observed climate/fire and fire frequency/size relationships to identify suitable model designs
    b. calibrating these models using satellite fire products and climate data
    c. developing methods for estimating the model parameters for given regions and time steps

(2) To incorporate the new models into a DGVM, by:

   a. coupling an existing fire model to the DGVM
   b. including the new models as alternatives to the existing process-based parameterisations for the respective processes

(3) To assess the suitability and accuracy of these models, by:

   a. running the DGVM using combinations of the new models and existing parameterisations
   b. comparing the resulting fire outputs to observations, and quantifying the spatial, temporal and magnitudinal accuracy of the estimates
   c. comparing the resulting fire outputs to each other, and identify whether the new models represent an improvement in the estimation of fire counts and burnt area.

1.8 THESIS STRUCTURE AND KEY FINDINGS

The first part of Chapter 2 details the development of a novel index of potential fire based on local climatic conditions and vegetation structure. A more in-depth analysis of existing fire danger models is given here, as well as a discussion of the theory used to develop this new index. The new index requires only easily obtainable datasets, and produces estimates of tropical fire activity that are spatially considerably better than existing fire danger indices and much easier to interpret. This section has been submitted for publication (Fletcher et al., submitted), as has a further publication that uses some of the same methodology (Murray-Tortarolo et al., 2014). The second part of Chapter 2 presents a method for modelling ignitions, and hence converting potential fire

into estimates of fire counts. This method enables the incorporation of the potential fire model into a standard fire modelling framework. It is not a model in itself, but rather a starting point from which future developments could be made.

In Chapter 3, observed fractal properties of forest fires are used as a basis for modelling burnt area, with the number of fires that are known (or predicted) to have occurred as a sole input. The resulting burnt area estimates for tropical forests are compared to satellite observations. The model is shown to be capable of reproducing spatial patterns and temporal trends of pan-tropical burning. This chapter has been published (Fletcher et al., 2014).

Chapter 4 describes the modelling framework used to test the new models presented in Chapters 2 and 3, and the difficulties associated with the implementation of existing fire models within a dynamic global vegetation model. Estimates of fire counts and burnt area are produced using every combination of the new and existing models, and compared to one another and to satellite-based active fire and burnt area products. The accuracy each set of estimates is assessed with regards to their magnitude, ranges and spatial and temporal distributions. The most accurate estimates of burnt area result from the use of the two new empirical models used in conjunction with one another.

In Chapter 5, the main conclusions and discussion points that arose in each of the preceding chapters are summarised. Areas of potential future improvement are identified.

1.9 CONTRIBUTION TO CO-AUTHORED PAPERS

The first-author paper resulting from Chapter 2 (Fletcher et al., submitted) is currently under review for Earth System Dynamics. The definitions of the

climate indices used in this work were developed with Guillermo Murray-Tortarolo (PhD candidate, University of Exeter) and also feature in another paper (Murray-Tortarolo et al., submitted). I did the rest of the other methodology and model development, under the guidance of Pierre Friedlingstein, Luiz Aragão and Stephen Sitch. The code for calculating the existing fire danger indices within the JULES DGVM was written by Richard Gilham (Met Office), and I wrote the code for the new index developed in the paper. I wrote the paper, and all authors made suggestions to improve the final manuscript.

The burnt area model in Chapter 3 has been published in Biogeosciences (Fletcher et al., 2014). I devised, developed and tested the model, supervised by Pierre Friedlingstein and Luiz Aragão. André Lima and Yosio Shimabukuro created the dataset used to calibrate the model, and André Lima and Luiz Aragão wrote the corresponding section of the publication, but I wrote the remainder of the manuscript, incorporating suggestions made by all of the co-authors.

1.10 ORIGINAL CONTRIBUTION TO THE RESEARCH FIELD

The models developed in this thesis are designed for use within a DGVM, yet, unlike existing models, they are not designed to directly represent physical processes. Instead, they rely on observed patterns and relationships between climatic and fire variables. These relationships have been shown in the literature to be true at regional scales, but have not previously been used for pan-tropical or global fire modelling.

Current fire models are complex, and increase in complexity with every

new version. This makes them difficult to reproduce, particularly if they are documented in a series of publications. In addition, they are generally designed for use with a particular DGVM, and hence are not always compatible with others, particularly if vegetation is modelled differently. The new models developed here rely only on readily available input data, and easily reproducible parameter values.

The fire count and burnt area estimates resulting from the models developed here capture the spatial distribution of fire activity in the tropics to a higher level of accuracy than existing models. The magnitude of the estimates is also considerably closer to observed data. The seasonal distribution of these estimates requires further development to capture the full seasonality of tropical fire, but is at least comparable in this respect to existing models. These results are given in full in Chapter 4.

2. Modelling fire occurrence

The following chapter consists of two main parts, followed by an overall discussion of them both together. Section 2.1 is a paper that details the development of a novel index of potential fire based on climate and fuel availability and has been submitted for publication in Earth System Dynamics as:

Fletcher, I.N., Friedlingstein, P., Murray-Tortarolo, G., Gilham, R.J.J., Sitch, S. & Aragão, L.E.O.C (submitted) *A novel index of tropical potential fire incidence based on the productivity-aridity gradient.*

The contributions of each of the co-authors to this paper are given in Section 1.9. The second part of this chapter, Section 2.2, describes a method for translating the fire potential into an estimate of actual fire counts. In other words, it represents the effect of ignition sources on fire activity. The discussion linking these two topics is given in Section 2.3.

2.1 THE POTENTIAL FIRE INDEX

2.1.1 Abstract

Tropical fires account for up to 90% of all wildfire carbon emissions, yet are poorly represented in existing dynamic global vegetation models. Commonly used fire danger indices are calibrated to specific forested regions using local, high-fidelity climate observations and ignore variability in fuel loading, making

them unsuitable for global analysis of fire risk. It has been shown that fire activity peaks at intermediate levels of annual precipitation, as a result of the combined effects of productivity and aridity, which increase fuel quantity and fuel dryness, respectively. Using products derived from precipitation and evapotranspiration data to approximate fuel production and moisture, we develop a new empirical index of potential fire incidence for all pan-tropical land cover types. Between 2003 and 2010, existing indices produce accurate spatial estimates of fire activity in forests, but correlate negatively or non-significantly with observations when tested across all pan-tropical vegetation types. The new index, however, shows a strong positive correlation of 0.661 ($p < 2.2 \times 10\text{-}16$, $df = 910$) with observed fire activity. Temporally, the new index produces estimates comparable to existing indices. It also allows us to identify the dominant limitation of fire occurrence, either fuel moisture or a lack of fuel. Fire activity in regions that consistently experience high levels of burning appears to be more likely to be controlled by changes in wet season moisture levels and the resulting fuel production, than by drought or the intensity of the dry season. Incorporation of this index into a dynamic global vegetation model could improve estimates of trace gas emissions from wildfires, and hence our understanding of the impact of tropical fire on the carbon cycle and climate change.

2.1.2 Introduction

Fires play a major role in the global carbon cycle, both directly, in the form of combustion emissions, and indirectly, due to the resulting decomposition and regrowth of vegetation (Mouillot and Field, 2005). Globally, anywhere between

1.4 and 4.1 Pg C are estimated to be released annually into the atmosphere by wildfires (e.g. Andreae, 1991; van der Werf et al., 2004; Ito and Penner, 2004; Lavorel et al., 2007; Schultz et al, 2008; Kloster et al., 2010), and tropical fires are believed to account for up to 90% of these emissions (e.g. Andreae, 1991; van der Werf et al., 2003; Cochrane et al., 2003; van der Werf et al., 2004; van der Werf et al., 2010). Despite this, wildfires are not included in many global carbon cycle models (le Quéré et al., 2009) and remain a major source of uncertainty in simulations of future climate (Scholze et al., 2006). Some dynamic global vegetation models (DGVMs) do include fire modules: MC1 (Bachelet et al., 2000) uses the MCFIRE model (Lenihan et al., 1998); the Lund-Potsdam-Jena DGVM (LPJ; Sitch et al., 2003, Gerten et al., 2004) was originally coupled to the Glob-FIRM (Thonicke et al., 2001) and Reg-FIRM (Venevsky et al., 2002) models, and later SPITFIRE (Thonicke et al., 2010) and its successor, LPX (Prentice et al., 2011); the Canadian Terrestrial Ecosystem Model (CTEM; Arora and Boer, 2005) also contains a fire parameterization. However, these models were mostly derived for high-latitude or Mediterranean ecosystems, and inadequately represent tropical fires (e.g. Prentice et al., 2011), due to an incomplete understanding of the complex interactions between fire, vegetation and climate, and the relatively recent changes in land-use that have exacerbated the tropical fire regime and increased its importance in the global carbon cycle (Cochrane, 2003).

The first and arguably most important step of fire modelling is predicting the likelihood of fire occurrence. The most commonly used fire danger indices (FDIs) were developed for forest management, so that advance warning could be used to prevent or more efficiently control fire spread. Hence, they are

developed for ecosystems with relatively constant fuel loading and human influence, and so consider only changes in fire danger associated with varying climatological conditions. The McArthur Forest Fire Danger Index (FFDI, e.g. Noble et al., 1980; Golding and Betts, 2008) is calibrated for forests only (although a grassland version does also exist), so an abundance of fuel is assumed, and not considered in the model calculations. The Canadian Fire Weather Index (FWI; Van Wagner and Pickett, 1985) similarly does not account for fuel loading. In the SPITFIRE model (Thonicke et al., 2010), the Nesterov Index (NI) is used to calculate an FDI. Although this calculation does include fuel load data, it uses only the proportion of the total fuel that is of each fuel class (e.g. 1hr fuel class: leaves and twigs; 10hr: small branches; 100hr: large branches), rather than the total quantity of available fuel. The only concession to the necessity of fuel for burning is that the FDI is set to 0 if there is no fuel: if there is even a small amount of fuel, the fuel load becomes irrelevant to the calculation. This omission means that additional fuel availability calculations should be used for extrapolation of these indices to ecosystems other than those for which they were originally developed. This is not, however, always the case: in SPITFIRE, for instance, the FDI is simply multiplied by the expected number of ignitions to obtain an estimate of fire occurrence. The spatial accuracy is therefore entirely dependent on the accuracy of the ignitions model, and fuel is not accounted for.

Another result of these indices being developed for operational use is that they make use of local, high resolution weather observations, which are rarely available across a larger spatial or temporal range at a sufficient quality, making these indices unsuitable for use in DGVMs without heavily

compromising on their accuracy. Both the McArthur and the Canadian indices use daily temperature, relative humidity, wind speed, and precipitation statistics as inputs, not all of which are easily obtainable at large temporal or spatial scales and high accuracy. Although these two indices are similar, there is a significant amount of variation between the two, due in part to different sensitivities to input variables. This leads, in some cases, to them producing considerably different fire danger ratings (Dowdy et al., 2009). The SPITFIRE FDI uses a simplified version of the Nesterov Index that requires only daily maximum and minimum temperatures and precipitation as inputs (dewpoint temperature is estimated from the daily minimum temperature), and model estimates of the distribution of fuel between each fuel class. The accuracy of these estimates is uncertain, since observations are not widely available.

Existing FDIs tend to be unitless, which makes them difficult to interpret and compare to each other. The McArthur, Canadian, and Nesterov indices are scalars that are meaningless without the context of values predicted for other years or locations. They are interpreted using index-specific lists of thresholds for various levels of risk, and the definitions of high or low risk are subjective and region-dependent, hence are not directly comparable to one another. These indices were developed to be practically useful in day-to-day fire management, not as conclusive measures of fire potential. The SPITFIRE FDI, a function of the Nesterov Index, is slightly easier to interpret physically, since it is the probability that an ignition event becomes a spreading fire.

To develop an index of fire risk that is suitable for large-scale climate modelling, rather than for the management of local fire danger, we must overcome each of the problems mentioned above. The index must:

1. take the quantity of available fuel into account, to make the index adaptable to a range of ecosystems;
2. only require input datasets that are readily available, to a reasonable degree of accuracy, at large temporal and spatial scales;
3. have units and a physical meaning, to facilitate ecological interpretation.

Additionally, to justify the use of such an index over existing indices, the following two conditions should also be met:

4. the index should be at least comparable to existing FDIs in forests or high-biomass vegetation;
5. the index should perform better than existing FDIs in non-forested regions.

The first two of these points can be satisfied by making use of the relationship between rainfall, productivity and fire activity that has been shown in several studies. Spessa et al. (2005), van der Werf et al. (2008), Prentice et al. (2011), and Bistinas et al. (2014) have, among others, demonstrated that fires are most abundant at intermediate levels of annual precipitation, as a result of the compounded effects of productivity and aridity: an increase in precipitation results in potential fires being extinguished or not taking hold at all due to excessive fuel moisture, but, conversely, also results in an increase in fuel that could be burnt (e.g. Krawchuk et al., 2009; Westerling et al., 2006). Similarly, fire is most likely to occur in ecosystems that are moderately productive. Unproductive regions lack sufficient fuel for fires to take hold, and highly productive biomes are often too wet to burn (Pausas and Bradstock, 2007; Pausas and Ribeiro, 2013; Bowman et al., 2014; Bistinas et al., 2014).

Hence, it is possible that in some regions a larger than average amount of rainfall at certain times of the year could lead to an increase in observed fire activity, due to higher fuel production, whereas elsewhere, the converse could be expected as a result of increasing moisture levels of the available fuel.

It is known that precipitation is a key driver of net primary productivity (NPP; e.g. del Grosso et al., 2008; Thomey et al., 2011; Bowman et al., 2014). Specifically, fire activity is promoted by strong seasonal patterns of wet and dry periods, due to biomass growth then drying (Westerling et al., 2006). Increases in precipitation in the wet (growing) season are expected to increase fuel loading and hence potential fire activity in the subsequent dry season, whereas increases in dry season rainfall, when the majority of fires occur (e.g. Archibald et al., 2009), are more likely to result in a decrease in fire activity. Therefore, we propose that wet and dry season water fluxes can be used as proxies for changes in fuel loading and fuel moisture stress, respectively, and that fire activity can be described as a function of these products. Since we are considering changes in fuel loading and moisture, rather than total fuel quantities, we expect the relationship between wet and dry season moisture levels and fire activity to vary between ecosystems, so land cover data is also required.

To ensure that the third condition, that of ecological interpretation, is met, we define the index first, and develop the model accordingly. The new index is designed to give an indication of potential fire: it is the expected maximum number of fires that could occur, given the climatic and ecological conditions. It is crucial to note that this index does not take changes in land use or human activity into account: the true number of fires may be considerably less than the

index suggests, if there are no ignition sources, or active fire suppression measures are in place. It may also possible for the actual number of fires to be larger than the index value, as a result of inevitable model error and the model fitting method, though not significantly higher. Converting the new index into expected fire frequency is a separate matter that is not dealt with explicitly in this study, but the need for such a method is explained in more detail in the Discussion.

We proceed in three stages. First, we define products that represent changes in fuel load and moisture. Second, we use these products, observed fire counts, and information about local land-cover to calibrate a model of maximum potential fire, given the climatic conditions. Finally, we incorporate the model into a DGVM and compare the resulting estimates of potential fire over the last 3 decades to observed fire activity and to estimates produced by existing FDIs.

2.1.3 Materials and methods

2.1.3.1. Data and study region

Moisture fluxes are given by two key variables. Precipitation provides information about the addition of moisture, and evapotranspiration indicates the rate at which moisture leaves vegetation. We use the Climatic Research Unit (CRU) version 3.21 global monthly time series of precipitation (University of East Anglia Climatic Research Unit, 2013), regridded to 1°x1° from its original 0.5° x 0.5° resolution. Each 1°x1° grid cell takes the mean value of its four constituent 0.5° x 0.5° cells. Mean monthly evapotranspiration data is taken from the TRENDY multi-DGVM ensemble (Sitch et al., 2013), with the DGVMs

forced with changing observed climate and CO_2, but no changes in land-use.

Fire activity is represented by the MODIS MCD14ML global monthly fire location product, as calculated from the TERRA and AQUA satellite observations (Giglio, 2010). The available time series for these three datasets overlap only between July 2002 and December 2009: since we are considering full calendar years, we start the analysis in 2003.

We are considering fire in tropical ecosystems, and therefore we restrict all datasets to land points that lie between 25°N and 25°S. We use the GLC2000 land cover data set (Bartholomé and Belward, 2005; Global Land Cover 2000 database, 2003) to identify the land points. We set the land cover type (LCT) of each 1°x1° grid cell as the LCT that covers the largest proportion of each grid cell.

To test the model, we run the JULES land surface model (Best et al., 2011; Clark et al., 2011), driven by the WFDEI dataset (WATCH Forcing Data methodology applied to ERA-Interim data; Weedon et al., 2014) with CRU precipitation, regridded from 0.5° x 0.5° to 2° x 2°, for 1980 to 2012 at a 3-hour timestep. This includes additional subroutines to calculate the new potential fire index (PFI), as well as the daily McArthur FFDI, Canadian FWI, and SPITFIRE FDI (based on the Nesterov Index, using SPITFIRE coupled to JULES as a diagnostic model) for comparison. The other commonly-used FDI, the National Fire Danger Rating System (NFDRS; Deeming et al., 1977) is omitted from this study since it is more complex than the others and hence harder to implement within the JULES framework. A more detailed description of JULES is given in Section 4.2.1.

2.1.3.2. Representing changes in fuel load and fuel moisture

The concept of wet and dry seasons is common in the literature, yet there is no single definition of these variables. Some studies use prescribed dry seasons, for example by defining the Amazonian dry season as October to September (Westerling et al., 2006), but this does not work for the tropics as a whole, since it does not account for spatial variability in the onset and ending of dry seasons, especially between the northern and southern hemispheres. Other studies apply arbitrary restrictions, for example by defining the dry season as the driest months of each calendar year that make up <30% of annual rainfall (Archibald et al., 2009). Instead of attempting to identify a dry season, characterised by low rainfall, we consider net moisture fluxes to identify seasons in which the ecosystem is becoming drier. We hence define a drying season as any period of time during which evapotranspiration (E) exceeds precipitation (P) at every consecutive time-step: in other words, when water is leaving the soil and fuel faster than it is being added. Hence, it is possible for a region to experience more than one drying season annually. Additionally, a drying season may overlap the transition between calendar years.

The drying season intensity (DSI) is the cumulative sum of the differences between evapotranspiration and precipitation over each drying season. This is similar, but not identical, to the maximum cumulative water deficit (MCWD) as defined by Aragão et al. (2007), but instead of using calendar years, it allows for more irregular seasonality. Unlike the MCWD, we also allow E to vary, rather than fixing it at 100 mm / month, since we are considering a range of vegetation types rather than just evergreen broadleaved forests.

The logical counterpart to the DSI is the wet season intensity (WSI), the cumulative sum of the differences between precipitation and evapotranspiration over each wet season. This represents fuel production, and therefore the change in total fuel load. These two indices can be summarised by Eqs. (2.1) and (2.2), below. They are also used in Murray-Tortarolo et al. (submitted).

.

$$DSI = \sum_{P<E} E - P \tag{2.1}$$

$$WSI = \sum_{P>E} P - E \tag{2.2}$$

We calculate the DSI and WSI for every grid cell, using precipitation and evapotranspiration interpolated to a daily timestep. Although these products can be calculated monthly, the daily interpolation allows for more accurate estimation of when the crossovers between drying and wet seasons occur.

Since we are interested in the water stress inflicted on vegetation that is already present, each DSI value is paired with the WSI from the preceding wet season. We assume that fire can only occur during the drying season. The MODIS fire dataset which will be used to calibrate the model begins in July 2002, so we use every set of WSI, DSI and drying season fire counts for which the drying season begins on or after 1st July 2002: the wet season can start before this date. We calculate these products up to the last complete drying season per grid cell.

2.1.3.3. Model equation

We define the potential fire index (PFI) as the minimum of two functions, one for each product, using Eq. (2.3):

$$\mathrm{PFI} = \max(\min(a\,\mathrm{DSI}, b\log(\mathrm{WSI}))\,, 0) \tag{2.3}$$

This model works on the assumption that fire activity has a dominant limitation: either a lack of fuel, or an abundance of water. The logarithmic transformation of WSI is due to a non-linear relationship between annual fuel production (NPP) and precipitation (e.g. Bowman et al., 2014). The PFI is restricted to being strictly greater than or equal to 0, to guard against negative values of the PFI in the case of the WSI being less than 1.

2.1.3.4. Consideration of local land cover

We expect the relationship between WSI, DSI and potential fire incidence to vary depending on the local vegetation type. This is predominantly due to the differences in total fuel load: since WSI represents the increase in fuel, rather than total biomass, information about the land cover is needed to complement this product. A high WSI value in a savannah represents a much larger percentage increase in biomass than an identical value in a dense forest. Hence, the model is calibrated separately for a range of land cover types representative of tropical ecosystems, based on the GLC2000 land cover dataset. LCTs that show very little to no fire activity, such as bare areas or regularly flooded forests have been excluded from the analysis.

2.1.3.5. Partitioning the fire data

We are modelling the maximum number of fires that could occur, given a pair of WSI and DSI values, rather than the expected number of fires. Hence the model cannot be fitted using all of the available fire count data for a given LCT. Instead, we consider only the largest numbers of observed fires in a grid cell and dry season for each WSI and DSI combination to be representative of maximum potential fire under those conditions. This assumes that in these cases, there has been little or no limitation on fire activity by a lack of ignitions or human suppression. To identify these data points, we first bin the data based on partitions of the ranges of both WSI and DSI, and then isolate the largest fire counts in each bin. These values, and their corresponding exact WSI and DSI values, are used to calibrate the model for each LCT.

We divide the ranges of DSI and WSI into 9 equally-spaced partitions. Increasing the number of partitions results in many of the bins containing no data points, and exponentially increases computational time, whereas reducing the number of partitions limits the accuracy of the model, since the range of DSI and WSI values in each bin becomes too large. The maximum DSI and WSI values per LCT for the given datasets are shown in Table 2.1 to enable these partitions to be recreated if desired. The minimum values in each range are always very small, so are assumed to be zero.

Once the WSI and DSI partitions have been identified, we isolate the largest x% of fire counts in each bin and fit the model to this data only. We choose the highest value of x such that the model fit has a coefficient of determination (R^2) of at least 0.7. This R^2-threshold is not strict - the final results change very little if this is changed to 0.6 or 0.8, for instance. For two LCTs

(evergreen, needle-leaved trees and sparse herbaceous or shrub cover) it was not possible to obtain an R^2-value greater than 0.7, so we chose *x* such that the coefficient of determination was as large as possible. The value of *x* changes considerably between LCTs, since some ecosystems are more prone to human intervention than others. The values of *x* for each LCT are given in Table 2.2.

Table 2.1: Maximum values of WSI and DSI using the calibration data, over the study period and time region.

Land Cover Type	Maximum WSI	Maximum DSI
Tree, broadleaved, evergreen	4344	727
Tree, broadleaved, deciduous, closed	3345	491
Tree, broadleaved, deciduous, open	1160	417
Tree, needle-leaved, evergreen	2041	484
Mosaic: tree/natural vegetation	1271	377
Shrub, evergreen, closed-open	4182	336
Shrub, deciduous, closed-open	1588	398
Herbaceous cover, closed-open	2862	614
Sparse herbaceous/shrub cover	1340	413
Cultivated/managed areas	3131	464
Mosaic: crop/tree/natural veg	3275	397
Mosaic: crop/shrub/grass	1569	427

2.1.3.6. Model calibration

The model parameters *a* and *b* are calibrated for each LCT using the largest fire counts per DSI and WSI partition. This is done by rearranging the right-hand side of Equation (2.3) into the format *a* log(WSI) min(DSI, *b*/*a*), optimising *b*/*a* by minimising the sum of squared errors of the corresponding linear model fit, and then using linear regression on the rearranged equation to estimate *a*, and

hence *b*. The estimates of these parameters are shown in Table 2.2.

It is important to note that the MODIS MCD14ML dataset does not give exact fire counts, but rather hotspot detections from four daily overpasses at a 1km resolution. As a result, a single fire event may correspond to multiple MODIS hotspots. Hence, the model parameters given in Table 2.2 are specific to this detection method.

Table 2.2: Model coefficients (*a* and *b*) per LCT, the corresponding percentage of data used to fit the model (*x*), and the model's coefficient of determination (R^2 value).

LCT	a	b	x	R^2
Tree, broadleaved, evergreen	10.7	604	11.3	0.70
Tree, broadleaved, deciduous, closed	16.8	476	76.5	0.70
Tree, broadleaved, deciduous, open	16.4	505	100	0.75
Tree, needle-leaved, evergreen	8.6	1604	0.8	0.54
Mosaic: tree/natural vegetation	13.8	676	100	0.76
Shrub, evergreen, closed-open	8.5	1435	20.9	0.70
Shrub, deciduous, closed-open	10.6	386	89.6	0.70
Herbaceous cover, closed-open	11.9	364	6.7	0.70
Sparse herbaceous/shrub cover	15.5	516	0.6	0.61
Cultivated/managed areas	5.3	1567	25	0.70
Mosaic: crop/tree/natural veg	11.4	424	32.9	0.70
Mosaic: crop/shrub/grass	6.9	266	87	0.70

2.1.3.7. Model testing

We test the model by adding a subroutine into JULES that calculates DSI and WSI using the model's precipitation and evapotranspiration variables, and

subsequently the PFI. The PFI is set to zero during wet seasons, and increases monotonically during the drying seasons, using the cumulative DSI values at the end of each timestep. Due to the resolution of the JULES simulations (2°x2°) being coarser than the resolution of the model calibration data (1°x1°), the PFI estimates need to be multiplied by 4 to account for the fourfold increase in grid cell area.

Although a daily timestep was used during the model calibration, daily precipitation and evapotranspiration at that stage were obtained by interpolating monthly values, resulting in relatively smooth time series. When calculated using JULES, the difference between precipitation and evapotranspiration is prone to many small fluctuations between positive and negative values at the crossover between wet and dry seasons. This results in many small WSI and DSI values per year, as well as a few larger values. Hence, an intense dry season is often paired with a very small WSI value, which does not represent the true level of fuel growth over the preceding wet season. To avoid this problem, we calculate the PFI on a monthly timestep. To facilitate comparison of the PFI to estimates of the Canadian FWI, McArthur FFDI and SPITFIRE FDI, also calculated within JULES, these indices are averaged over each calendar month.

The indices are not directly comparable with one another, due to the range of purposes and interpretations. Hence, in order to compare the spatial and temporal patterns to each other, and to the MODIS MCD14ML fire data, we first calculate the mean annual grid cell values, mean seasonal cycle, and mean annual time series of the indices and fire counts, and then standardise these products. Annual values are the sum of the monthly values in the case of the

PFI, and mean monthly values for the other indices. The seasonal cycle of each index is the mean value for each calendar month. Standardisation is done by subtracting the minimum value of each product from every value, and dividing the result by the full range of values. This restricts each index to values between 0 and 1. We compare the standardised products to the MODIS MCD14ML active fire count dataset by calculating the pairwise Pearson's correlation coefficients between them.

2.1.4 Results

2.1.4.1. Spatial patterns of fire

All of the indices, including the PFI, show strong positive spatial correlations to the MODIS fire counts within forested regions (Fig. 2.1, left-hand plots, Table 2.3). The PFI gives the strongest correlation ($r = 0.715$, $p < 2.2 \times 10^{-16}$, $df = 377$), followed by the SPITFIRE FDI ($r = 0.618$, $p < 2.2 \times 10^{-16}$, $df = 358$), the McArthur FFDI ($r = 0.533$, $p < 2.2 \times 10^{-16}$, $df = 358$), and the Canadian FWI ($r = 0.520$, $p < 2.2 \times 10^{-16}$, $df = 358$).

The PFI has been calibrated to multiple land cover types and therefore we expect it to produce better spatial patterns of fire estimates than the McArthur, Canadian or SPITFIRE indices when the analysis is extended to include non-forested regions, for which these existing indices have not been calibrated. When considering the full range of LCTs in the tropics, the existing indices perform poorly (Fig. 2.1, right-hand plots). The McArthur and Canadian indices correlate negatively to the MODIS data (Table 2.3), which is to be expected given that they are known to perform poorly outside of the regions for which they were calibrated (Australia and Canada, respectively; Planas and

Pastor, 2013), and the SPITFIRE FDI shows no significant correlation to the MODIS fire counts at a 10% significance level. This is due in part to the high predicted fire danger in barren regions, most notably on the edge of the Sahara desert. Additionally, these indices show relatively high fire dangers in western Australia and south-western Africa, whereas the MODIS data shows peaks in fire activity on the northern edge of Australia, and immediately south of the Congo basin. By considering the spatial correlations for each individual LCT, we observed that the overall negative correlations are a result of the indices performing badly for the majority of LCTs, despite very strong positive correlations for a few LCTs (Table 2.3). Both the McArthur and the Canadian

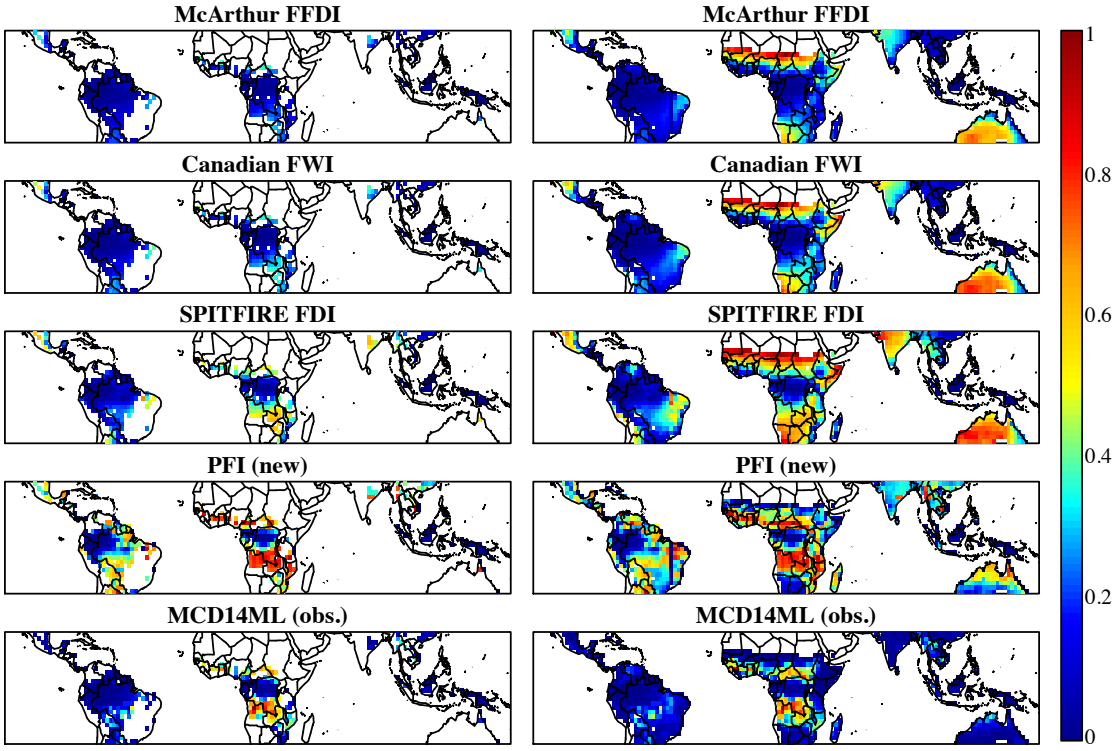

Figure 2.1: Mean annual fire danger or potential fire per grid cell in the tropics, for forested areas (left) and all non-bare LCTs (right). The corresponding maps for the MODIS MCD14ML active fire dataset are shown at the bottom, to facilitate comparison. The values for each product are normalised through subtraction of the minimum value and division by the range, and are thus limited to between 0 and 1.

have coefficients of correlation of over 0.55 for 3 LCTs, but negative correlations for 6 LCTs and negligible correlations that are insignificant at a 10% level for the remaining 3 LCTs. The SPITFIRE FDI shows negligible correlations for 6 out of the 12 PFTs considered and moderately strong negative correlations for a further 2 PFTs.

The PFI is the only index that shows a significant, strong and positive correlation with the observations ($r = 0.661$, $p < 2.2 \times 10^{-16}$, $df = 910$). It captures the obvious regions of high and low fire activity shown by the MODIS fire data in most regions. In Africa, particularly, the PFI identifies the ecosystems that are most at risk of fire, and shows very low fire potential on the southern edge of the Sahara desert where there is very little fuel. It shows a much higher level of potential fire in South America relative to the rest of the tropics than actually occurs, but captures the location of the curve of fire from Bolivia to the eastern tip of the continent much more accurately than the other indices. Similarly, the PFI indicates a much higher level of potential fire than actually occurs in S.E. Asia and Australia, but peaks in the right places: Burma, Thailand and northern Australia. The correlations for individual LCTs are positive, strong ($r > 0.4$) and significant at a 10% level in all but 3 cases, which is a considerable improvement on the other indices.

2.1.4.2. Seasonality of fire predictions

Comparison of the mean annual cycle of each of these indices across tropical forests (all tree LCTs, the area shown in the left-hand plots of Fig. 2.1) shows that the PFI performs similarly to the other indices (Fig. 2.2a). It is lowest in April and November, which corresponds to the dips in fire activity shown by the

Table 2.3: Pairwise correlations between the annual means, cycles and time series of the indices and the MODIS MCD14ML active fire count product. Correlations that are insignificant at a 10% significance level are given in brackets.

Land Cover Type	McArthur	Canadian	SPITFIRE	PFI
	Spatial distribution: pairwise correlation between annual means per grid cell			
Forests (1st 4 LCTs)	0.533	0.520	0.618	0.715
All LCTs	-0.121	-0.121	(0.04)	0.661
Tree, broadleaved, evergreen	0.614	0.650	0.658	0.603
Tree, broadleaved, deciduous, closed	(-0.229)	-0.288	(0.057)	0.582
Tree, broadleaved, deciduous, open	-0.223	-0.301	(-0.003)	0.615
Tree, needle-leaved, evergreen	-0.575	-0.579	(-0.394)	(-0.044)
Mosaic: tree/natural vegetation	0.667	0.583	0.545	0.912
Shrub, evergreen, closed-open	(0.055)	(0.127)	0.581	(0.372)
Shrub, deciduous, closed-open	-0.296	-0.418	(0.132)	0.580
Herbaceous cover, closed-open	-0.441	-0.485	-0.427	0.526
Sparse herbaceous/shrub cover	-0.232	-0.293	-0.260	0.671
Cultivated/managed areas	-0.194	-0.177	(-0.099)	0.448
Mosaic: crop/tree/natural veg	0.663	0.566	0.419	0.564
Mosaic: crop/shrub/grass	(-0.008)	(-0.070)	(0.132)	(-0.114)
	Temporal distribution: pairwise correlation between mean global annual cycles			
Forests (1st 4 LCTs)	0.771	0.888	0.887	0.794
All LCTs	(-0.415)	(0.204)	0.723	(0.208)
	Temporal distribution: pairwise correlation between annual global time series			
Forests (1st 4 LCTs)	0.813	0.764	0.816	0.659
All LCTs	(0.454)	(0.445)	(0.239)	(0.525)

MODIS fire count data: all of the indices capture the April dip, but the SPITFIRE FDI is the only other index to correctly predict the timing of the November dip. The PFI peaks in June and January, rather than August and December, as shown by the MODIS data. None of the existing indices capture the timing of the December peak, with the McArthur and Canadian indices peaking in February and the SPITFIRE FDI in January. However, the McArthur and Canadian indices do capture the large peak in fire in August, and the SPITFIRE FDI predicts this peak one month earlier in July. Hence, none of the indices capture all of the four peaks and troughs of the annual fire cycle: all of them correctly identify two, and are one or two months out for the other two.

The correlations between these seasonal cycles of the indices and the MODIS data are all above 0.75 (Table 2.2). Although the PFI shows weaker correlation ($r = 0.794$, $p < 0.002$, $df = 10$) than the Canadian FWI ($r = 0.888$, $p = 0.0001$, $df = 10$) and the SPITFIRE FDI ($r = 0.887$, $p<0.0002$, $df = 10$), it is nonetheless a very strong, positive correlation, and is strong than that of the McArthur FFDI ($r = 0.771$, $p = 0.003$, $df = 10$). The PFI is therefore comparable to the other indices in terms of capturing the seasonality of fire in tropical forests, though no better in this respect.

When extending this analysis to all LCTs, none of the indices except for the SPITFIRE FDI capture the observed seasonality of fire particularly well (Fig. 2.2b). This is the only index that correlates strongly and significantly with the observations (Table 2.3). The McArthur and Canadian indices are both between 2 and 3 months late in predicting peaks and dips in fire activity, and the Canadian FWI barely identifies the spring dip at all. The PFI captures the low fire activity observed in April, and is only one month late in predicting the

October dip and the peak in December, though it does predict the August peak 2 months early. Hence, although it is not as good as the SPITFIRE FDI at estimating pan-tropical fire seasonality, it is more accurate than the Canadian and McArthur indices.

2.1.4.3. Annual fire estimates

At an annual scale, we observed strong positive correlations between all of the indices and the MODIS fire count time series when we restrict the analysis to forested regions only. The PFI is slightly worse than the other indices in this sense, but nonetheless correlates strongly with the observations (r = 0.659, p-value = 0.075). Every index captures the main peaks in fire activity in 2005 and 2007, which were years of intense drought in Amazonia, as well as the large decrease in fire counts in 2006 (Fig. 2.2c). When the analysis is extended pan-tropically, the PFI gives the strongest correlation. However, none of these correlations are statistically significant, which may be due to the small number of data points being considered.

2.1.5 Fuel and water limitations

We use the model parameters to identify what percentage of the fire data points used to calibrate the model is limited by an excess of fuel moisture. If the DSI term of Equation 2.3 is less than the WSI term (i.e., a*DSI < b*log(WSI)), this indicates a water limitation. We call this statistic the PWL (percentage water-limited). The higher the values of a or b, the lower the likelihood that a grid cell will be identified as water or fuel limited, respectively.

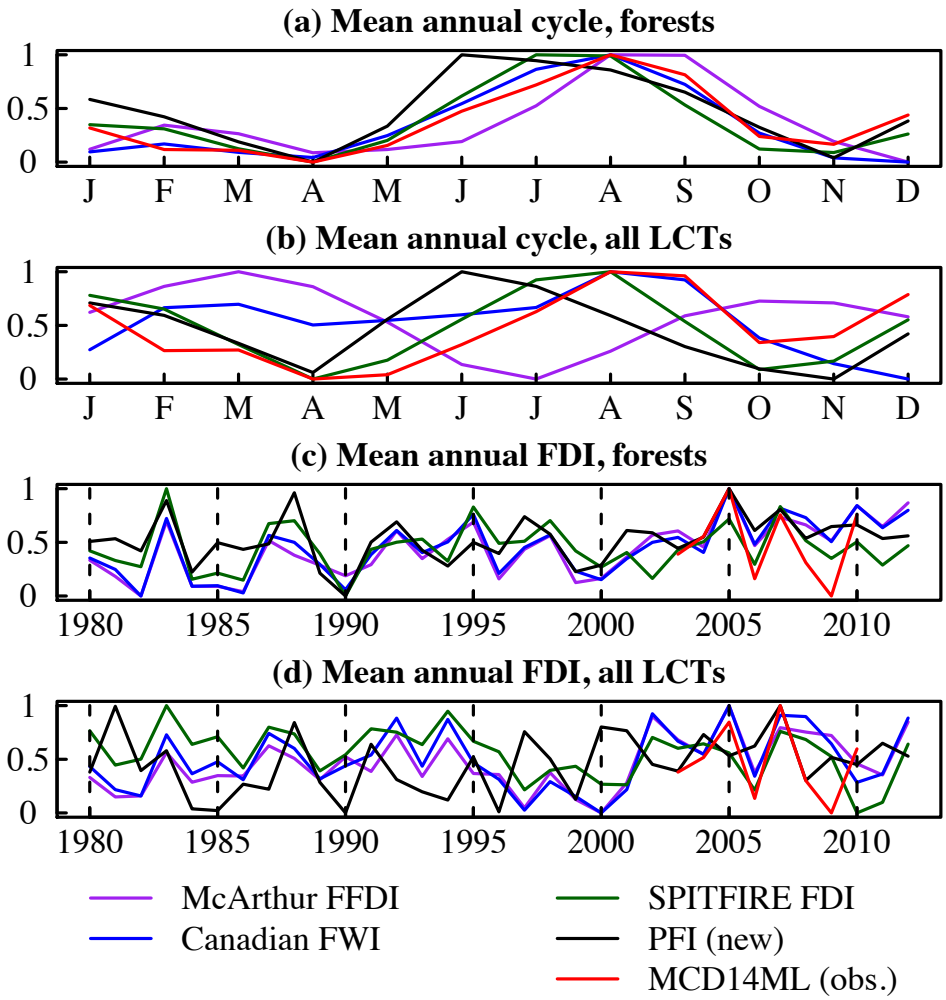

Figure 2.2: Standardised time series of the grid cell mean McArthur, Canadian and SPITFIRE fire danger indices, the new potential fire index (PFI), and the MODIS MCD14ML fire count product for comparison. Plots (a) and (c) plot use only forested grid cells (the top 4 LCTs in Table 2.2), and (b) and (d) plots use all grid cells that are covered by any of the LCTs to which the model is fitted. Plots (a) and (b) show the mean annual cycle of each index, averaged over all available years (1980 to 2012 for the indices, 2003 to 2010 for MCD14ML), and (c) and (d) show the full time series.

By considering the percentage of fire seasons per grid cell that are predominantly limited by water excess, rather than a lack of fuel, we can identify which regions or ecosystems are most at risk of extreme fire seasons as a

result of drought. The LCTs that are almost entirely limited by excess fuel moisture are evergreen trees and shrubs (PWL > 95%), cultivated or managed areas (PWL = 97%), or mosaic areas of trees and other natural vegetation (PWL = 94%). The only LCTs that are identified as being fuel-limited the majority of the time are broadleaved, deciduous trees (open: PWL = 28%, closed: PWL = 38%). Deciduous shrubs are limited by both factors to equal extents, with a PWL of 50%. The remaining LCTs have PWLs of between 60% and 83%.

The expectation is that fire in barren, arid and semiarid regions is limited predominantly by a lack of fuel that is sufficiently connected to allow fire to spread, and yet the opposite appears to be true in some of these areas, such as the Sahel region (Fig. 2.3a). This can be explained by comparing the PWL to mean grid cell DSI and WSI (Fig. 2.3b,c): the drying seasons are less intense in the Sahel than they are in areas with higher levels of precipitation (Fig. 2.3d), as a result of less evapotranspiration (Fig. 2.3e). The hypothesis that the DSI is controlled primarily by evapotranspiration is further supported by a correlation of 0.91 ($p < 2.2 \times 10^{-16}$) between the grid cell means of DSI and dry season evapotranspiration, but of only 0.40 ($p < 2.2 \times 10^{-16}$) between DSI and dry season precipitation.

Spatially, the PWL distribution correlates closely with the mean pattern of fire activity ($r = -0.60$, $p < 2.2 \times 10^{-16}$). In other words, areas of high fire activity are more likely to be limited by a lack of fuel than by an excess of water. Conversely, the fire regime in regions that rarely burn is predominantly controlled by fuel moisture in the dry season, rather than by fuel load.

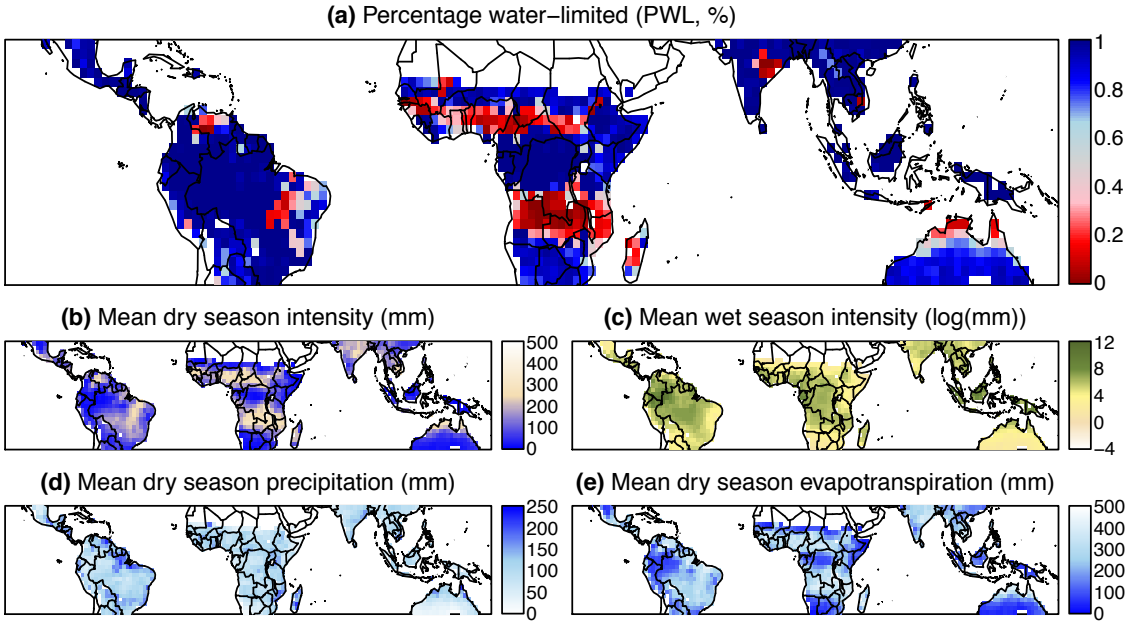

Figure 2.3: (a) Map showing the regions in which the PFI model identifies fire activity as being predominantly limited by an excess of fuel moisture (blue) or a lack of fuel (red). The corresponding mean (b) dry season intensity, (c) wet season intensity, (d) dry season precipitation (mm), and (e) dry season evapotranspiration (mm) are shown for comparison.

2.1.6 Discussion

The potential fire index presented here has four clear distinguishing factors. First, it reproduces available fuel loads, making it applicable to virtually all tropical ecosystems, rather than a single, specific region. Second, the PFI requires only three readily available and reliable datasets: precipitation, evapotranspiration and land cover. Third, it has a definite ecological interpretation. Finally, it can be used to identify regions that are most at risk of extreme fire seasons due to changes in climate.

Temporally, the PFI performs similarly to existing FDIs, both in forested regions and across the tropics: its simplicity does not majorly compromise its performance. This shows that using measures of dry and wet season moisture

levels as proxies for fuel loading and moisture is sufficient for predicting fire occurrence in the tropics, and that the inclusion of temperature, wind speed, humidity or fuel quantity datasets is not essential.

The main issue with the timing of the PFI is that it predicts the main August peak in fire activity two months too early. It allows fires to occur from the beginning of the drying season, but during this time the fuel is becoming drier: it is not yet dry. Hence, fire should not be predicted at the beginning of a dry season, but the optimal time delay is likely dependent on the vegetation type, the WSI of the preceding wet season and the rate of increase of the DSI, since different fuels dry at different speeds. Additionally, the timing of ignitions may also have a significant effect. For instance, the predominantly human-driven fires of Northern Australia occur mainly near the beginning of the dry season (Russell-Smith et al., 2007). Further analysis of the seasonal cycles for individual biomes may provide insight into where the major discrepancies are. The December peak in fire activity is predicted one month too late by the PFI, but the observations are of similar magnitude in both December and January, so this is not necessarily a major problem. This may also be an effect of the monthly (rather than daily) calculation of the PFI.

Although an improvement in the timing of the PFI predictions would undoubtedly be beneficial, it is more important that the magnitude and spatial distribution of the estimates is adequate. The goal of fire modelling within a DGVM is to improve estimates of emissions and carbon cycling, which depend much more on the location and extent of burning than on the timing of fires. The PFI does not represent an improvement over the existing indices in terms of temporal fire predictions, but it does perform significantly better on a spatial

scale, making it much more suitable for use within a DGVM.

By representing fuel availability indirectly as a function of moisture availability, the PFI not only avoids the major problem of high fire predictions in sparsely vegetated area such as the Sahara desert, but also captures many of the finer nuances of the fire distribution pattern across all LCTs. This gives the PFI a distinct advantage over existing FDIs due to its suitability for long-term, large-scale, within-DGVM analysis of climate change and the environmental impacts of fire across the globe.

Additionally, it is likely that many of the remaining discrepancies between the spatial distribution of the PFI and the MODIS active fire product are caused by ignition patterns. The PFI represents the maximum possible number of fires that could occur, but in many areas, the true number of fires will be considerably smaller, as a result of a lack of ignition sources or active measures taken to prevent fires. Hence, the areas in which the PFI appears to be too high, such as South America or northern Australia, are not necessarily a sign of a shortfall of the index. Rather, these regions have the potential to provide interesting insight into human behaviour with regards to wildfire.

A particular advantage of the PFI model is being able to calculate fuel and water limitations to fire activity. The PWL gives an interesting insight into the way certain LCTs may react to changes in seasonal patterns of precipitation or temperature. Areas that have low PWL values are much more prone to increased fire risk if there is above-average rainfall in the wet season, whereas water-limited ecosystems are much more susceptible to dry season drought. Since fire-prone ecosystems are more likely to have low PWL values, changes in precipitation in the wet season have more impact on fire activity than changes

in dry season precipitation. The main focus of existing fire danger indices and current fire literature is on the effect of drought on fire occurrence: these results suggest that moisture levels in wet seasons preceding droughts are of more importance to fire prediction.

Contrary to expectations, fire in dry, barren regions such as the Sahel is predominantly limited by an excess of moisture, as well as the expected dense, tropical forests, while it is the intermediate LCTs that are more prone to fuel-limitation. While this may, in part, stem from the difficulties faced when fitting the model to the sparse herbaceous and shrub cover LCT, which covers a large proportion of the Sahel, we hypothesise that this might also be a result of drought-adapted vegetation in the region. Many plants, such as the baobab tree, store large quantities of water and transpire very little: the low evapotranspiration levels in the area results in very low-intensity drying seasons, despite long periods without rain. Additionally, the effect of changes in moisture on the growth of such plants is small. Therefore, if a drying season is exceptionally long or intense, this could be more likely to increase flammability by depleting water stores, than a long wet season would be by increasing fuel production. However, this is would require substantial further research to be confirmed.

There are many benefits of having an FDI that works well across multiple ecosystems. We can quickly and easily investigate the effects of changes in climate on pan-tropical fire activity, rather than focusing on small, individual regions. We can therefore further investigate claims such as that presented by Krawchuk et al. (2009) of increases in fire activity in some regions being balanced out by decreases in other areas, and the resulting effects, if any, on

carbon emissions. Additionally, we can analyse whether fires in specific biomes are predominantly limited by a lack of fuel or an excess of moisture, and pinpoint the thresholds at which this limitation switches.

As mentioned in the Introduction, the PFI represents potential fire, rather than expected fire activity: the index does not take the presence or absence of ignition sources into consideration. Hence, the PFI is only a realistic representation of fire activity in regions with high levels of human fire-causing activity or lightning strikes. Elsewhere, it is bound to be too high, as seen in Figure 2.1. Despite this, the index is of considerable use. It can be used to identify changes in flammability in specific regions as a result of a changing climate, thus aiding in fire management. It can also be combined with an ignitions model within a DGVM, and its improved accuracy over the other indices suggests that the resulting estimates of pan-tropical burning and resulting trace gas emissions will consequently be enhanced. Additionally, a detailed ignitions model may improve the temporal accuracy of the index, since ignitions are unlikely to be evenly distributed throughout the fire season, though further research is required to confirm this.

The PFI should be easy to implement within a DGVM. The main obstacle is that the model LCTs may not correspond to those used to calibrate the model, or, more likely, that the model may use plant functional types (PFTs) rather than LCTs, which by definition do not characterise mixed/mosaic classes or biomes. In the first case, the LCTs could be grouped appropriately and parameter means can be used. If LCTs are not included in the model, a method similar to that used by Pacifico et al. (2011) could be used to transform each LCT into a PFT, where necessary. It is also possible to read the GLC2000

dataset into the DGVM as an ancillary, and use it directly (as was done for this study), although this would not allow for future changes in land cover. Alternatively, it may be easier to recalibrate the model so that the parameters are functions of biomass. Since the values of *a* and *b* roughly correlate to the biomass gradient, this should be a feasible option, and shouldn't cause major changes to the model results. This would also make the model more dynamic since it would allow the land cover to change temporally. However, this would be dependent on the model being able to accurately estimate biomass, which is not straightforward (e.g. Lu, 2006).

Finally, it would be useful if the model could be extended to extra-tropical regions, so that it could be run on a global scale. The model may prove to be unsuitable in ecosystems that do not experience strong, distinct drying and wet seasons, but since there is no restriction on how many drying/wet season pairs per year the model can take as input, the model may still work. Indeed, Westerling et al. (2006) found that extra-tropical fires are still strongly driven by oscillations between wet and dry periods, but that the presence of snow adds to the complexity of determining dry seasons.

In conclusion, therefore, the fire risk model developed here, the Potential Fire Index has many advantages over existing fire danger indices. It is applicable to a range of ecosystems as a result of considering fuel availability. It is simple to calculate, and requires only precipitation, evapotranspiration and land cover type as inputs, all of which are readily available datasets. It can be clearly interpreted as the maximum possible number of fires that can occur, given the local climatic and vegetative conditions. Its estimates are comparable to existing FDI predictions when looked at temporally, both for forested parts of

the tropics and across all LCTs, and are much closer to observed spatial patterns of fire activity. The PFI works well as a standalone model, but could be implemented within a broader model with some further development, and should be extendable to a global scale with little modification.

NB: This is the end of the content of Fletcher et al. (submitted).

2.2 FROM POTENTIAL FIRE TO EXPECTED FIRE COUNTS: MODELLING IGNITIONS

The potential fire index (PFI) developed in the first part of this chapter represents the number of fires that could occur as a result of the local climatology: it is not equivalent to active fire counts, despite strong correlations between the PFI and observed fire activity. In order to make full use of the PFI, it is therefore necessary to develop a method for converting the PFI into an expected number of fires. This method should represent the effect of the presence of ignition sources on fire occurrence. The purpose of this is not to produce a generalised ignitions parameterisation that can be used in any fire model, but rather to develop a simple method that specifically applies to the PFI and enables its incorporation into a DGVM.

2.2.1 Existing model approaches

Modelling ignition events is arguably the most complicated aspect of fire modelling, as evidenced by the range of parameterisations used by existing models. The Glob-FIRM model (Thonicke et al., 2001) simply assumes that ignition sources are always present, thus avoiding the problem, but likely

resulting in a significant loss of accuracy, since it is an unrealistic assumption. This would be equivalent to using the PFI as an estimate of expected fire counts, which would result in an overestimation of fire activity. MCFIRE (Lenihan et al., 1998) uses an ignition and fire spread probability, derived from simulations of fuel flammability, rate of spread and a basic indicator of the presence of lightning. The exact calculation is not given, and this method is designed to identify only extreme fire events. Other fire models tackle the problem of ignitions in two parts, by dividing them into natural ignitions caused by lightning, and anthropogenic causes of fire. These are modelled independently, with the complexity of the approaches varying considerably between models.

2.2.1.1. Natural ignitions

Natural ignitions, with only one main driver, are theoretically straightforward to predict, but the models nonetheless all use slightly different parameterisations. Reg-FIRM (Venevsky et al., 2002) prescribes a constant number of lightning ignitions per grid cell per day. SPITFIRE (Thonicke et al., 2010) and its successor, the fire component of LPX (Prentice et al., 2011), both calculate lightning ignitions as a constant fraction of observed lightning flashes, yet don't agree on the value that this should take. The CLM fire parameterisations (Li et al., 2012a,b; Li et al., 2013) take a similar approach, but allow this fraction to vary based on a grid cell's latitude. CTEM (Arora and Boer, 2005) has the most complex method for modelling natural ignitions, using a non-linear function of lightning flashes between upper and lower bounds.

2.2.1.2. Anthropogenic ignitions

Anthropogenic ignitions are unquestionably the hardest driver of fire occurrence to model. The CTEM fire model, despite having the most detailed lightning ignition parameterisation, does not attempt to model human ignitions, instead stating that the probability of fires being started by humans "may be selected depending on location and human activity". This method is therefore impossible to reproduce. SPITFIRE uses a function of population density (PD) that requires region-specific parameter values denoting the propensity of humans to cause fires, but this equation is then removed from the model during the LPX development and not replaced, emphasising the inadequacy of the parameterisation. Reg-FIRM calculates human ignitions as proportional to the product of $PD^{0.43}$ and the natural logarithm of PD, whereas the first CSM fire parameterisation (Li et al., 2012a) goes for the less complex option of $PD^{0.4}$. The subsequent CSM fire parameterisation (Li et al., 2013) uses a much more detailed function of PD along with additional functions of gross domestic product, the seasonality of agricultural fires, and the fractional coverage of cropland to estimate fire.

There is a clear lack of agreement about the exact nature of the relationship between population and fire, even when PD is used as the sole driver of anthropogenic ignitions. It may be that the functions of PD used are too simple. For instance, Bistinas et al. (2013) suggests that the relationship between PD and burnt area varies based on land use, and it would therefore be logical to assume that the relationship between PD and fire occurrence does as well. Many other factors that influence the occurrence of fire have been identified in the literature: their inclusion would undoubtedly exacerbate the

discrepancies between the models, but their exclusion inevitably limits the potential accuracy of the models. These factors include proximity to roads, forest edges or clearings, degradation levels from previous burns, and distance from agricultural settlements or charcoal pits, to name just a few (e.g. Cochrane et al., 1999; Alencar et al., 2004; Alencar et al., 2006). Cultural and political factors may also affect the location and timing of anthropogenic fires. For instance, the relative values of timber and pasture, and education about the economic consequences of wildfire, can have large impacts on the extent of deforestation (Guyette et al., 2002), as can the intensification of agriculture (Morton et al., 2008). Additionally, it seems likely that intentional human ignition events are dependent on fire potential, since humans are less likely to attempt to ignite fires while it is raining or the fuel is saturated, or if there is no fuel to ignite, yet this interaction is not considered by any of the models.

2.2.1.3. Limitations of existing ignition models

The ignition models described above are generally described as “process-based”. As explained in Chapter 1, this implies that the individual processes that ultimately come together to cause fire are represented mathematically. There are several problems with a process-based approach when attempting to model ignitions. The first of these is that we, as a scientific community, do not understand all of the processes driving ignitions. We understand that lightning can cause fires if it is not accompanied by heavy rainfall, but do not know why some lightning strikes trigger burning and others do not. Similarly, we know that anthropogenic ignitions are linked to human activity, but we have not identified every factor that influences human fire-causing behaviour, hence our reliance

on general functions of population density. Despite extensive research into the drivers of the anthropogenic fire regime, no consensus has been reached.

This complexity means that it is impossible to include all of the driving factors in an ignition model, but limiting restricting ignition parameterisations to functions of lightning and population density does not give adequate results, suggesting that this is an oversimplification. If more drivers are included, additional input datasets will be required, which are not necessarily available at large temporal or spatial scales.

Another obstacle to the development of an accurate process-based ignitions model is that ignitions are not, in themselves, observable. An ignition event is a spark that may take hold to become a fire, if the local conditions are favourable to fire. Some ignitions will not take hold to become fires, and hence are not accounted for in active fire datasets. The lack of quantifiable data makes any “process-based” ignition models difficult to calibrate. There is little explanation in the literature about what data is used to calibrate existing parameterisations. Furthermore, it is difficult to distinguish between fires caused by lightning and fires resulting from human activity, especially as the two are believed to be co-dependent: it is believed that anthropogenic fires pre-empt the natural fire regime (Keeley and Bond, 2001; Prentice et al., 2011). Some documentation of lightning ignitions in specific areas is available (Tutin et al., 1996; Middleton et al., 1997; Ramos-Neto and Pivello, 2000), but this is rare, and not comprehensive.

Finally, due to the differences in meaning between the new PFI and commonly-used fire danger indices, it would not be possible to use an existing ignition model in the way it was designed, by multiply the resulting estimates by

the potential fire. Such an approach would make no physical sense, and would result in extremely inflated fire estimates. It would be plausible to take the minimum value of the expected ignitions and PFI in order to obtain a sensible fire count prediction. However, this would rely heavily on the somewhat dubious accuracy of current ignition modelling methods.

2.2.2 An empirical approach to ignition modelling

It seems that a logical approach for converting the potential fire index into fire count estimates would be to develop a new, empirical model, which makes use of the observable relationships between the PFI and fire counts. Using empirically derived parameters that represent the proportion of the potential fires that are expected to occur would implicitly account for the local effects of human activity, lightning strikes, and any other factors on fire occurrence, thus removing the need for complex, process-based simulations of these drivers.

It is likely that the local land cover type influences the PFI to fire count ratio. However, there is no obvious linear relationship between these two variables per LCT (Fig. 2.4). Although for some LCTs, the linear regression fits between the two give relatively high R^2 values, suggesting a linear relationship may work as an approximation, there is a visible lack of linearity for all LCTs. The use of a single parameter per LCT would therefore not be suitable for modelling purposes. We consider instead individual parameters specific to each grid cell.

This choice of method would not allow for temporal changes in the distribution of ignitions, but could be modified in the future to look at monthly, seasonal or annual patterns in ignitions. For now, however, we can assume that

significant changes in human activity or lightning patterns do not occur rapidly.

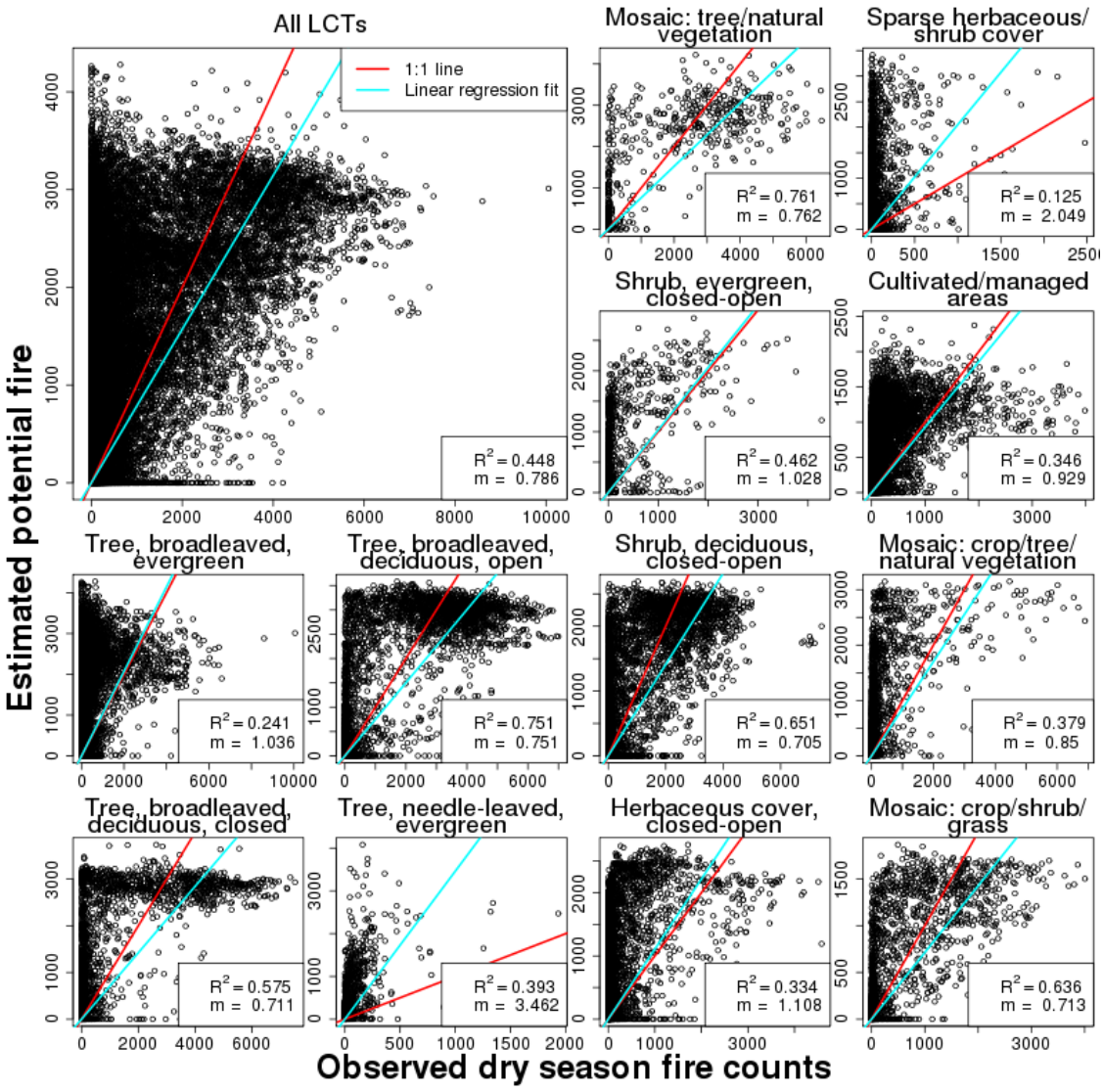

Figure 2.4: Estimated dry season potential fire (PFI) against observed dry season active fire (MODIS MCD14ML satellite product), for the tropics (top left) and each individual land cover type. The corresponding least-squares regression lines are given in blue, with their gradients and the R^2-values of the regression fit. The 1:1 lines are shown in red, for comparison.

Interannual variability in lightning occurrence is general assumed to be small (Thonicke et al., 2010), and, barring sudden policy changes, people are unlikely

to drastically change their habits from one year to the next.

It is worth noting that the use of a prescribed map of parameters to represent human ignitions is not entirely new: SPITFIRE uses a prescribed map for the values of $a(N_D)$, the propensity of humans to produce ignition events, although this is not reproducible without more information. The parameters used here simply provide a more direct approach, by eliminating the need for equations of population density or lightning flashes.

2.2.2.2. Parameter calibration

The average proportion of estimated potential fires that actually occur in each grid cell i, henceforth denoted δ_i, can be calculated in one of two ways. The first option is to fit a linear model of observed dry season fire to PFI for each grid cell. The linear model is restricted to passing through the origin, since a PFI of 0 indicates that no fire should be present, and the gradient of the resulting regression line is taken as δ_i. Non-linear relationships between the PFI and fire counts were also considered, but display no significant improvement in fit over the basic linear model. The second option is to divide the mean grid cell dry season fire counts by the mean grid cell PFI.

The two methods give very similar results for an average grid cell (Fig. 2.5, Scenario 1), though the linear model is slightly less susceptible to extreme outliers. If the PFI is consistently calculated to be larger than zero, but no fires ever occur in the grid cell (Fig. 2.5, Scenario 2), indicating a complete lack of ignitions, the resulting estimate of δ will be zero, regardless of the estimation method. The main difference occurs in Scenario 3, in which the PFI is always 0,

suggesting that fire should not be possible, but at least one fire has been shown to have taken place. In this case, the fraction method involves an attempt to divide by zero, resulting in $\delta = \infty$, whereas the linear model method returns a missing value in any statistical software. In fact, this scenario is rare, and for the calibration data only occurs in one single grid cell. Based on these scenarios, the linear model method of estimating δ is used from now on, though the fraction method would be adequate.

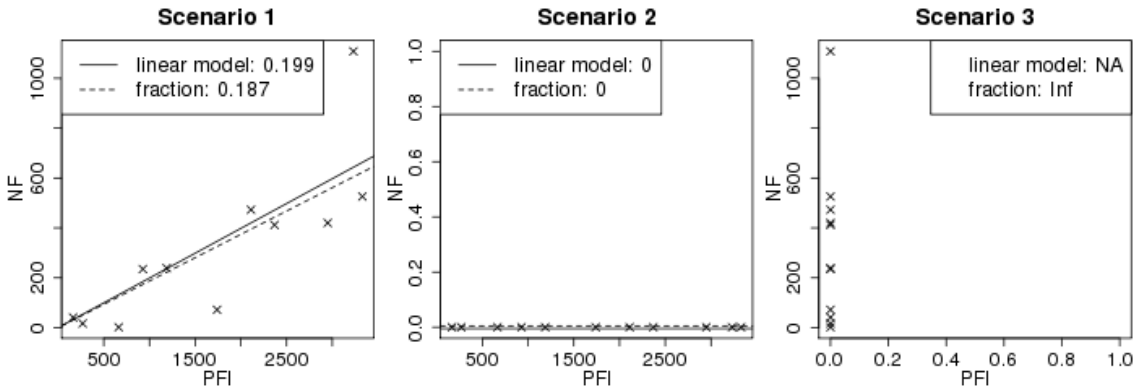

Figure 2.5: Comparison of the two methods of estimating the fire counts (NF) to PFI ratio (linear model vs. fraction of means) in three possible scenarios.

The same data used to calibrate the PFI model is used here, for consistency. The PFI is estimated, as before, using the CRU version 3.21 global monthly time series of precipitation (University of East Anglia Climatic Research Unit, 2013), the TRENDY ensemble mean for evapotranspiration (Sitch et al., 2013) and the GLC2000 land cover data set (Bartholomé and Belward, 2005; Global Land Cover 2000 database, 2003). The observed fire counts are from the MODIS MCD14ML global monthly fire location product (Giglio, 2010). Dry season PFI and fire counts are used instead of monthly or annual values, for

consistency with the methods used to calibrate the PFI model. The analysis is performed on all 1ºx1º grid cells between 25ºN and 25ºS, from July 2002 through to December 2010.

Theoretically, the values of δ_i should never be larger than 1, since the PFI represents the largest number of fires that can occur given the fuel availability and moisture. However, since the PFI model was fitted to the largest x% of fire counts, rather than using the absolute upper limit of fire counts, the PFI is likely to be slightly lower than the true maximum number of potential fires. Additionally, a small amount of model error is inevitable. Imposing an upper limit on the values of δ_i for theoretical purposes would only serve to reduce the accuracy of the final fire count estimates. The calculated values of $\delta_{i,}$ shown in Fig. 2.6, are larger than 1 in just over 11% of land grid cells in the study area, and above 1.5 in under 5%.

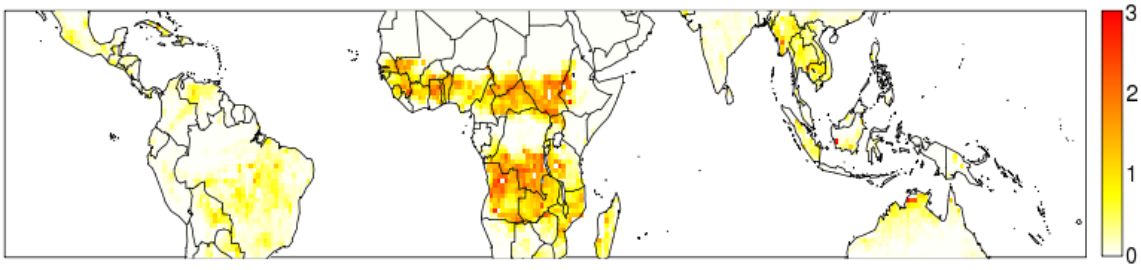

Figure 2.6: Calculated values of $\delta_{i,}$ which represent the proportion of estimated potential fires that are expected to actually occur for each grid cell.

2.2.2.3. Suitability of the proportional adjustment method

By comparing the observed fire counts from the MODIS dataset to $\delta_i \cdot \mathrm{PFI}$ for every dry season and grid cell, we can test the assumption that a constant value of δ_i per grid cell is suitable, and that allowing δ_i to vary per month, dry season, or year is not necessary over the given study period. In other words, we

are testing the assumption of negligible interannual variability in ignition patterns.

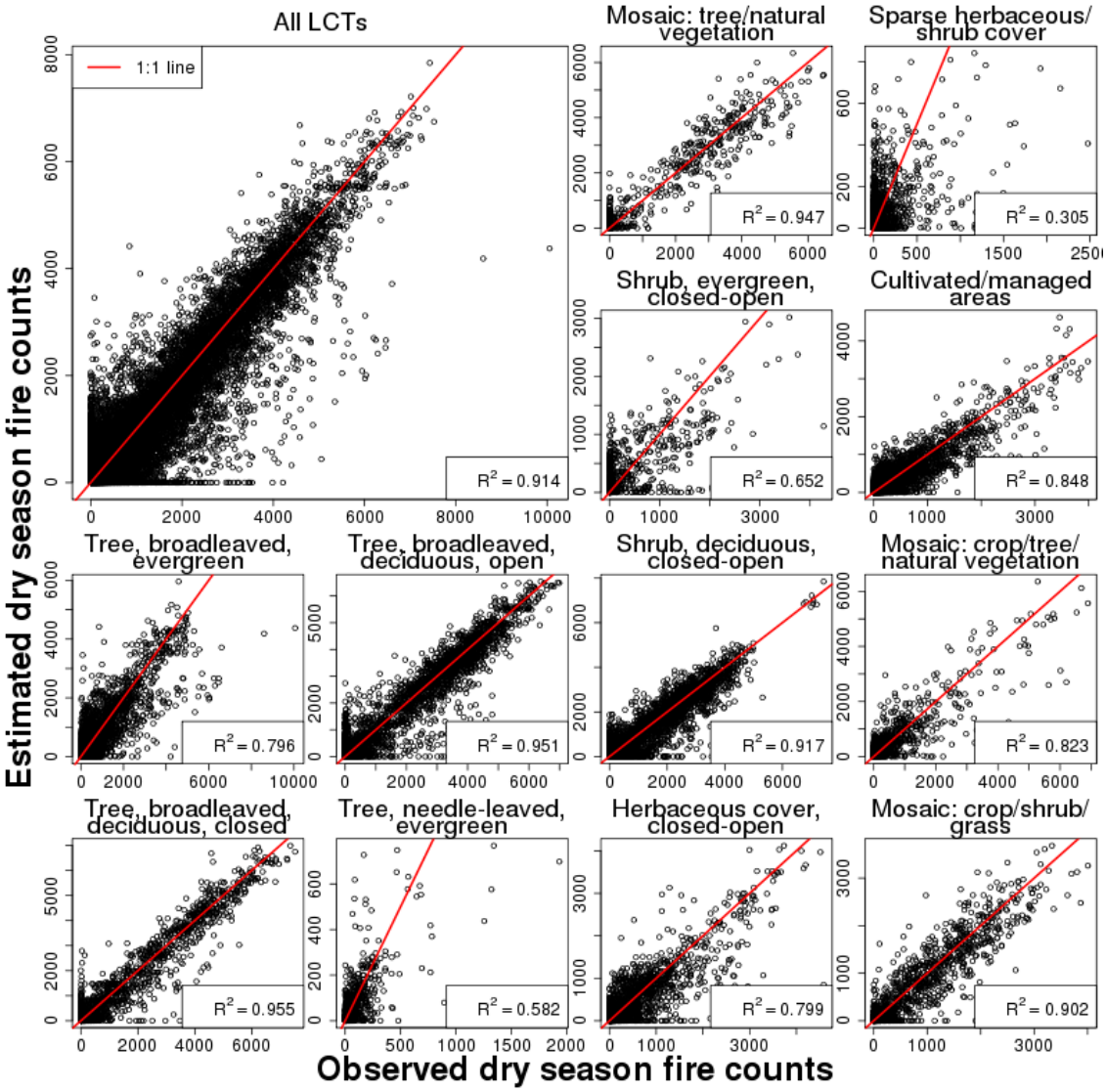

Figure 2.7: Estimated against observed dry season fire counts for all tropical LCTs (top left) and each LCT individually. The corresponding 1:1 line is shown in red, which is equivalent to the linear regression fit, which has a gradient of 1 in all cases. The R^2-values of each linear regression fit are given for each plot.

Due to the way in which the δ_i were calculated, the least-squares regression lines between the estimated and observed active fires will have a gradient of 1, both overall and per land cover type. These are equivalent to the

1:1 lines shown in red in Fig. 2.7. The statistics of interest are the R^2-values of these regressions: if they are low, this suggests that there is a significant amount of variability in each grid cell of the fire count to PFI ratio, implying a grid-cell specific constant value of δ_i may not be appropriate.

When tested over all LCTs, the coefficient of determination of the regression fit between estimated and observed fire counts is very high at 0.914. This shows that, overall, not allowing δ_i to vary temporally is not problematic for the time period studied. This is true for the majority of LCTs when considered separately. The R^2 values are low for sparse herbaceous or shrub cover and needle-leaved evergreen trees. However, these are the same LCTs for which is was difficult to fit the PFI model (Table 2.2), suggesting that the poor linear relationship between PFI and observed fire counts for these vegetation types is a limitation of the PFI model, rather than an indication of significant seasonal variability in ignition patterns.

2.2.3 Magnitude of the fire count estimates

The MODIS MCD14ML dataset gives information about hot pixel detections, rather than individual fires. The dataset is derived from information from 2 satellites, Terra and Aqua, which often both detect the same fire (Giglio, 2010). Large fires are also prone to multiple detections. We can obtain an approximation of the average number of times a single fire event is detected by each satellite by grouping the detections into probable single fire events. This is done by binning the detections from each satellite by day, latitude and longitude, with these two latter dimensions rounded to the neared arcminute, and calculating the mean number of detections in each bin.

Using this method, a single fire is detected approximately 1.94 times by each of the two satellites. Hence, we assume that a fire is detected an average of 4 times. All estimates of fire counts produced using the methods described in this chapter should be divided by 4 to account for multiple detections in the calibration dataset.

2.3 DISCUSSION

This chapter deals with the development of a potential fire index, and a method for using the PFI to estimate fire activity, so that the PFI can be used within a standard framework of a fire model.

The PFI is useful in its own right. It can be used as a standalone predictor of potential fire occurrence, and it has many advantages over existing fire danger indices. It accounts for changes in fuel availability, making it suitable for use over all tropical ecosystems, as is shown by the high spatial correlations between the PFI and observed active fire. It requires only precipitation and evapotranspiration data as input, which are more readily available at large spatial or temporal scales than relative humidity or wind speed, for instance. It can also be used to identify the regions in which an excess of fuel moisture, rather than a lack of fuel, predominantly limits fire activity.

In addition to this, the PFI can be incorporated into a fire model when combined with the ignition parameters shown in Fig. 2.7. The spatial and temporal accuracy of the resulting fire count predictions depends on the accuracy of both the PFI and the ignition parameters. The improvement in spatial accuracy of the PFI over existing FDIs that are currently used in fire models is likely to be beneficial. The PFI is temporally comparable to other

FDIs. Whether the resulting fire count estimates are also temporally comparable to those produced by existing fire models depends on the suitability of keeping the ignition parameters constant in time, as well as the temporal accuracy of current ignition models. For the study period assessed in this Chapter, July 2002 to December 2010, the assumption of little interannual variability in ignitions per grid cell appears to be sound. However, this does certainly limit the model, since it can't reliably be used for palaeontological predictions of fire activity, or for estimates in the far future. This method of modelling ignitions is therefore a temporary solution. Once the processes driving ignitions are better understood, this method should be updated.

A full assessment of the performance of this fire count model in comparison to existing models and observations is given in Chapter 4.

3. Fire spread and burnt area

The following chapter has been published as:

Fletcher, I.N., Aragão, L.E.O.C., Lima, A., Shimabukuro, Y. & Friedlingstein, P. (2014) *Fractal properties of forest fires in Amazonia as a basis for modelling pan-tropical burnt area.* Biogeosciences, 11, 1449 – 1459, doi: 10.5194/bg-11-1449-2014.

The contributions of each co-author are detailed in Section 1.9.

3.1 ABSTRACT

Current methods for modelling burnt area in dynamic global vegetation models (DGVMs) involve complex fire spread calculations, which rely on many inputs, including fuel characteristics, wind speed and countless parameters. They are therefore susceptible to large uncertainties through error propagation, but undeniably useful for modelling specific, small-scale burns. Using observed fractal distributions of fire scars in Brazilian Amazonia in 2005, we propose an alternative burnt area model for tropical forests, with fire counts as sole input and few parameters. This model is intended for predicting large-scale burnt area rather than looking at individual fire events. A simple parameterization of a tapered fractal distribution is calibrated at multiple spatial resolutions using a satellite-derived burnt area map. The model is capable of accurately reproducing the total area burnt (16,387 km^2) and its spatial distribution. When

tested pan-tropically using the MODIS MCD14ML active fire product, the model accurately predicts temporal and spatial fire trends, but the magnitude of the differences between these estimates and the GFED3.1 burnt area products varies per continent.

3.2 INTRODUCTION

Fires are a major component of the global carbon cycle. Globally, they release an average of 2.0 Pg C yr^{-1} into the atmosphere and over a third of this amount can be attributed to tropical fires (van der Werf et al., 2010). A changing climate is expected to increase the occurrence of droughts in tropical regions (e.g. Booth et al., 2012; Cox et al., 2008), which in turn will make extreme tropical fire regimes more likely (Aragão et al., 2007; van der Werf et al., 2008).

Despite their importance, representing fire dynamics within dynamic global vegetation models (DGVMs) to model their impacts upon the structure and functioning of ecosystems and their potential feedbacks on the climate system has been challenging. Their accuracy depends, in part, on an accurate representation of fire dynamics, yet many DGVMs do not contain a wildfire component (Piao et al., 2013). For quantifying carbon emissions from fires, three main steps are required: (i) predicting how many fires will occur, (ii) modelling the spread of these fires in order to determine burnt area, and (iii) calculating the expected quantity of biomass that will be combusted as a result. In this study we focus specifically on the second of these steps.

Within existing fire models, the spread of fire is one of the more complex processes. Many fire models implemented in DGVMs – including the most detailed fire models to date, SPITFIRE (Thonicke et al., 2010) and its

successor, the fire component of LPX (Prentice et al., 2011) – use an approach based on the Rothermel equations (Rothermel, 1972) to model the rate of fire spread. The area burnt in a given grid cell is then calculated using the rate of spread, expected number of ignitions and calculated fire danger index. This estimate relies on the assumption that fires generate elliptical burn scars. The Rothermel approach requires data about the distribution, density and moisture content of fuel in the area, the velocity of wind, and assumptions about when fires stop spreading. Data about the fuel needed to sustain fire spread are generally calculated by the DGVM itself, and therefore prone to substantial uncertainties. Wind velocity is routinely measured at meteorological stations; however, the accuracy of wind estimates from climate models that extend past the time frame of available measurements is uncertain, further limiting the potential of such an approach for palaeontological or future projections of fires. Additionally, a large number of prescribed parameters are used to describe processes such as the effect of damp fuel combustion on fire intensity. These parameters are generally estimated, and therefore likely to differ from their true values. Hence, each additional parameter introduces a new level of uncertainty into the modelled fire simulations. Because simulated area burnt is dependent on several separate assumptions, expressed as parametric equations, its accuracy is highly susceptible to both parameterization and forcing data errors, especially for tropical forest ecosystems.

It is undeniable that fire spread, as a physical process, must be dependent on ecological and climatic conditions, and that details of these conditions are essential for predicting the spread of any individual fire. The traditional approach of modelling the spread of individual fire events requires

detailed, localized data such as wind speed, fuel moisture and fuel loading. However, if the aim is to estimate the total burnt area resulting from all fires in a given region or biome over a certain time period, we can greatly reduce the number of input data sets required. For the model developed in this study, by using the theory of a scale-invariant fire size distribution, we need only ecological information about the dominant land cover type of the study area.

Scale invariance manifests itself as a fractal distribution, where the probability that an event of a certain size will occur decreases proportionally as the size increases. The exact distribution that is appropriate for a given system is debatable, and a range of possibilities are suggested in the literature. It has been shown that a huge range of complex dynamical systems and extreme events are scale-invariant, from earthquakes (Sornette and Sornette, 1989) and solar flares (Bofetta et al., 1999), to the extinction of species (Solé and Manrubia, 1996). More importantly for this work, numerous studies have shown scale invariance in the distribution of wildfire sizes, for certain regions and time frames (Cui and Perera, 2008). Significant power-law distributions of fires were found in regions of the US and Australia (Malamud et al., 1998), Spain (Moreno et al., 2011) and Amazonia (Pueyo et al., 2010). Some studies showed that either a truncated, piecewise or tapered distribution might be more appropriate for certain regions (Cumming, 2001; Holmes et al., 2004; Ricotta et al., 1999; Schoenberg et al., 2003; Pueyo et al., 2010) than an unbounded one.

The consensus among these studies is that variation in the parameters of these distributions between ecosystems and regions is associated with differences in land cover and local climate, and as such there has been no previous attempt to generalize the distributions over larger regions and time

periods. In this study, we consider only tropical forests. Although there is variability in land cover within tropical forests, we do not investigate the effect of land cover on the distribution parameters in this study. Local climate affects both the number of fires or fire fronts that occur as well as the spread of these fires. However, in this study we hypothesize that the effects of climate variations on active fires and fire spread are closely correlated, and hence, if fire counts are known, then the distribution parameters can be estimated from this single input variable, without the introduction of a weather variable.

To test this hypothesis, we proceed in three successive steps. First, we identify a distribution that is a suitable approximation of the observed distribution of fire sizes in the forests of Brazilian Amazonia. Second, we develop methods for estimating the distribution parameters, and check the accuracy of the model simulations of both the spatial distribution and total accumulation of burnt area across the whole region. Third, we test the suitability of the model for use with all tropical forests, as well as its ability to capture both spatial and temporal patterns of burnt area.

3.3 MODEL DEVELOPMENT

3.3.1 Data

In this work we used a burn scar data set for 2005 produced by Lima et al. (2009), restricted to the forested areas within the Brazilian Legal Amazonia limits, to calibrate the model. The burn scars were mapped using a linear spectral mixing model (LSMM; Shimabukuro and Smith, 1991) applied to the MOD09 daily reflectance product from Moderate Resolution Imaging Spectroradiometer (MODIS) onboard of NASA's Terra satellite, using the red

(band 1), near-infrared (band 2) and short-wave infrared (band 6) bands at a 250 m spatial resolution (Justice et al., 2002) (band 6 data were regridded from its original 500 m resolution). The MODIS images were chosen based on the following criteria: (1) images should be within the fire season period, identified by analysing daily active fire information from MYD14 product; (2) images should be free or partially free cloud images; and (3) images should be acquired with a view angle close to the nadir to minimize panoramic distortion.

The mapping was carried out in four steps, following the methods of Shimabukuro et al. (2009): application of an LSMM, segmentation of shade fraction image, unsupervised classification by regions and visual interpretation.

The LSMM was applied to the composite bands 1, 2 and 6 to generate the shade fraction image, which highlights low-reflectance targets – the case of burnt areas. Shade fraction images were subsequently classified in two steps. The first consisted in the application of a segmentation algorithm. The second encompassed the use of an unsupervised classification method (ISOSEG, Ball and Hall, 1965; Kawakubo et al., 2013) applied to the segmented images.

For the segmentation procedure two thresholds were defined: a) the similarity threshold, a minimum threshold below which two regions are considered similar and grouped into a single polygon, and b) the threshold area, minimum area value, given in pixels numbers, for a region to be individualized. A value of eight digital numbers and an area equal to four pixels were used for the similarity and area threshold, respectively. These thresholds were set based on the complexity of shape and size as well as from the mean deviations of digital number values of burn scars samples visually identified.

After segmentation, the ISOSEG algorithm was applied to the three

bands generated by the LSMM, shade, soil and vegetation with a 75% similarity limit (Shimabukuro et al., 2009). From the resulting classes, those corresponding to burnt areas were merged into a single “burn scar” class, and the remaining classes were discarded.

All water bodies were masked out and editing based on visual interpretation was performed to differentiate between burn scars and terrain shadow. All maps produced for each date were combined into a single yearly map depicting the total area of burn scars in 2005.

Finally, to quantify the forest burnt area, the burn scars map generated was overlapped by the 2005 forest mask provided by PRODES project (INPE, 2013). The final map used for the model calibration was the result of the intersection between the burn scars and PRODES forest area maps.

We compare the total area of burn scars mapped with a higher resolution map (30 m spatial resolution) derived from visual classification of Landsat 5/TM false-colour composite scenes for three Amazonian states following a west-to-east transect: (1) Acre (path 001/ row 67), (2) Amazonas (path 230/ row 65) and (3) Maranhao (path 221/ row 65). For the classification of the total burnt area for 2005 based on Landsat 5/TM data we used seven, five and six cloud-free scenes acquired during the fire season for Acre, Amazonas and Maranhao, respectively. We also compare our results with the MODIS burn scar product MCD45. Overall, using the LSMM algorithm produces a total area of burn scars consistent with the higher resolution map, apart from the state of Amazonas, where an underestimation is clear. Surprisingly, the MCD45 product well underestimates the burn scar area for the regions analysed in comparison to both Landsat 5/TM and our MODIS LSMM mapping procedure (Fig. 3.1).

For the purpose of our analysis we used point data corresponding to the LSMM image data, at a 500 m resolution. We treated every group of adjacent 500 m x 500 m pixels as a single fire event, and counted the number of fires of each size, *A*, in every grid cell, repeating the procedure for four different grid-cell resolutions: 0.5º x 0.5º, 1º x 1º, 2º x 2º and 4º x 4º. Any fire event that crossed a boundary between two or more grid cells was attributed to the grid cell in which the majority of the burn scar could be found. In this way, we obtained information about the number of fires of each size in each grid cell.

Due to the use of logarithms in the distributions, all calculations use the number of pixels as the fire size measure, rather than an area value, to ensure that $0 \leq \log(A)$ at all times.

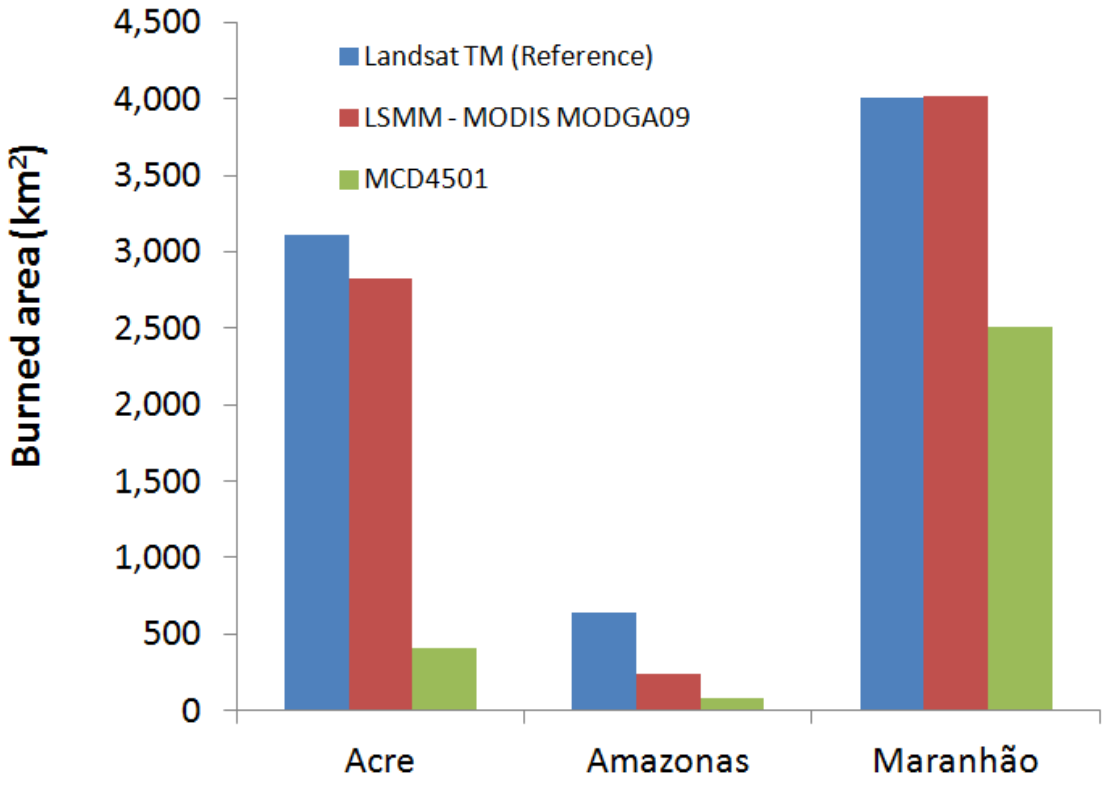

Figure 3.1: Comparison of the Landsat TM, LSMM-MODIS MODGA09 and MCD4501 burnt area products.

All analyses presented below were performed for each of these four grid-cell resolutions, to assess the effect of changing the resolution on the accuracy of the results. The suitability of the distribution for estimating burnt area was assessed at both a grid-cell level and over the whole Brazilian Amazon domain. The exact use of this data set in the overall work presented here is shown in Fig. 3.2.

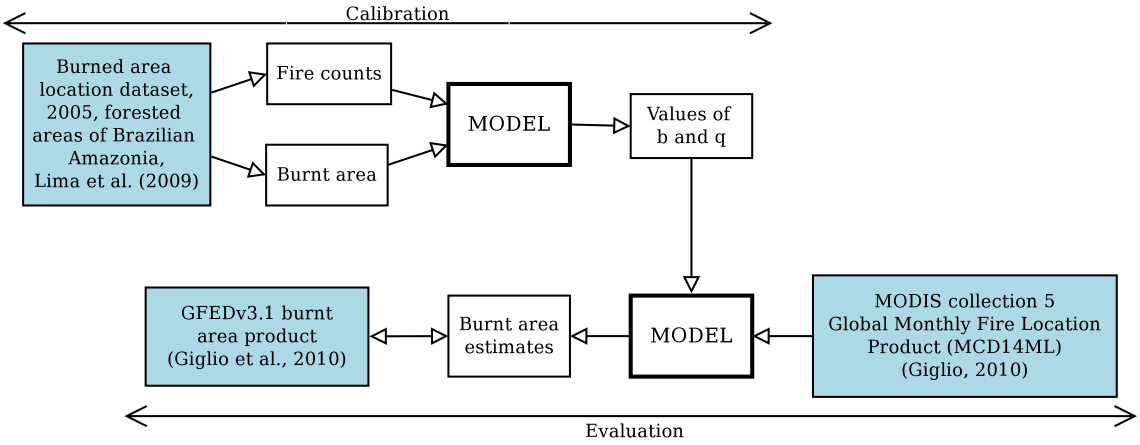

Figure 3.2: Flow diagram detailing the data sets and parameters used in calibrating and evaluating the model.

3.3.2 Representing the fractal properties of fire size distributions

A range of distributions has been used in the literature to describe fire size distributions. The most common is the Pareto distribution, sometimes referred to as the power-law distribution. This states that the probability that fire X is of size A or larger is proportional to A^{-b}, for a constant b. Other studies use variations of this distribution to allow for the fact that fires in many regions show scale invariance only for a particular range of sizes. One of these variations is truncation, i.e. ignoring all fires smaller than a lower threshold and/or larger than

some upper threshold. Although this yields interesting information about the behaviour of fires, it is not useful in the context of this study, since all fires must be considered if an accurate prediction of burnt area is to be produced. Small fires contribute greatly to total burnt area: Randerson et al. (2012) found that accounting for small fires resulted in a 35% increase in total global burnt area estimates. Another variation prevalent in the literature is a piecewise distribution, where the parameters of the Pareto distribution are distinct for two or more ranges of fire sizes. Although possible, this would require the estimation of many more parameters, and hence could have a large effect on the accuracy of the model. The other commonly used option is to modify the Pareto distribution to include a tapering function (e.g. Schoenberg et al., 2003). However, this generally only allows for the distribution to tail off as the fires become extremely large: it does not take into account the fact that there may be a tail at the low end of the distribution as well.

Based on the burn scar data we are using to calibrate the model, we use the following distribution:

$$n_{X \geq A} = \alpha A^{-b} \exp\left(-\frac{1}{A} - \frac{A}{\theta}\right), \tag{3.1}$$

where $n_{X \geq A}$ is the number of fires of size A or larger, and α, b and θ are grid-cell-dependent parameters. θ is known as the tapering parameter. The -1/A term represents the small-fire taper. Although an additional parameter could be introduced into this term, this tapering is most likely a result of limitations in the detection of small fires, and hence should remain constant. The estimate of

such a parameter for the whole region is 0.99 ± 0.075 (using least-squares regression, as described below), so the use of the number 1 in this term is reasonable. For ease of use, Eq. (3.1) can be rewritten by taking the logarithm of both sides, resulting in Eq. (3.2):

$$\log\left(n_{X\geq A}\right) = \log(\alpha) - b\log(A) - \frac{1}{A} - \frac{A}{\theta}. \tag{3.2}$$

By setting A = 1 and solving Eq. (3.2) for α, we get log(α) = log(n_f) +1 + 1/θ. Substituting this back into Eqs. (3.1) and (3.2), they can be rewritten as Eqs. (3.3) and (3.4), respectively:

$$n_{X\geq A} = n_f A^{-b} \exp\left(1 - \frac{1}{A} - \frac{(1-A)}{\theta}\right), \tag{3.3}$$

$$\log\left(n_{X\geq A}\right) = \log\left(n_f\right) - b\log(A) + 1 - \frac{1}{A} - \frac{(1-A)}{\theta}. \tag{3.4}$$

We check that this distribution fits the data by estimating parameters b and θ using least-squares regression on Eq. (3.4), and comparing the resulting fitted cumulative frequencies to the data points. This is not an optimal fitting method, since a condition of least-squares optimization is that the errors are independent of one another. This is obviously not the case when cumulative frequencies are used. However, alternative methods such as maximum likelihood regression or the method of moments are not suitable in this case. These methods are commonly used for similar problems in the literature, using logarithmically binned data (e.g. Pueyo, 2007; Pueyo et al., 2010; Moreno et al.,

2011). Binning the data results in the loss of information about extreme fire sizes, hence our reluctance to use this technique in this instance. If the data are used unbinned, we encounter the problem of trying to fit a continuous, monotonically decreasing probability density function to a set of data in which many sizes can take the same frequency and some intermediate fire sizes do not occur at all (this pattern can be seen in the top right plot of Fig. 3.3). Ultimately, this results in a large underestimation of fire frequencies. Least-squares regression, although not a perfect option, provides decent approximations of the parameters.

The estimated cumulative frequencies of each fire size are close to the observed, with very small errors. This can be seen in Fig. 3.3 in the left-hand plots. The frequencies of each fire size can be calculated by differentiating Eq. (3.4) with respect to *A*, and this should give the best estimates of burnt area. Alternatively, burnt area can be calculated directly as the area under the cumulative frequency curve. In order to see whether the true distribution of fire size frequencies can be recreated, however, we round the cumulative frequencies to restrict the frequencies to integer values, and calculate the difference between cumulative frequencies for each consecutive integer value of *A*. This results in a similar frequency distribution to that observed in the data (Fig. 3.3, top right) but with increasing uncertainty as the frequencies decrease (Fig. 3.3, bottom right). The resulting burnt area estimate is only 5% lower than the observed total, and overall there is no evidence to suggest that this distribution does not fit the data.

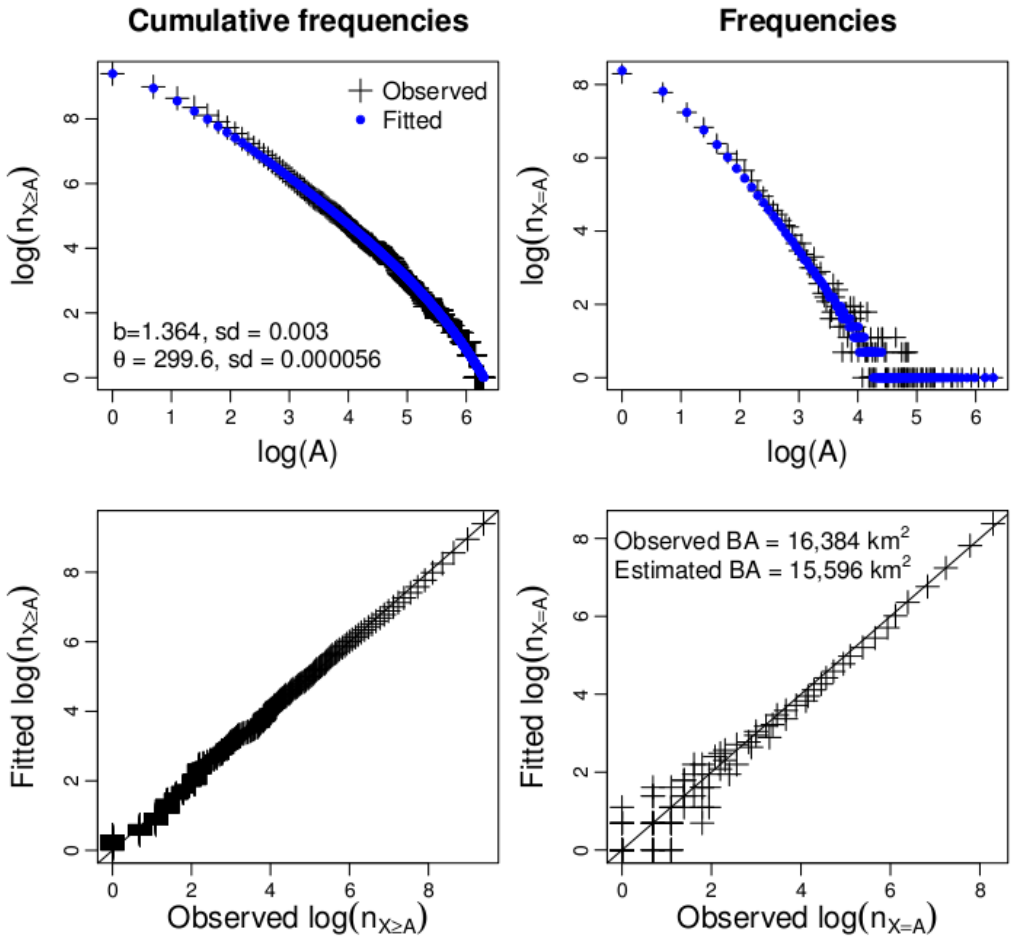

Figure 3.3: Plots of the observed (black) and fitted (blue) cumulative frequency distribution (top left) and non-cumulative frequency distribution (top right), with the corresponding plots fitted against observed values (with 1:1 lines, bottom row). Logarithmic axes are used for all plots. The burnt area values given in the bottom-right plot are the total observed and estimated burnt area over the whole study region.

3.3.3 Estimating the distribution parameters

In order for this model to be of use, there needs to be a simple way to estimate parameters *b* and θ, preferably without introducing other input variables. To do so, we first of all approximate these parameters using least-squares regression for every grid cell, as well as a range of resolutions: 0.5º x 0.5º, 1º x 1º, 2º x 2º and 4º x 4º. This allows us to see patterns in the parameters, and determine

whether either of them is resolution-dependent.

3.3.3.1. Estimating gradient *b*

The parameter *b* in the distribution represents the underlying rate at which the cumulative frequencies of each consecutive fire size decrease. There is an extra adjustment to this in the form of the exponential component of Eq. (3.3).

By plotting the fitted values of *b* for each grid cell against a range of other variables, such as n_f, θ, or max(*A*) (the largest observed burn scar in each cell), there is a consistent lack of correlation. We have not included all of the plots mentioned above, as this would be somewhat redundant, due to the similar patterns of each one: only *b* against n_f is shown in Fig. 3.4. This suggests that *b* is approximately constant, and can be estimated by taking the mean value of the observations. Although there is a large amount of variation in *b* when n_f is small, this can be attributed to the difficulties of parameter estimation when the model is fitted to a small number of data points.

There appears to be a slight effect of resolution on the mean value of *b* per grid cell. The coarser the resolution, the larger the value of *b* is. This is further supported by the significantly higher value of *b* obtained when the distribution is fitted to the whole region. However, performing Student *t* tests on the estimates of *b* for each pair of resolutions shows that there is not enough evidence at a 5% significance level to suggest that there is a difference between the means calculated here. This is true even if a one-sided *t* test is used on the estimates of *b* for 0.5º x 0.5º and 4º x 4º, which give the smallest and largest values of *b*, respectively (p-value = 0.2487). The mean of the *b* across these four resolutions is 1.27. The change in the total burnt area

estimates over the study region if a fixed *b* is used instead of the individual *b* per resolution is at most 4%. Hence, it is best for this study to keep *b*=1.27.

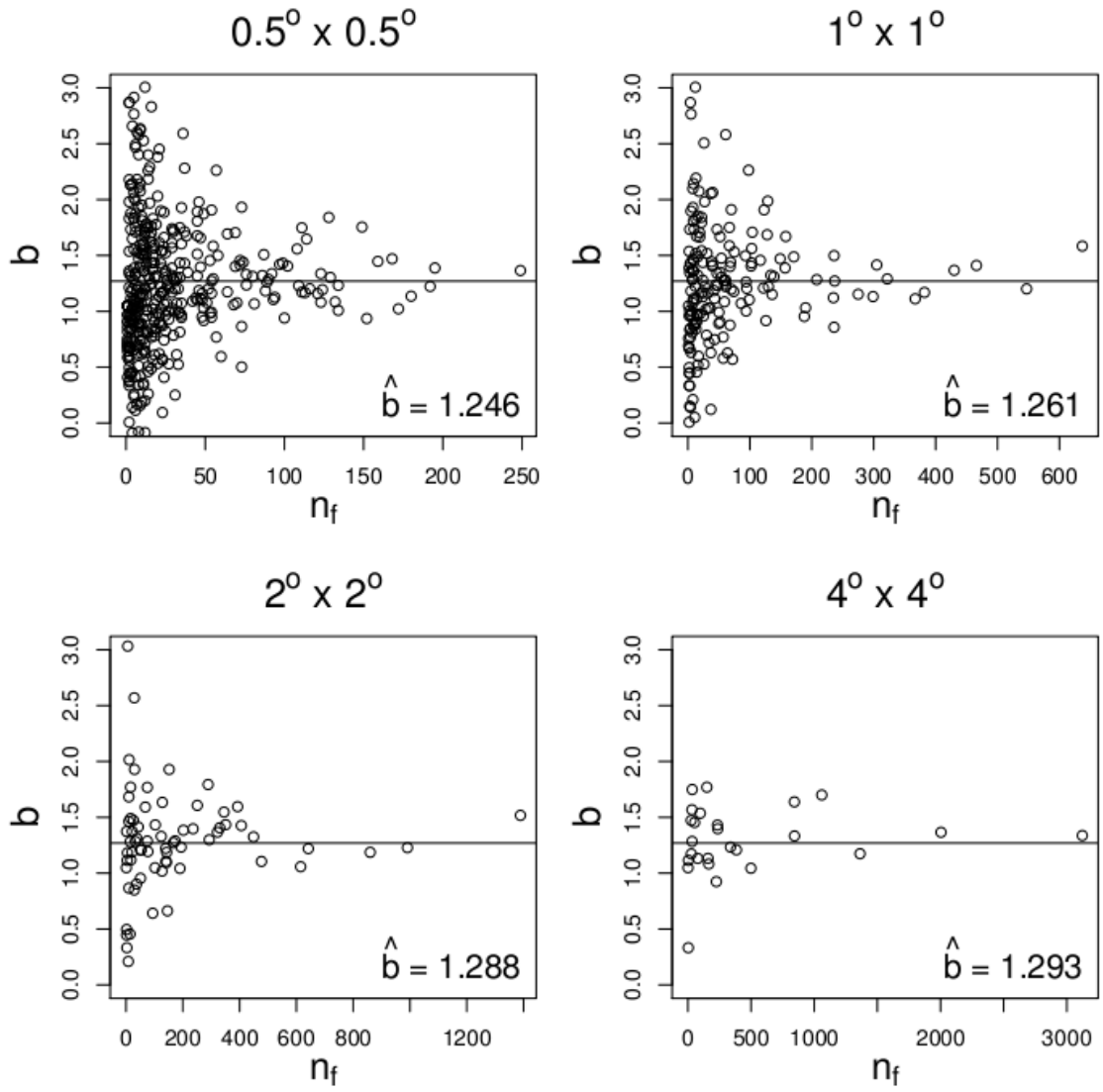

Figure 3.4: Plots of estimated values of parameter *b* against fire counts, n_f, for all four resolutions. The solid horizontal lines are at *b*=*b* for the values of *b* shown on each plot.

3.3.3.2. Estimating tapering parameter θ

We assume that there is always one single largest fire in each grid cell, so $n_{X \geq \max(A)} = 1$. By setting $A = \max(A)$ in Eq. (3.4) and rearranging, we get the

following approximation of θ:

$$\hat{\theta} = \frac{\max(A) - 1}{\log(n_f) + 1 - \frac{1}{\max(A)} - b \log(\max(A))} \quad (3.5)$$

Since $\hat{b}$ = 1.27 from Section 3.3.3.1 and n_f is an input variable, if a method of estimating max(*A*) is found, then θ can be calculated directly from Eq. (3.5).

The maximum size a fire can take in a grid cell is dependent on many factors. From a purely statistical viewpoint, the more fires in a cell, the larger max(*A*) is likely to be. The value of max(*A*) also depends on local climatic and ecological conditions. For example, fragmented fuel or a high fuel moisture content can severely limit fire spread, while high winds and a high litter load encourage fire propagation. Additionally, the largest potential fire size is not necessarily similar to the actual achieved max*(A),* which makes this a difficult value to predict.

The estimate used in this model is simple: it is a log-linear function of fire counts, as described by Eq. (3.6):

$$\log(\max(A)) \approx q \log(n_f) \quad (3.6)$$

This obviously takes the statistical likelihood of large fires given the sample size into account, and restricts max*(A)* to 1 pixel if there is only one fire, which is a reasonable assumption. Also, since fire occurrence is itself dependent on the same climatological and ecological conditions as fire spread, we would expect max(*A*) and n_f to covary. We see a correlation between the logarithms of the

two variables of between 0.73 and 0.85 for the range of resolutions, and this relationship can be observed in Fig. 3.5. While the introduction of additional input variables could potentially improve the estimates of max*(A),* the added complexity of the model and errors present in the input data sets may counteract any potential improvement in the model performance.

The value of *q* is estimated for each resolution: $\hat{q}$ = 0.95, 0.87, 0.81 and 0.78 for 0.5º x 0.5º, 1º x 1º, 2º x 2º and 4º x 4º, respectively. There is a sizeable amount of variation in the data, and hence the errors are relatively large. This may be due, in part, to the use of such a simple relationship between the variables. Particularly for high resolutions, there appears to be a slight decay in the linearity of the relationship as n_f becomes small: the values of max(*A*) seem to flatten out rather than continue decaying (Fig. 3.5). However, the introduction of a more complex relationship is difficult, due to the need for additional prescribed parameters, and hence is not attempted here. The value of $\hat{q}$ is clearly resolution-dependent, decreasing from 0.94 at 0.5º x 0.5º to 0.81 at 4º x 4º. This decrease can be generalized by:

$$\hat{q} = 0.88 - 0.44 \log (A_c) \tag{3.7}$$

where A_c is the size of the grid cell in degrees squared.

By substituting Eq. (3.6) into Eq. (3.5), we obtain a final equation for estimating θ:

$$\hat{\theta} = \frac{n_f^q - 1}{\log(n_f) + 1 - \frac{1}{n_f^q} - b \log (n_f^q)} \tag{3.8}$$

Since q and b are fixed, as n_f becomes large there comes a point at which θ becomes negative. Where this is the case, we prescribe $q = \infty$, so that the tapering term disappears.

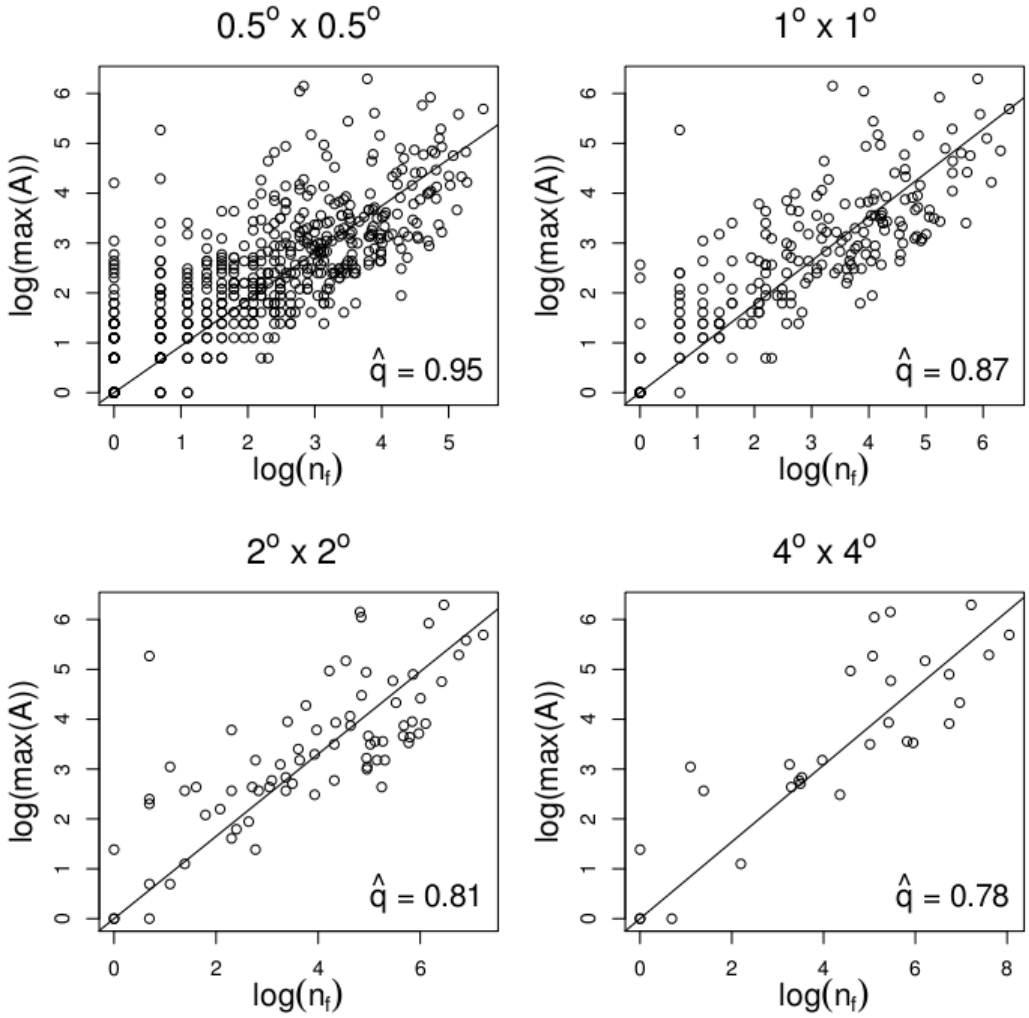

Figure 3.5: Plots of the largest fire per grid cell against fire counts, on logarithmic axes, for four resolutions. The solid lines are straight lines through the origin with gradient $\hat{q}$, as given in the plots.

3.3.3.3. Correcting for data detection resolutions

The parameter estimation methods described above are calibrated to a data set detected at 500 m x 500 m resolution. If another data set is used that has been detected at a different resolution, gradient b will remain the same, but the 1-1/A

+(1-*A*)/θ component of Eqs. (3.3) and (3.4) needs to be scaled inversely proportional to the change in detection resolution: if the data driving the model are detected at 1 km^2 (i.e. grid cells that are 4 times larger than those used to calibrate the model), then this term must be divided by 4 to compensate. The value of max(*A*) would also need to be divided by 4 in this example. It is crucial to note that θ should be estimated from Eq. (3.8) rather than by estimating max(*A*) first and substituting the corrected version of this into Eq. (3.5), or otherwise the correction will be applied twice.

3.3.4 Predictions of burnt area

Once the distribution parameters *b* and θ have been estimated using the above methods, they are substituted back into Eq. (3.3) to obtain estimates of the cumulative frequencies of the calibration data set. No parameter correction is needed in this case. The area burnt can be predicted by summing these cumulative frequencies over the range $A = 1,\ldots,\max(A)$, for the estimated value of max(*A*). Failing to restrict the possible fire sizes to this range negates the previous assumption of there being a single, largest fire per grid cell. It is theoretically possible at this stage to integrate Eq. (3.3) over this range for a more accurate result, but the complexity of the equation makes it an unsuitable method in this case. Additionally, it is necessary to impose an upper limit on burnt area estimate per grid cell, equal to the area of that cell, in order to avoid unrealistic estimates. The area of each grid cell is estimated using the raster package in R (Hijmans, 2013; R Core Team, 2013).

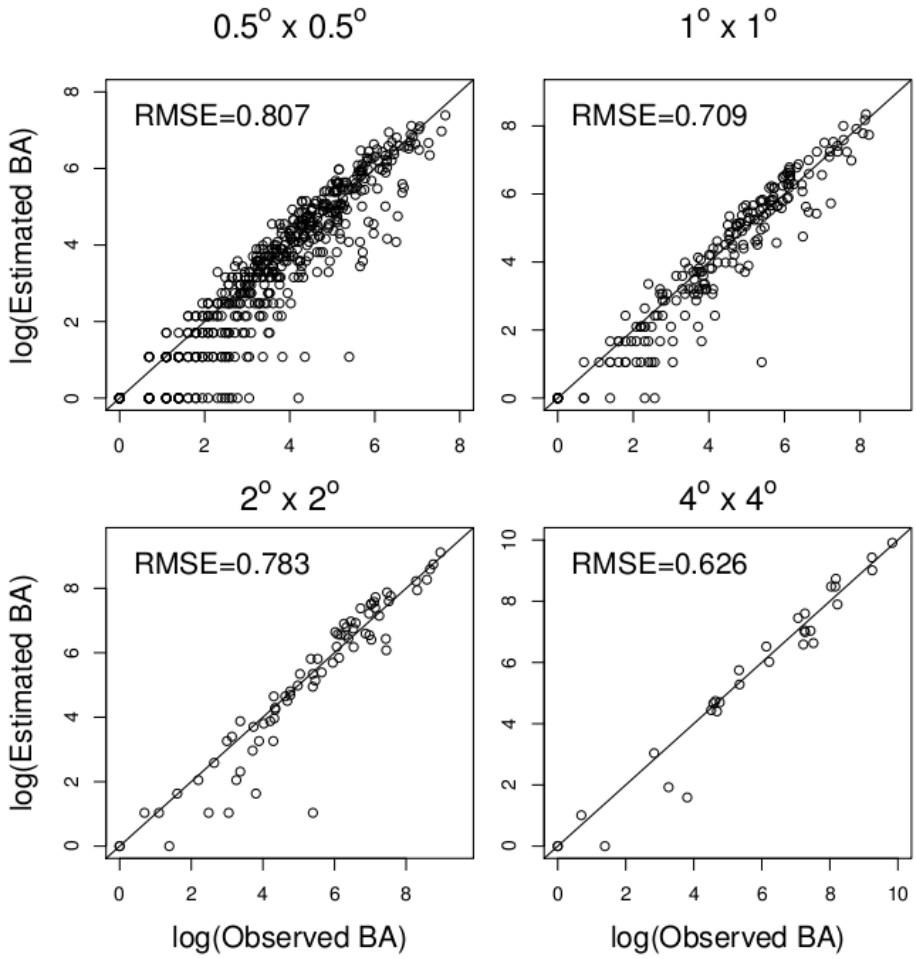

Figure 3.6: Estimates of burnt area in Brazilian Amazonian forested areas, in number of pixels (500 m x 500 m) for a range of resolutions, on a logarithmic scale. The solid line in each plot is the 1:1 line, and the root-mean-square errors are given for each resolution.

The model is capable of predicting burnt area to a reasonably high degree of accuracy, although it is more prone to underestimating burnt area in grid cells with little fire activity. This slight skew can be seen in Fig. 3.6, and is most apparent at finer resolutions. There is a strong link between this underestimation and the underestimation of max*(A)* when using Eq. (3.6): for the range of resolutions studied, an underestimation of max(A) resulted in an underestimation of burnt area in between 87 and 92% of grid cells. The coarse

resolutions generally produce smaller errors, and the root-mean-square-error (RMSE) values decrease as the grid cell size increases. The spatial distributions of the burnt area estimates closely match those of the observations for all resolutions (Fig. 3.7).

The total burnt area over the study region is 65,535 pixels, which equates to just under 16,400 km^2. The total BA estimates for each resolution are presented in Table 3.1, and highlight the effect of the resolution on the final estimates: the larger the grid cells, the larger the overall estimate will be, though none of the estimates are unrealistically far from the observed value.

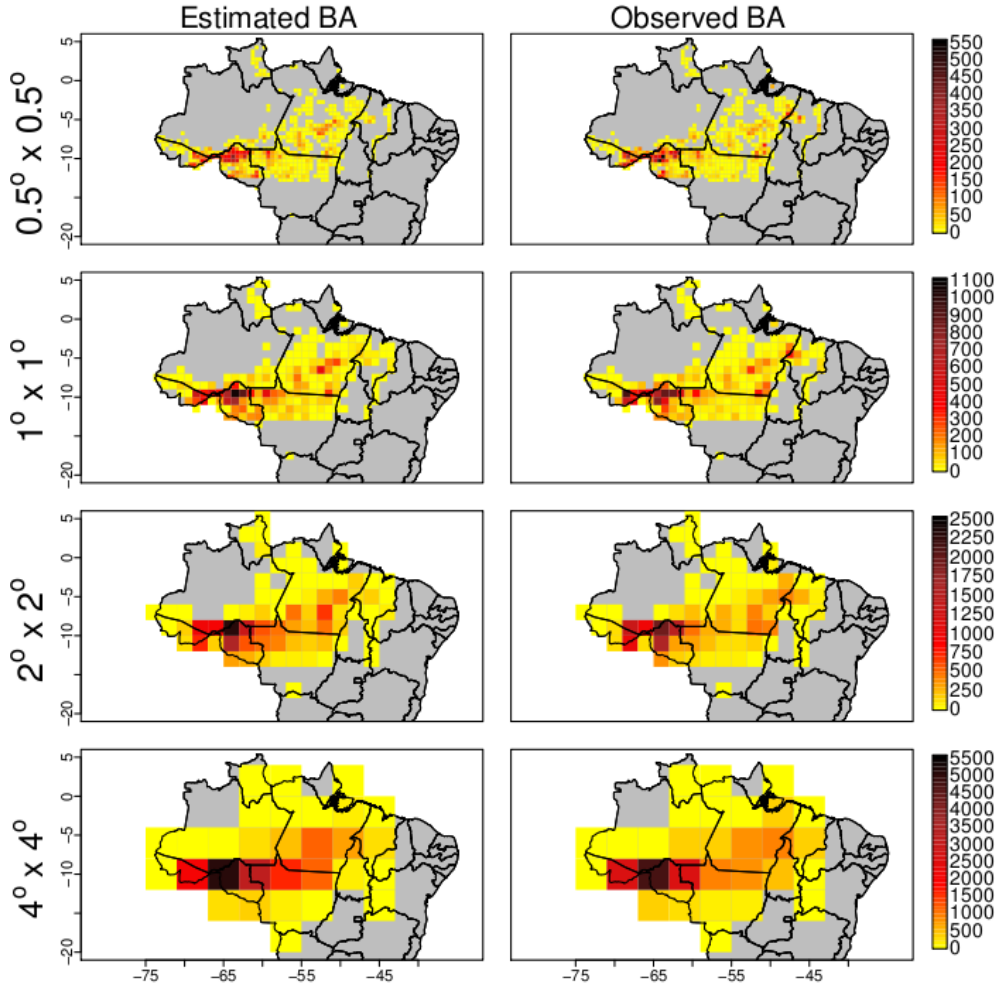

Figure 3.7: Maps of burnt area estimates (left) and observations (right), in km^2, for each resolution.

Table 3.1: Total burnt area estimates over the study region, in pixels and km^2, for each resolution.

Resolution	Total burnt area	
	Pixels	km^2
0.5° x 0.5°	59 039	14 760
1° x 1°	65 019	16 255
2° x 2°	67 794	16 949
4° x 4°	69 880	17 470
Observed	65 535	16 384

3.4 MODEL TESTING

3.4.1 Data

After calibration, the model was tested using the MODIS collection 5 Global Monthly Fire Location Product (MCD14ML) (Giglio, 2010) as input. This data set provides the geographic coordinates of each individual 1 km^2 fire pixel detected by the TERRA and AQUA satellites across the globe for every month between January 2001 and December 2010. For use with our model, only the TERRA observations were used to avoid fires being detected twice. The fire pixels were summed over each 0.5º x 0.5º grid cell and each year from 2001 to 2010. This data set is not an ideal input for the model, since a single fire can be detected multiple times, either spatially or temporally, if it is a large or long-lasting fire. Hence, the true number of fires per grid cell will be lower than the number given by this data set, and the model will overpredict burnt area. However, this is the closest approximation to true fire counts that is currently available and based on observations rather than model output.

The burnt area estimates produced by driving the model with this fire count data were compared to the GFED3.1 burnt area product (Giglio et al.,

2010), in hectares, at its original 0.5º x 0.5º resolution, restricted to the same time frame. We expect the estimates produced by the model to be considerably higher than those given by this data set, since it is known that it under-represents burning in dense forests.

We limited both of these data sets to tropical, forested regions, since the model has been calibrated for this land cover type. To do so, the GLC2000 land cover data set (Bartholomé and Belward, 2005; Global Land Cover 2000 database, 2003) was used to identify the grid cells between 25ºN and 25ºS that were covered by at least 75% forest (classes 1 to 8 in the GLC2000 data set).

Again, a clear description of the exact use of these data sets is shown in Fig. 3.2.

3.4.2 Spatial predictions

We ran the model using the MODIS fire count data for 2005, and compared the resulting burnt area estimates directly to the GFED3.1 burnt area product for the same year. The model produces burnt area estimates that are generally much larger than those given by the GFED3.1 data set for tropical South America. For Africa, Asia and Australia there are patches of overestimation and of underestimation, but no obvious spatial biases (Fig. 3.8, left and middle).

3.4.3 Temporal predictions

Annual burnt area predictions were calculated for every grid cell, for 2001 to 2010. By looking at the mean annual grid-cell burnt area for each continent, we can again see that the model generally overestimates burnt area in South America by quite a considerable amount (Fig. 3.8, top right, solid lines),

whereas the predictions for the other two continents are generally of the same orders of magnitude as the GFED3.1 burnt area product (Fig. 3.8, middle- and bottom-right). For all three regions, the estimates capture the main features of the temporal patterns as identified by the GFED3.1 data. This is especially noticeable for South America, which experiences much more interannual variability than the other two regions. Africa, on the other hand, shows remarkably little interannual variability, despite the mean burnt area per grid cell being roughly 10 times as large as in the other two regions.

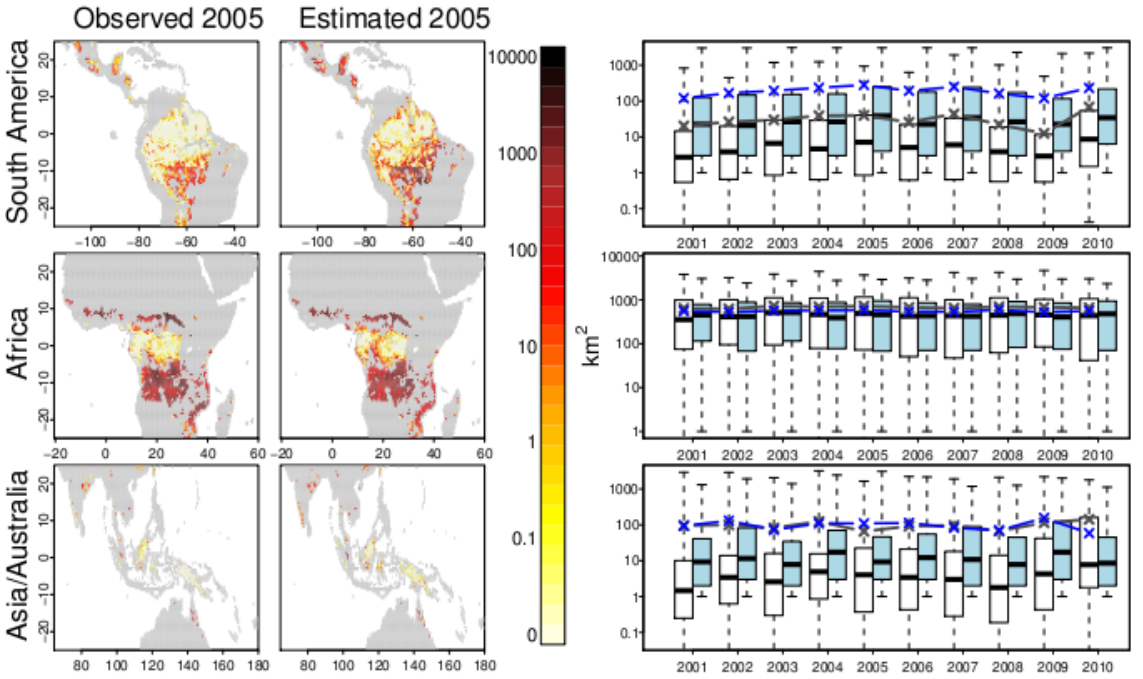

Figure 3.8: Maps of the total observed (left) and estimated (middle) burnt areas for the tropical regions of South America, Africa and Asia/Australia in 2005, in hectares. The corresponding time series for these regions are shown on the right: the box plots illustrate the median burnt area values, interquartile ranges and full ranges of the annual, grid cell observations (white/black) and estimates (blue), and the connected points show the mean annual grid cell values.

By considering the corresponding medians and ranges of the data (Fig. 3.8, right, box plots), we can see that in Australia and Asia, the majority of the

model estimates are considerably higher than the GFED3.1 burnt area values, despite the means being very similar for most years. This suggests that burning in this area is dominated by a few very large fires, which our model is failing to identify. In the other study areas, the differences between the medians and ranges of the model and GFED3.1 burnt area products are reflected by the means.

3.5 DISCUSSION

We have shown that the distribution chosen for our model is capable of recreating the 2005 pattern of burnt area in the Amazonian forests of Brazil, as given by the LSMM calibration data set, as well as producing accurate total burnt area estimates, despite doubts in the literature about the suitability of fractal distributions in describing fire spread. Reed and McKelvey (2002) argue that fractal distributions are too simple and do not make physical sense unless fire growth and fire extinguishing are independent of fire size. Their main reasoning is that small fires are more likely to be extinguished than large fires, either by rain or as a result of a limited amount of fuel, and therefore their spread is not size-independent. Despite this, fractal distributions have proved useful in many studies in the literature, and for this work. Additionally, the added complexity introduced by the tapering terms of the distribution overcomes some of the perceived problems with other possible distributions.

Testing the model with the MODIS active fire and GFED3.1 burnt area products shows us several important things. First, it demonstrates that the model is capable of producing the expected spatial patterns and temporal trends of burning. For South America, the peaks in burning in 2005, 2007 and

2010 (Aragão et al., 2007; Chen et al., 2013; Zeng et al., 2008) are correctly identified. Tropical Africa, Australia and Asia show much less interannual variability, but nonetheless, the model successfully recreates the temporal patterns. This confirms the hypothesis that active fire is sufficient as an input variable, and the introduction of other inputs is not necessary, although it may be useful in future model development, especially if the model were to be extrapolated to different biomes with considerably different climates and vegetation. It could be argued that, since burnt area and active fire are strongly correlated, the intermediate steps of calculating model parameters and estimating the largest fire per grid cell are unnecessary: while it is true that rough estimates of burnt area can be produced as a simple linear or log-linear function of active fire, there is a considerable amount of variation in the data which would not be captured, but is by our model. A simple log-linear relationship can produce estimates with RMSEs that are approximately twice as large as those predicted by the model. Our model may be of less benefit in other regions, such as savannahs, where the correlation between active fires and burnt area is larger (Randerson et al., 2012).

The second interesting point of discussion resulting from Section 3.4 is that of the magnitude of burnt area predictions. We see in Fig. 3.8 that the model produces burnt area estimates that are considerably higher than their GFED3.1 counterparts in South America. This is expected because the burn scar data set used to calibrate the model was specifically designed to include understory fires, which are hard to detect in dense forest. For these reasons we would expect a slight overestimation in the other two regions tested as well, but the burnt area predictions for Asia and Australia are very close to the GFED3.1

values, and in Africa, the model actually underestimates burnt area with respect to GFED3.1, albeit only slightly. Although this may be due in part to more accurate predictions from the GFED3.1 product for these regions, it is likely that the model parameters need to be recalibrated for these regions, as some of the modelling assumptions may not hold outside of Brazilian Amazonia.

Although it would be difficult to calibrate the model to another region without extensive fire size data for the desired region, there are three points at which the distribution is likely to change. First, the underlying distribution gradient, *b*, is assumed to vary based on land cover type, but may also vary due to other local variables, such as mean local temperature or precipitation, or human activity. Second, the relationship between fire counts and the largest fire per grid cell may also vary from region to region, based on the same factors. Third, the small-fire taper currently has a prescribed numerator of 1, but there is no reason why this might not change. If this tail is solely due to issues with the resolution at which fires are detected, as currently presumed, then theoretically this should not be difficult to account for.

The choice of parameter estimation methods was not without its difficulties. We feel that the final options used are capable of producing decent burnt area estimates, and have reasonable physical interpretations. Parameter *b* represents the gradient of the distribution, i.e. the underlying rate of decay of fire sizes. We are assuming that this is predominantly dependent on land cover, and since we are only considering tropical forests, there is no reason to allow *b* to vary. This does not mean that the rate of decay is fixed across all grid cells, since the value of θ can have a large effect on the gradient of the distribution at a given fire size. Hence, whereas *b* represents the general land-cover-

dependent decay of fire size frequencies, θ represents the specific grid cell decay.

As mentioned in Section 3.3.3.2, it is possible that the method for estimating θ could be improved upon by including climatological input variables in the estimation of max(*A*), such as precipitation or temperature. This is something that would be interesting to look into further at a later stage, but is beyond the scope of this study. As it stands, θ takes the effect of climate into account implicitly, since fire counts are heavily influenced by climate, and n_f is used in the prediction of θ. Additionally, if Eq. (3.6) could be modified to be non-linear, therefore removing the slight skew of the data for low values of n_f, the propensity of the model to underestimate small burnt areas might also be reduced.

The purpose of this model is for it to be incorporated into a DGVM. We will be able to use modelled fire counts instead of active fire pixel data as an input, and as a result it should be possible to identify how much of the difference between modelled and observed burnt area seen in Section 3.4 is due to the under-representation of fires in the GFED3.1 product. The model will then also be comparable to existing, process-based fire models: the effect of replacing the existing rate-of-spread equations with this distribution on trace gas emissions and vegetation structure will be easy to quantify.

3.6 CONCLUSIONS

We have shown the main hypothesis presented in the Introduction to be true; it is possible to use the theory of scale invariance to calibrate a burnt area model with only fire counts as input, as well as accurately reproduce the observed

pattern of burn scars in the forests of Brazilian Amazonia in 2005. The model can be extended, with a few modifications, to forests across the tropical latitudes, and fully captures temporal variability in burning. The total, annual burnt area predictions are difficult to compare, due to the lack of a completely suitable input data set. The accuracy and adaptability of the model to other ecosystems and non-tropical regions is something that remains to be tested further.

4. Model intercomparison

4.1 INTRODUCTION

As stated in Chapter 1, the aim of this thesis is to develop empirical models that facilitate the prediction of fire occurrence and spread by minimising the required number of input variables, parameters and calculations, and that improve these estimates in tropical latitudes. These models should work both on their own, and within the framework of an existing fire model, coupled to a dynamic global vegetation model (DGVM). The models developed in Chapters 2 and 3 have been shown to work well as standalone models: they are easy to calculate and require only easily obtainable datasets. In this chapter, the suitability of these parameterisations for use within a DGVM is considered, and the accuracy of the estimates of fire activity resulting from the use of these models, both separately and together, is assessed.

Section 4.2 explains the way in which the new models are incorporated into a fire model, and the way in which this fire model is coupled to a DGVM, including any obstacles that were encountered and the solutions that were found. In Section 4.3, fire count estimates resulting from the new model described in Chapter 2 are compared to predictions from two existing models, and to two different satellite-derive active fire products. Burnt area estimates from all possible combinations of fire count and burnt area parameterisations are compared to each other and to an observational burnt area product in Section 4.4. Finally, the relative merits and limitations of each parameterisation are summarised and discussed in Section 4.5.

4.2 METHODS: THE MODELLING FRAMEWORK

4.2.1 JULES

The Joint UK Land and Environment Simulator (JULES; Best et al., 2011; Clark et al., 2011) is used in this chapter to drive the fire models by providing the necessary climatic and ecological variables. JULES is a community land surface model (LSM) that can either be driven by standard forcing data, or coupled to an atmospheric global circulation model (GCM): for this thesis, it is driven by the data described in Section 4.2.1.2. Its modular structure facilitates the modification of existing modules or the incorporation of new ones. More importantly, fire is one of the main land processes still missing from JULES, so the incorporation of a fire component into the LSM is a beneficial development.

4.2.1.1. Version

JULES version 3.2 was the current version when the work presented in this thesis was started, and is used throughout. The current version 3.4 does not vary significantly from version 3.2. The main changes that have been made improve the functionality of the code and facilitate the use of the model, rather than affecting the science. A fully summary of the changes can be found at http://www.jchmr.org/jules/documentation/user_guide/vn3.4/release_notes/JULES3-4.html (last accessed: 26 September 2014).

4.2.1.2. Driving data

The data used to drive JULES is the WFDEI dataset (WATCH Forcing Data methodology applied to ERA-Interim data; Weedon et al., submitted 2014). This provides two options for precipitation, based on data from the Climatic

Research Institute (CRU), or from the Global Precipitation Climatology Centre (GPCC). For consistency with the precipitation data used to calibrate the potential fire index in Chapter 2, the CRU option is used. The WFDEI data was regridded by Eleanor Burke (Met Office) from 0.5° x 0.5° to 2° x 2°, for 1980 to 2012 at a 3-hour timestep.

4.2.1.3. Switches and settings

JULES is run with all switches set to their defaults, with a few important exceptions: the vegetation phenology model is switched on, as is the dynamic vegetation model (TRIFFID) in equilibrium. This allows local fuel loading to vary, which influences the spread of fires. Vegetation competition is supressed. An additional switch for fire modelling is introduced.

4.2.2 SPITFIRE and the LPX fire model

The SPITFIRE model (Thonicke et al., 2010) is a modular, process-based fire model. As one of the more recently-developed fire models, it has considerable advantages over some of the alternatives: it allows fuel distribution to influence fuel moisture, it uses the full Rothermel equations for the rate of fire spread rather than a simplified version, and it considers fuel characteristics specific to each plant functional type (PFT). Moreover, its structure makes it easy to add the new models developed in this thesis as alternatives to the existing parameterisations.

The fire modelling component of the LPX-DGVM (henceforth referred to as “the LPX fire model”) developed in Prentice et al. (2011) is a later version of SPITFIRE. The main difference between the models is that LPX does not

account for anthropogenic ignitions. The authors claim that in many ecosystems, the natural fire regime is preempted rather than augmented by human-caused fires, and thus lightning ignitions capture the main features of the global fire regime. Ecosystems that are not naturally fire-prone, such as tropical moist forests, are the main exceptions to this rule, making this model perhaps unsuitable for tropical fire modelling: however, it provides a good point of reference to which new fire parameterisations can be compared.

The other significant difference between the LPX fire model and SPITFIRE is the calculation of fire danger. The estimate of the relative moisture content of fuel has been modified to allow different drying rates for each fuel class, and an additional factor adjusting the probability of an ignition event becoming a fire based on the monthly fraction of wet days is introduced. This latter term is omitted from the code, since its accuracy is dubious, according to the discussion of Kelley et al. (2014). This should not have a large effect on the fire danger estimates, since this factor is close to one in most instances.

Since LPX makes use of the SPITFIRE framework and most of its equations, it is added to the SPITFIRE code as an option, and provides an additional set of outputs to which new models can be compared.

Existing code for SPITFIRE was written for the LPJ-DGVM (Sitch et al., 2003; Gerten et al., 2004), but has undergone many modifications since its implementation, and is no longer consistent with the Thonicke et al. (2010) model description. It would also require a significant amount of recoding to make it compatible with JULES. Therefore, the neatest approach for incorporating SPITFIRE into JULES was to recode the model directly from the literature. I did the majority of the recoding myself, with the guidance and help of

Richard Gilham (Met Office), and some contribution from Ioannis Bistinas (University of Lisbon).

SPITFIRE has only been partially coupled to JULES as a diagnostic model. This means that JULES model variables are used as inputs to SPITFIRE, but no feedback from SPITFIRE into JULES has been included at this stage. Although a full coupling is possible and would certainly be beneficial in the future, it is not necessary for the work presented in this thesis, and is hindered by some of the problems highlighted in the remainder of this chapter.

The majority of the SPITFIRE model is coded exactly as described in Thonicke et al. (2010). However, there are a few parameters and variables that are missing or require adjustment to enable the incorporation of SPITFIRE into JULES. All instances where the code differs from the model description are described below.

4.2.2.1. Ancillary data

Lightning flash data are given by the High Resolution Monthly Climatology of lightning flashes from the Lightning Imaging Sensor-Optical Transient Detector (LIS/OTD) produced by the Global Hydrology Resource Center (GHRC) (Cecil et al., 2014). This data set is a more up-to-date version of that used by Thonicke et al. (2010). Mean monthly lightning flashes are given for each grid cell.

4.2.2.2. Input data from JULES

Most of the input variables needed to run SPITFIRE can be obtained directly from JULES. These include temperature, relative humidity, air pressure,

precipitation, wind speed and local canopy height per plant functional type (PFT).

The only variable that needs to be explicitly calculated from existing JULES variables is the quantity of each fuel class present per grid cell. This is estimated using JULES modelled values of litter and vegetation carbon. The former is attributed entirely to the 1-hr fuel class (leaves and twigs), along with 4.5% of the vegetation carbon. The remaining vegetation carbon is distributed between the 10-hr (small branches, 7.5%), 100-hr (large branches, 21%) and 1000-hr (trunks and boles, 67%) fuel classes (Thonicke et al., 2010). The resulting estimates are converted from carbon to biomass by dividing them by 0.47: this represents the expected proportion of carbon in biomass, and is based on the 2006 IPCC guidelines for national greenhouse gas inventories (IPCC, 2006).

SPITFIRE requires fuel to be broken down into live and dead biomass, since the model distinguishes between surface fires and crown burning, and the consumption of dead fuel differs considerably from live fuel consumption. However, there is limited information about dead fuel within JULES, let alone dead fuel per PFT and per fuel class. Hence, for the calculation of the daily fuel moisture for surface fires, proxies for dead fuel are used. The 1-hr, 10-hr and 100-hr dead fuel quantities are made up of the corresponding fuel classes from the grass and shrub PFTs, and the litter load from JULES is added to the 1-hr dead fuel. For all remaining calculations, the total fuel load per grid cell is used.

4.2.2.3. Conversion of PFT-dependent parameters

The JULES plant functional types in this version do not match up with those

used in SPITFIRE. The SPITFIRE PFTs are therefore grouped to correspond to JULES PFTs and averaged across each group. The groupings are shown in Table 4.1. All of the PFT-dependent parameters given in Table 1 of Thonicke et al. (2010) are averaged over the respective SPITFIRE PFTs to produce appropriate values for the JULES PFTs. These parameters are fuel bulk density, scorch height, parameters for the calculation of bark thickness and crown damage, and trace gas emission factors.

Table 4.1: Grouping of SPITFIRE PFTs to correspond to existing JULES PFTs.

JULES PFT	Contributing SPITFIRE PFT(s)
Broadleaved trees	Tropical broadleaved evergreen
	Tropical broadleaved raingreen
	Temperate broadleaved evergreen
Needleleaved trees	Temperate needleleaved evergreen
	Boreal needleleaved evergreen
Shrub	Temperate broadleaved summergreen
	Boreal summergreen
C3 grasses	C3 grasses
C4 grasses	C4 grasses

4.2.2.4. Grid cell area calculation

The size of each grid cell in hectares is required to convert the predicted area burnt per hectare and per day into an estimate of total grid-cell burnt area. No explicit calculation is given for this in Thonicke et al. (2010), since this information is already present within the LPJ DGVM, but this is not available in JULES.

The great circle distance between two sets of geographic co-ordinates is

calculated using the Haversine formula (Sinnott, 1984). This distance, d, is defined in Eq. 4.1, where r is the radius of the earth, in km (in JULES, $r = 6371.229$ km), and the two coordinates have co-ordinates (lon_1, lat_1) and (lon_2, lat_2).

$$d = 2r \arcsin\left(\sqrt{\sin^2\left(\frac{lat_2 - lat_1}{2}\right) + \cos(lat_1)\cos(lat_2)\sin^2\left(\frac{lon_2 - lon_1}{2}\right)}\right) \quad \textbf{(4.1)}$$

For a grid cell, the co-ordinates (lon_1, lat_1), (lon_1, lat_2), (lon_2, lat_2) and (lon_2, lat_1) represent the south-west, north-west, north-east and south-east corners, respectively.

The height of a grid cell is only affected by latitude. By setting $lon_2 - lon_1 = 0$, Eq. 4.1 can be simplified to calculate the height, h, as in Eq. 4.2.

$$\begin{aligned} h &= 2r \arcsin\left(\sqrt{\sin^2\left(\frac{lat_2 - lat_1}{2}\right)}\right) \\ &= 2r\left(\frac{lat_2 - lat_1}{2}\right) \\ &= r\,(lat_2 - lat_1) \end{aligned} \quad \textbf{(4.2)}$$

The width, w, of a grid cell is affected by both latitude and longitude, and hence must be calculated at both lat_1 and lat_2 using Eq. 4.3: the average width, $\overline{w}$, is then used to calculate the grid cell area.

$$w = 2r \arcsin\left(\cos^2(lat)\sin^2\left(\frac{lon_2 - lon_1}{2}\right)\right) \quad \textbf{(4.3)}$$

The grid cell area is the product of h and $\overline{w}$.

4.2.2.5. Fuel threshold

Fire is considered to be impossible in SPITFIRE if there is no fuel available. The existence of any fuel, however little, is deemed sufficient for fire to occur. Although the relative quantities of each fuel class are included in the calculation of fire danger, no consideration is made of how much fuel in total is available to burn. When run using JULES, this results in estimates of extremely high fire danger in desert regions, most notably the Sahara desert. This threshold has been increased from 0 g C m^{-2} to 10 g C m^{-2}. This is sufficient for masking out areas in which very small quantities of fuel are simulated.

The LPX fire model includes a lower fuel threshold of 90 g C m^{-2}, below which fire is deemed impossible. This appears to be too high, perhaps due to differences between LPJ and JULES: too many regions are masked out as a result. Hence, this threshold is changed to 10 g C m^{-2}, to conform with the fuel threshold chosen for use with JULES-SPITFIRE.

4.2.2.6. Moisture of extinction

No value is given in the documentation of either SPITFIRE of the LPX fire model for the moisture of extinction, m_e, the moisture threshold above which fire is assumed to be impossible. Values in the literature range from 0.2 for woody vegetation and 0.3 for herbaceous vegetation (Thonicke et al., 2001; Venevsky et al., 2002), to 0.69 (Li et al., 2012; Li et al., 2013). The majority of literature values are towards the lower end of this range. Personal communication with Colin Prentice (Imperial College London), a co-author of SPITFIRE, resulted in a suggestion of setting m_e to 0.3. The suitability of this value can be tested by running JULES-SPITFIRE with this value for 1982 to 1999, and comparing the

resulting mean annual fire danger index (FDI) to Fig. 3a in Thonicke et al. (2010). To facilitate comparison, the colours of the maps have been matched as closely as possible, and combined to make Fig. 4.1.

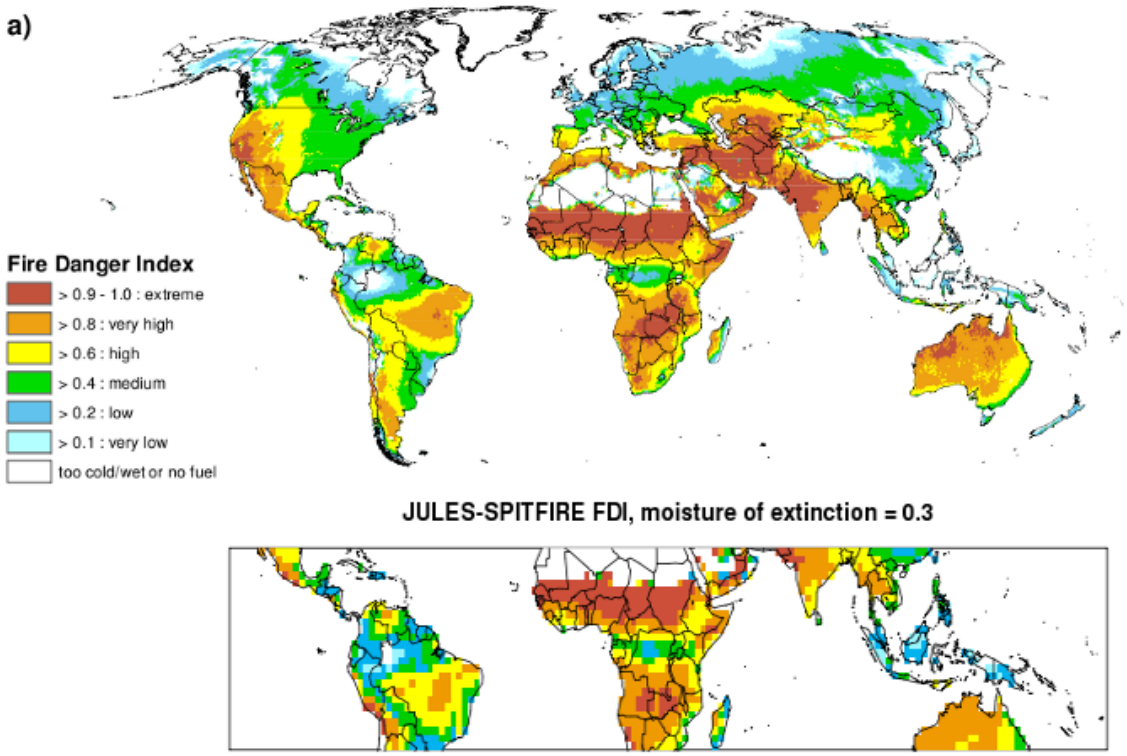

Figure 4.1: Mean annual values of the SPITFIRE fire danger index, as shown in Fig. 3a of Thonicke et al. (2010) (top, full globe), and as calculated using JULES-SPITFIRE (bottom, restricted to tropical latitudes).

The mean annual FDI predictions can only be compared visually at this point. The spatial distributions of fire danger appear to be consistent with one another in most areas, although there are a few slight differences. These could be caused by differences between JULES and LPJ, the adapted fuel bulk density parameters used to calculate litter moisture, or the choice of m_e. However, the two sets of values are similar enough to suggest that 0.3 is a

suitable estimate of the value of m_e.

4.2.2.7. Propensity of humans to ignite fires

A key set of parameters missing from Thonicke et al. (2010) are the region-specific values of $a(N_D)$, which represent the propensity of humans to cause ignition events. These values are described as estimates derived for a series of regions, and subsequently extrapolated across similar ecosystems. There is no obvious way to reproduce this set of parameter values, especially since all but one of the datasets used to produce these estimates are unpublished, and no explanation of the extrapolation method is given. Obtaining these values from the existing code or the authors of SPITFIRE has not been possible, since the later developments of the model, namely the LPX fire model, no longer use this parameter.

One option for dealing with this would be to set $a(N_D)$ as a single, constant parameter across the whole study region. It is theoretically possible to work backwards from observed fire count data to estimate this value, but the accuracy would be dubious, as best. Keeping this parameter constant is bound to result in a loss of accuracy throughout the fire modelling process: since humans are the main causes of tropical fires. The magnitude of the effect of this parameter on the model accuracy is impossible to quantify without further information, but likely to be large.

There is therefore no realistic way to make use of the SPITFIRE calculations of human ignitions. The only option is to remove human ignitions entirely, and rely solely on lightning ignitions, as is done in LPX. However, the fire count estimates are likely to be lower than the true values for the tropics,

where the majority of fires are anthropogenic in origin, even if the natural fire regime does pre-empt anthropogenic fires, as suggested by Prentice et al. (2011).

Removing human ignitions from SPITFIRE results not only in a drastic change in the magnitude of fire count estimates in comparison to Fig. 3b in Thonicke et al. (2010), but also in their spatial distribution (Fig. 4.2). The exact magnitude of the differences is impossible to quantify visually, especially owing to the non-linear scale used to colour the maps. However, it can be clearly seen that SPITFIRE coupled to JULES with no anthropogenic fires produces generally lower estimates of fire counts than the original SPITFIRE model. This is especially apparent in the areas of normally very high fire activity, such as the Sahel, the savannah region below the Congo, eastern Brazil, India and S.E. Asia. Interestingly, given the reduction in ignition sources, more fires are predicted in Australia than originally. Since fire counts are calculated as a function of lightning flashes and the FDI, this must be due to differences in the lightning data, since it is certainly not a result of the new FDI values, which are lower than those given in Thonicke et al. (2010).

Despite this, however, the resulting fire count estimates are still higher than those produced using the LPX fire model, driven by JULES. The only difference between the two models at this stage is the calculation of fuel moisture, suggesting that fuel in the LPX model is modelled as drying more slowly than in SPITFIRE.

4.2.2.8. Surface-area-to-volume ratios

The surface-area-to-volume ratios, σ_i, for each fuel class i, needed for the

calculation of the overall surface-area-to-volume ratio of the available fuel and hence the spread of fires, are not given in Thonicke et al. (2010). From the existing SPTIFIRE code in the LPJ-DGVM, it appears that these should be equal to 80.66, 3.58 and 0.98 for livegrass and the 1hr, 10hr and 100hr fuel classes, respectively. For the 1000hr fuel class, a value of 0.5 is used, although this is commented in the code as “highly subjective”.

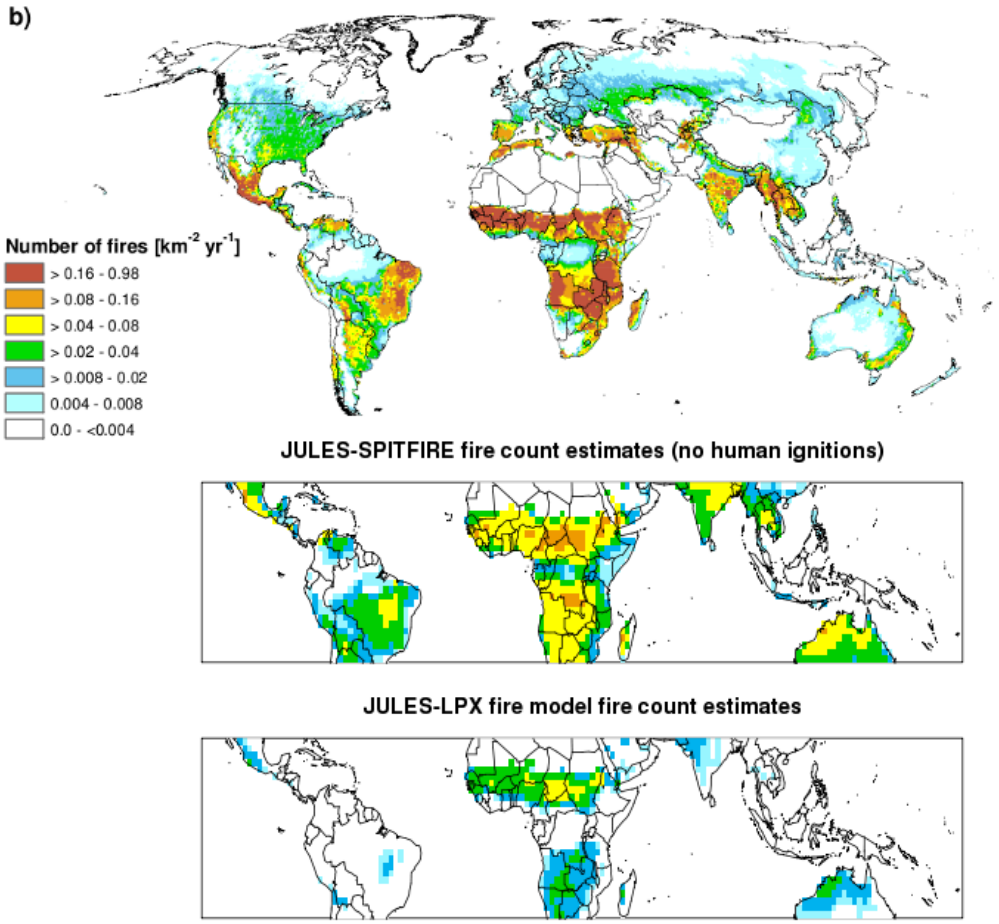

Figure 4.2: Mean annual values of the SPITFIRE fire count estimates, as shown in Fig. 3b of Thonicke et al. (2010) (top, full globe), and as calculated using JULES-SPITFIRE without anthropogenic fires (middle, restricted to tropical latitudes) and the LPX fire model (bottom, tropical latitudes).

4.2.2.9. Fuel bulk density weighting factors

The fuel bulk density calculation that is used in the estimation of the rate of fire spread is described by Thonicke et al. (2010) as having “weighting factors for 10- and 100-h fuel classes”. However, although the 10-hr fuel load is multiplied by 0.2, the 100-hr fuel is not modified in any way. This suggests that a weighting factor should be present, but was accidentally omitted: this is further confirmed by burnt area estimates that are far too low (< 6.5% of a grid cell in a year, in comparison to up to 95% in the original SPITFIRE output), even after consideration of the lower fire count estimates resulting from the removal of human ignitions. The weighting factors supposedly originate from Brown (1981), but could not be identified in this publication. Hence, a value of 0.05 is used as the 100-hr weighting factor. This results in burnt area estimates that seem sensible. However, this choice is bound to impact the accuracy of the burnt area predictions produced by either SPITFIRE or the LPX fire model when run in JULES.

4.2.2.10. Calculation of fuel consumption and trace gas emissions

The equation given in Thonicke et al. (2010) for the calculation of trace gas emissions resulting from fires appears at first glance to be simple: it is the product of biomass burnt and the trace gas-specific emission factor, with a simple unit conversion factor applied. Biomass burnt is described as “the sum of dead and live fuel consumption as the result of surface fire and crown scorching”. However, as mentioned previously, this is problematic due to the lack of distinction between dead and live fuel. Using the proxies for dead fuel described in Section 4.2.2.2 does not work in this instance, since it detracts

from the live fuel load, and hence all resulting emission estimates are considerably too low.

In addition to this, there appears to be a slight issue with the equations given for dead fuel consumption. These are piecewise linear and use rounded values for the intercepts and gradients of each section. This results in disjointed functions that exceed 1 in some circumstances, which makes no physical sense, as it is impossible for more than 100% of the available fuel to burn.

Owing to the incompatibility of this part of the SPITFIRE model with the JULES framework, the fuel consumption and trace gas emission estimates are not used. This is one of the main reasons for not fully coupling SPITFIRE to JULES, as mentioned previously: the feedbacks to the JULES vegetation would be inaccurate.

4.2.3 Study area and time period

The models are run on all land points in the tropics, generally defined as all latitudes between the Tropic of Cancer (23° 27’ N) and the Tropic of Capricorn (23° 27′ S) (e.g. Latrubesse et al., 2005). The limits of 25°N and 25°S are used for compatibility with the 2° x 2° resolution of the JULES driving data (Section 4.2.1.2).

The models are run from 1980 to 2012, the full time period for which the WFDEI driving data is available. The time periods used for comparing the models to observational datasets depends on the temporal availability of this data.

4.2.4 Incorporation of new parameterisations into JULES-SPITFIRE

The new models developed in Chapters 2 and 3 are designed to be compatible with the framework of SPITFIRE and the inputs available from JULES. Switches are added to the JULES code to allow the user to choose between the different fire count and burnt area parameterisations. The new models can be called completely independently from SPITFIRE, but can also be used in conjunction with the SPITFIRE or LPX fire count or burnt area calculations.

The GLC2000 dataset and the map of parameters for converting the potential fire index into estimates of fire counts are read in as ancillary datasets.

4.2.5 Model options

After incorporating the new models into the SPITFIRE framework, there are three options for predicting fire counts, namely:

1) the SPITFIRE fire count parameterisation, without human ignitions, as described above;
2) the LPX fire count parameterisation – different fuel drying calculation to SPITFIRE, and hence different fire danger estimates;
3) the newly-developed empirical fire count model, described in Chapter 2, henceforth referred to as the PFI fire count model.

There are additionally two options for predicting burnt area once fire counts have been estimated:

i) the SPITFIRE rate of spread and burnt area parameterisation (the same is used in the LPX fire model)
ii) the new fractal burnt area model developed in Chapter 3, referred to as the empirical BA model.

Hence, there are a total of six possible combinations of fire count and burnt area parameterisations that can be used when running JULES.

4.3 RESULTS: FIRE COUNT ESTIMATES

As stated above, JULES is run with three alternative fire count parameterisations. The predictions of fire activity resulting from each of these models are compared to two active fire satellite products: the MODIS MCD14ML dataset, which was used to calibrate the new fire count model, and the ATSR ESR2 World Fire Atlas from July 1996 to March 2012 (Along Track Sensing Radiometer / European Remote Sensing Satellite 2; Arino et al., 2012).

4.3.1 Spatial estimates of fire counts

It is difficult to quantify the accuracy of the spatial distributions of the mean annual fire count estimates, since the two sets of satellite observations do not fully agree with one another. Spatially, there is a moderately strong correlation of 0.437 between the two ($df = 991$, $p < 2.2 \times 10^{-16}$), but ideally this would be much higher. The major discrepancy comes from the values for Africa: these show a correlation of only 0.41 ($df = 514$, $p < 2.2 \times 10^{-16}$), in comparison to correlations of 0.886 in South America ($df = 263$, $p < 2.2 \times 10^{-16}$), 0.862 in Australia ($df = 77$, $p < 2.2 \times 10^{-16}$) and 0.777 for India and South-East Asia ($df = 89$, $p < 2.2 \times 10^{-16}$).

An initial visual comparison of the mean annual fire counts per grid cell as estimated by each of the models with the satellite products shows that the PFI-based fire count estimates have a better spatial distribution than the LPX fire parameterisation or the SPITFIRE model (Fig. 4.3), although SPITFIRE is

missing the human ignitions equation, which has some effect on its accuracy. This has been shown already in Fig. 4.2 and discussed in Section 4.2.2.7. The PFI-based estimates not only capture the regions of high fire activity, such as the Sahel, sub-congolean Africa, Thailand, and the northern tip of Australia, but also the areas in which fire is not particularly prevalent, including India, the Congo and the remote central parts of the Amazon.

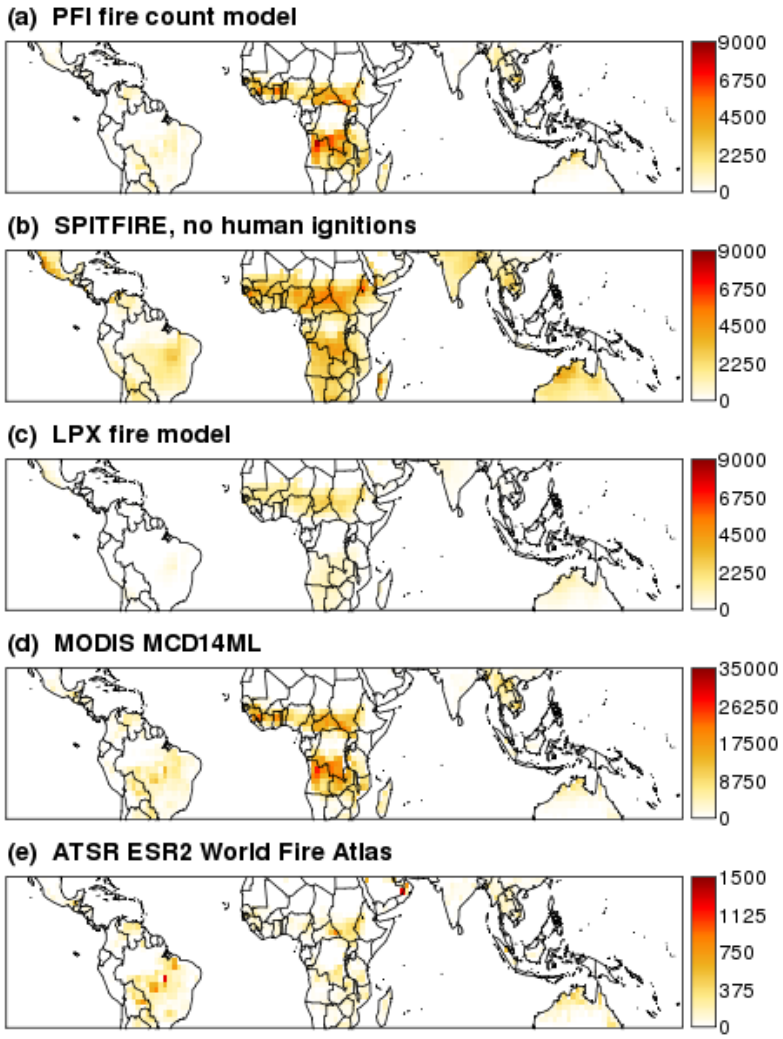

Figure 4.3: Maps of fire count estimates from JULES, using (a) fire counts derived from the PFI using the δ_i adjustment, (b) SPITFIRE, without human ignitions, and (c) the LPX fire parameterisation. For comparison, maps of satellite hot pixel detections from (d) the MODIS MCD14ML dataset and (e) the ATSR ESM2 World Fire Atlas are also shown. Note that although the same scale is used for each set of estimates (a – c), different scales are used for the satellite products (d – e).

Table 4.2: Spatial correlations between the mean annual grid cell estimates of fire counts from three fire parameterisations, and the satellite-derived fire count products MODIS MCD14ML and ATSR ESM2 World Fire Atlas. The parameterisations tested are SPITFIRE without human ignitions, the LPX fire model, and the new PFI-based fire count estimation method. The degrees of freedom for all of the correlations is 991.

	MODIS MCD14ML		**ATSR ESM2 World Fire Atlas**	
	r	**p-value**	**r**	**p-value**
SPITFIRE, no human ignitions	0.593	2.2×10^{-16}	0.241	1.2×10^{-14}
LPX fire model	0.275	2.2×10^{-16}	0.072	0.023
PFI fire count model	0.955	2.2×10^{-16}	0.326	2.2×10^{-16}

This visual assessment is further confirmed by the Pearson's correlation coefficients between the sets of estimates shown in Fig. 4.3, given in Table 4.2. The fire count estimates from the two existing models, SPITFIRE and the LPX fire model, both correlate positively with MODIS MCD14ML (r = 0.593 and 0.275, respectively). Their correlations with the ATSR fire product are worse (r = 0.241 and 0.072). The PFI-based fire count estimates also do not correlate particularly strongly with the ATSR product (r = 0.326), but this is nonetheless considerably better than the other models, and with the MODIS MCD14ML product, a correlation of over 0.95 is observed. Such a high correlation is partially expected, given that this dataset was used to calibrate the model, but it confirms that the effect of keeping ignitions constant in time is minimal at this timescale. Additionally, this correlation is significantly higher than the spatial correlation of 0.661 between the raw PFI estimates and MODIS fire detections (Table 2.3), which suggests that such an adjustment from the PFI to fire counts

is both necessary and beneficial.

4.3.2 Temporal estimates of fire counts

To test the temporal accuracy of the various model predictions of fire counts, the correlations between the monthly estimates and satellite products are calculated for each grid cell. This removes the effect of the spatial distribution of the estimates: if time series of the mean fire counts estimates and observations over the entire study period are compared, none of the resulting correlations are significant at a 5% level. The LPX fire model estimates do show temporal correlations with the observations that are significant at a 10% level: for both of the satellite products these are strong, negative correlations (< -0.3). Table 4.3 details the percentage of grid cells with observed fire (at least one hot pixel detected in the corresponding satellite product) in which the correlations between estimates and observations are significantly positive or negative, respectively, at a 5% significance level.

The SPITFIRE fire count estimates correlate positively with the observations in the majority of grid cells, and in more grid cells than the other models (Table 4.3). Very few of the grid cells in the study region show negative correlations. The PFI-based estimates give positive correlations in fewer grid cells, but these correlations are, on average, stronger than those of the SPITFIRE fire counts (Table 4.4). When the correlations are averaged over all grid cells that show significant correlations, either positive or negative, the PFI has the highest values of the three models. The LPX fire model estimates consistently perform the worst of all the models, with the lowest percentages of positive temporal correlations and the weakest mean correlations.

Hence, the PFI-based fire count predictions are comparable to the SPITFIRE estimates, and better than the LPX predictions. This is consistent with the comparable temporal accuracies of the respective fire danger indices shown in Table 2.3.

Table 4.3: Percentage of fire-prone grid cells in which monthly model fire count estimates correlate positively or negatively with observations, at a 5% significance level. "Fire-prone" implies at least one fire has been detected by the respective satellite product over the study period. The models tested are SPITFIRE without human ignitions, the LPX fire model, and the new PFI-based fire count estimation method. The observations are the MODIS MCD14ML and ATSR ESM2 World Fire Atlas datasets.

	MODIS MCD14ML		**ATSR ESM2 World Fire Atlas**	
	+	**-**	**+**	**-**
SPITFIRE, no human ignitions	74.5%	0.79%	62.7%	0.12%
LPX fire model	48.1%	1.5%	44.5%	0.24%
PFI fire count model	52.4%	0.79%	45.6%	1.1%

Table 4.4: Mean grid cell level correlations between modelled and observed fire counts. The means are calculated for all grid cells that show significant positive correlations at a 5% significance level, significant negative correlations, and significant correlations of either sign.

	MODIS MCD14ML			**ATSR ESM2 World Fire Atlas**		
	+	**-**	**all**	**+**	**-**	**all**
SPITFIRE, no human ignitions	0.52	-0.22	0.52	0.46	-0.21	0.46
LPX fire model	0.43	-0.25	0.41	0.44	-0.21	0.44
PFI fire count model	0.55	-0.22	0.54	0.49	-0.22	0.47

4.3.3 Magnitude of fire count estimates

The MODIS product is larger than the true number of fires, since it is a measure of hot pixels detected by two overlapping satellites, and therefore a single fire may be detected multiple times. As estimated in Chapter 2, each fire appears to be detected approximately 4 times, on average. The ATSR product, on the other hand, is based on only night-time satellite observations, and is known to underestimate the total global hotspot number (Arino et al., 2012). Hence, it is no surprise that the model estimates of fire counts from SPITFIRE and LPX lie between these two observation sets, as can be seen in Fig. 4.3. The LPX fire model estimates are clearly lower than those produced by JULES-SPITFIRE, as has already been seen in Figure 4.2.

4.4 RESULTS: BURNT AREA ESTIMATES

4.4.1 Burnt area predictions from SPITFIRE and the LPX fire model

Before comparing the estimates of burnt area to each other and to observations, it is first necessary to assess how close the predictions from SPITFIRE and the LPX fire model coupled to JULES are to the predictions shown in the relevant literature. This allows us to see how much the new estimates have been affected by coupling the models to a different DGVM and modifying the parameters, where necessary, as described in Section 4.2.2.

The new SPITFIRE burnt area estimates are generally lower than those shown in Thonicke et al. (2010) (Fig. 4.4), which follows from the lower than documented fire count predictions shown in Fig. 4.2. Spatially, there are some obvious differences. In South America, the JULES-SPITFIRE predictions are highest in central Brazil, whereas Thonicke et al. (2010) predict peaks in

Paraguay, northern Argentina and the eastern tip of Brazil. In Africa, the new distribution shows the most fire activity immediately surrounding the Congo, whereas the peaks in the original estimates are slightly further away from this forest. The high burnt area in India is no longer captured.

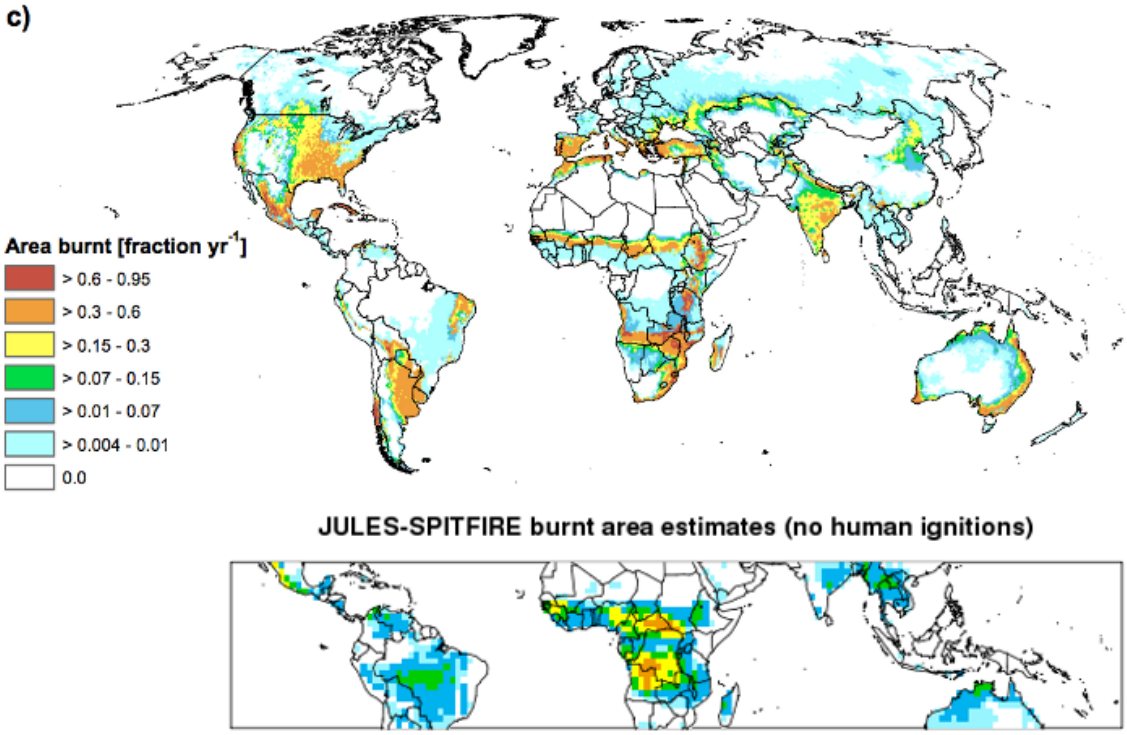

Figure 4.4: Mean annual fractional burnt area from 1982 – 1999 estimated by SPITFIRE, shown in Fig. 3c of Thonicke et al. (2010), and as calculated by SPITFIRE implemented in JULES.

The new predictions from the LPX fire model coupled to JULES are also considerably lower than in the original model documentation (Fig. 4.5). This makes it difficult to compare the spatial distributions, but it appears as if the main features are still captured, particularly in Africa and Australia. In South America, very little burnt area is seen in the new predictions, but the little that has been predicted is closer to the centre of Brazil, which is more consistent

with the distribution shown by the GFED3 BA product than with the original LPX predictions.

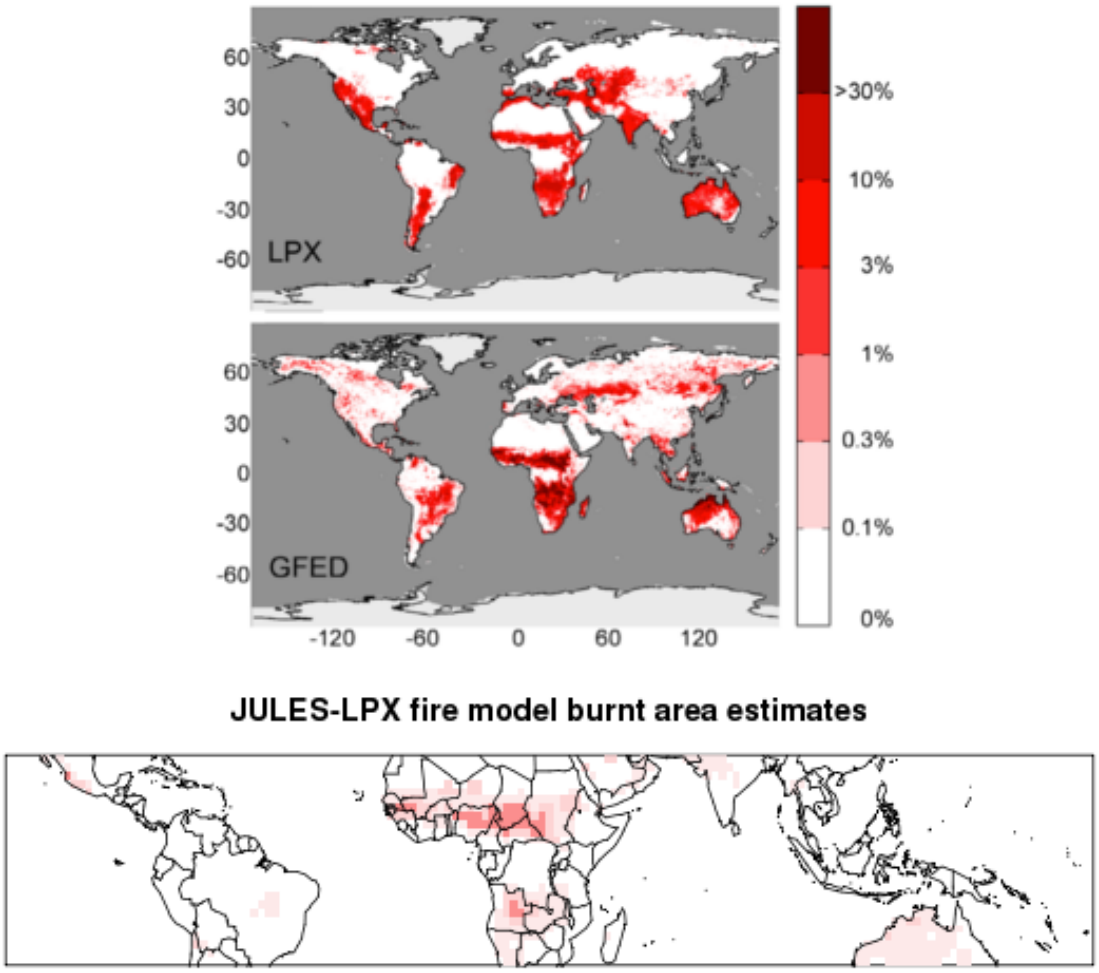

Figure 4.5: Mean annual fractional burnt area from 1997 – 2005 estimated by the LPX fire model, shown in Fig. 2 of Prentice et al. (2011) with the corresponding map of GFED3 BA (Giglio et al., 2010; van der Werf et al, 2010), and as calculated by the LPX fire model implemented in JULES.

These comparisons suggest that any issues that arise with the spatial distribution or magnitude of burnt area estimates in Sections 4.4.2 or 4.4.3 would not indicate a fundamental problem with either the SPITFIRE or LPX fire models, but instead shows either that the difficulties faced when attempting to

recreate these models have large impacts, and therefore better documentation is needed, or that the models are not compatible with JULES, which may signify an incompatibility with any DGVM other than the one for which they were originally designed.

4.4.2 Spatial distribution of burnt area estimates

An initial assessment of the spatial accuracy of the burnt area estimates produced using each of the six model combinations given in Section 4.2.5 can be done visually, by inspecting maps of the mean annual estimated burnt area alongside the mean annual observed burnt area, as given by the GFED4 BA product (Giglio et al., 2013; Fig. 4.6). Combining this visual aid with statistical information about the correlations between these mean annual grid cell values and the observations (Table 4.5) provides a detailed insight into the ability of each of these model combinations to produce burnt area estimates that have accurate spatial distributions.

The predictions of burnt area that are based on the LPX fire model fire count estimates are poor, regardless of the choice of burnt area calculation. If the original SPITFIRE BA calculation is used, the burning is clustered in Africa with virtually no burnt area predicted elsewhere. Using the new burnt area model results in much higher burnt area in the Sahel than in southern Africa, and more burning in India than in S.E. Asia, both of which contradict the patterns visible in the satellite data. This is confirmed by the values of the Pearson's correlation coefficient between these estimates and the GFED4 BA dataset, both across the full study region and for individual continents. These

are generally lower than for estimates produced using either the SPITFIRE or the PFI-based fire count estimates. The only exception to this is found in Australia, where the LPX fire model with its original BA calculation correlates better with the observations than if the PFI-based fire counts are used.

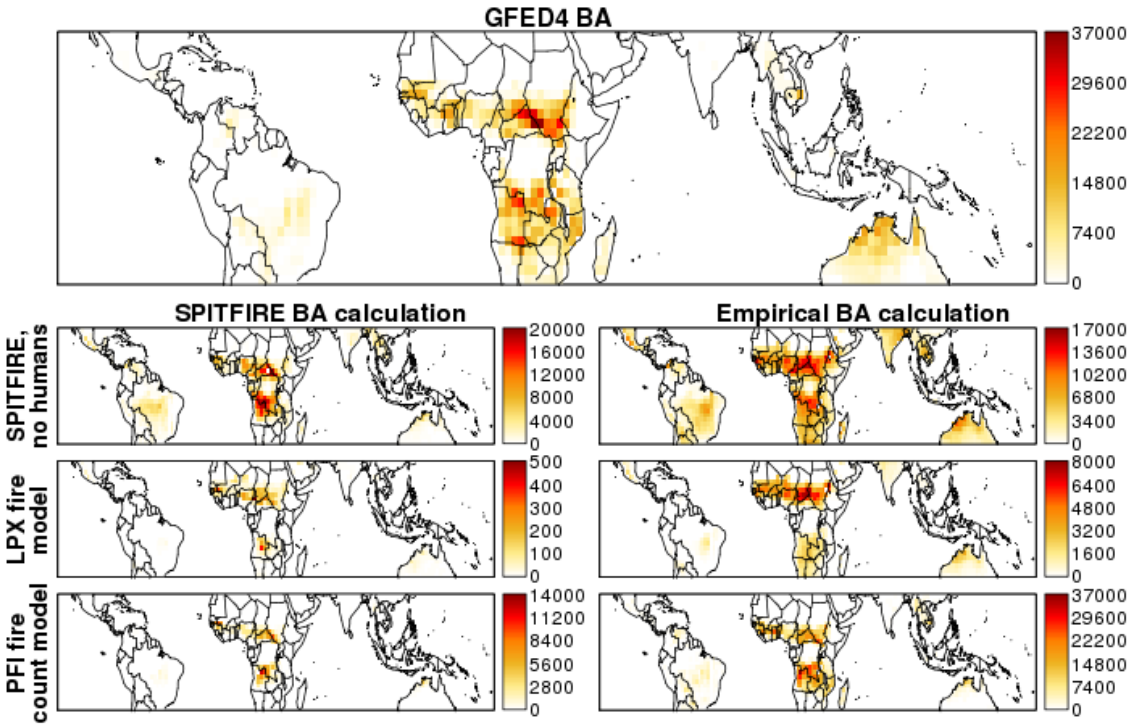

Figure 4.6: Mean annual burnt area (km^2 per 2°x2° grid cell) as detailed in the GFED v4 burnt area product (top) and for each combination of fire count and burnt area parameterisations.

With the same single exception (Australia, SPITFIRE BA calculation), estimates produced using the PFI-based fire counts are more spatially accurate than if the SPITFIRE fire counts are used. Although the SPITFIRE estimates identify the regions of high and low fire activity, the former appear to be underestimated, and the latter overestimated.

Over the full study region, using the empirical BA calculation results in a significant increase in the correlation coefficients between the estimates and the

observations, for each choice of fire count calculation. The same is true for South America, but the pattern is less consistent for other continents. However, this is always the case when the PFI-based fire counts are used.

The combined use of both of the new, empirical models is the only method that consistently produces burnt area estimates that show a strong positive (>0.4) and statistically significant correlation ($p < 0.05$) with the observations.

Table 4.5: Spatial correlations (Pearson's correlation coefficient) between the mean annual burnt area estimates from six possible model combinations and the GFED4 BA product, for the entire study region ("tropics") and individual continents. Correlations given in brackets are non-significant at a 5% level.

	Tropics	South America	Africa	India & S.E. Asia	Australia
SPITFIRE	0.586	0.331	0.597	0.304	0.732
LPX fire model	0.475	0.323	0.440	(0.106)	0.539
PFI fire counts	0.642	0.593	0.647	0.351	0.496
SPITFIRE, empirical BA	0.644	0.551	0.617	(0.152)	0.704
LPX fire model, empirical BA	0.485	0.473	0.406	(-0.069)	0.704
PFI fire count, empirical BA	0.790	0.630	0.803	0.842	0.724

4.4.3 Magnitude of estimates

The accuracy of the magnitudes of the burnt area estimates produced by each combination of the fire count and burnt area models is difficult to quantify, since there are several distinct metrics to consider. The range of estimates that are observed in each grid cell is the easiest to assess: the further the maximum

value is from the observed maximum as given by the GFED4 BA product, the worse the magnitude of the estimates. However, it is possible for some estimates to have a similar range of values as the observations, but with much more weight at one end of the range. For instance, if all but the highest few values are underestimated, the overall area burnt will be considerably too low. Hence, the total annual burnt area summed over the entire study region is also considered, both as a proportion of the mean total annual observed BA (Table 4.6), and its median and range (Fig. 4.7). Additionally, these same metrics are considered per continent, to identify whether some of the models work particularly well or badly in certain regions, and how this affects the overall model performance.

The burnt area estimates based on the LPX fire counts are considerably too low. The maximum mean annual estimated BA using the LPX model in its original form is approximately 75 times smaller than the corresponding value from the GFED4 BA product (Fig. 4.6), and the predicted total annual area burnt is 170 less than observed, when averaged over the study period (0.59%, Table 4.6). For no continent does the mean total annual BA exceed 1% of the GFED4 value.

Using the empirical BA model improves the magnitude of the estimates produced using the LPX fire counts by a huge amount, but they still do not come close to the observations. The largest grid cell estimates of mean annual BA are just over a fifth of the size of the largest detected values (Fig. 4.6), and when summed over the entire study period or individual continents, annual BA estimates range from 16% to 46% of the observations (Table 4.6).

Table 4.6: The percentage of the total mean burnt area given by GFED4, summed over the entire study region ("tropics") or the individual continents, that is estimated by each of the six model combinations.

	Tropics	South America	Africa	India and S.E. Asia	Australia
SPITFIRE	63%	186.9%	58.2%	180.6%	17.1%
LPX fire model	0.59%	0.14%	0.68%	0.43%	0.23%
PFI fire counts	11.8%	6.3%	14.2%	7.0%	3.0%
SPITFIRE, empirical BA	127.3%	358.5%	105.5%	526.7%	91.7%
LPX fire model, empirical BA	26.4%	16.2%	28.1%	46.4%	18.1%
PFI fire count, empirical BA	89.5%	172.0%	95.5%	195.9%	23.9%

The magnitude of the estimates produced by SPITFIRE and the PFI fire count models with the SPITFIRE BA calculation is unexpected: the PFI produces fire count estimates that are similar in magnitude to the SPITFIRE estimates (once adjusted to account for multiple satellite detections), and the burnt area calculation is identical, yet the resulting burnt area estimates are considerably lower for the former than for the latter. This is true of the maximum annual grid cell estimates (Fig. 4.6), and the mean and range of total annual area burnt summed over the study region (Table 4.6, Fig. 4.7). The only difference between the burnt area calculations is that SPITFIRE is calculated daily, whereas the PFI requires a monthly timestep.

Using the empirical BA calculation with SPITFIRE fire counts gives estimates of burnt area that are higher than the observations on all continents except Australia (Table 4.6) and 27% higher when summed over the study area, despite a much lower maximum annual BA per grid cell (approx. 17000) than

the observations (approx. 37000; Fig. 4.6). This suggests that the overestimation of low burnt area mentioned in Section 4.4.2 has more impact than the underestimation of high burnt area. This is further confirmed by the very high total burnt area estimates for South America (> 350% of observations; Table 4.6) and India and South East Asia (> 520%), where relatively little burnt area is observed, but much closer magnitudes for Africa (106%) and Australia (92%), which are much more fire-prone. In fact, SPITFIRE fire counts with the empirical BA model gives the best magnitude of estimates of burnt area for Australia out of all of the model combinations, although the variability between years is much less than in the GFED4 data (Fig. 4.7).

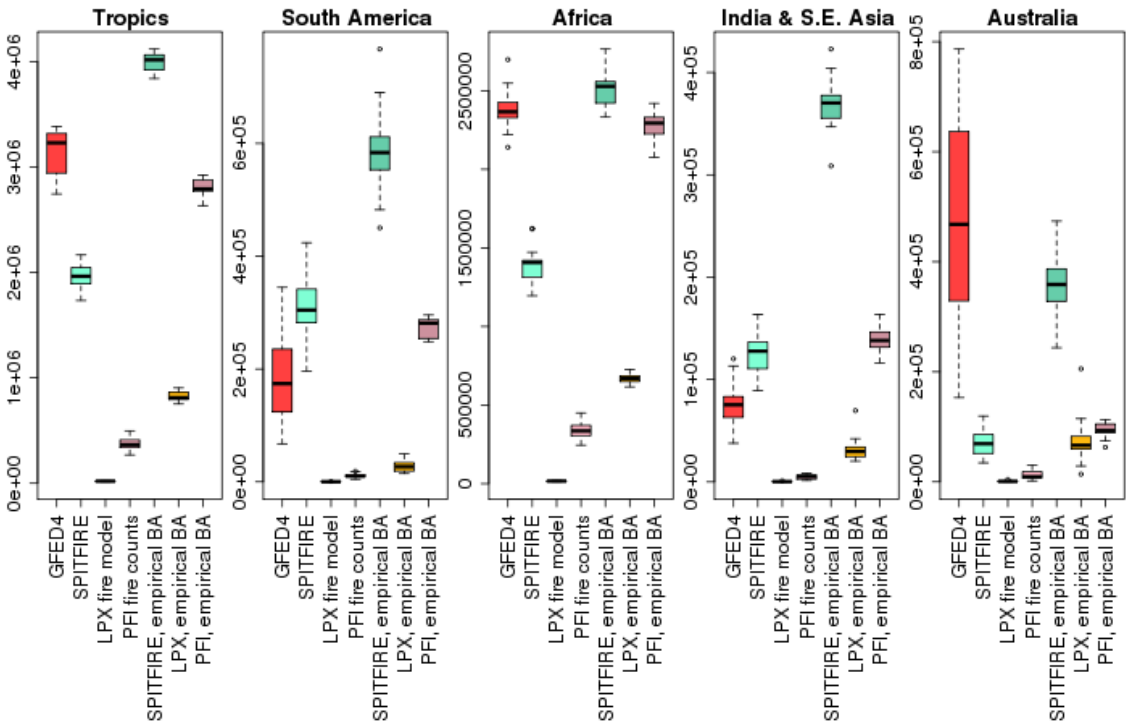

Figure 4.7: Boxplots showing the median, interquartile range and full range of total annual burnt area estimates (for each of the six model combinations) and observations (from GFED4), summed over the entire study period ("tropics") and each continent individually.

The burnt area estimates resulting from the PFI-based fire counts with the empirical burnt area calculation appear visually to be the right order of magnitude (Fig. 4.6), and give the closest annual total burnt area predictions to the observations when summed across the full study region (Table 4.6, Fig. 4.7). Although the interquartile ranges of these estimates and the GFED4 BA product do not overlap, the full ranges do, unlike any of the other model combinations. This parameterisation gives the best results for Africa in terms of magnitude, and despite being 72% larger than the observations, is nonetheless the closest to the GFED values in South America.

4.4.4 Temporal accuracy of burnt area estimates

Time series of burnt area are produced by summing burnt area over the study region (or continent of interest) at each timestep. Annually, none of the time series of estimated BA for the entirety of the tropical latitudes correlate significantly with the GFED4 BA time series at a 5% level. With only 17 full years to analyse, it is difficult to obtain significant correlations, so this is not necessarily a sign of poor temporal performance of the models, but rather an indication of a need for datasets with longer time periods.

At a monthly scale, time series for the full study region from both LPX-based model combinations show a strong negative correlation with the observations (Table 4.7). Estimates based on the SPITFIRE fire counts correlate positively with GFED4, as does the PFI fire count with SPITFIRE burnt area calculation option, though to a lesser degree. Using both of the new models together gives a monthly time series of burnt area that does not correlate strongly or significantly with the observations.

Table 4.7: Temporal correlations between the monthly time series of burnt area estimates from each of the six model combinations and the GFED4 BA product. Time series are produced by summing burnt area over the entire study period ("tropics") or each continent individually. Correlations that are not significant at a 5% level are shown in brackets.

	Tropics	South America	Africa	India and S.E. Asia	Australia
SPITFIRE	0.37	0.48	0.60	0.60	(0.01)
LPX fire model	-0.54	0.69	-0.54	0.16	0.63
PFI fire counts	0.21	0.78	0.32	0.44	(-0.03)
SPITFIRE, empirical BA	0.30	0.66	0.43	0.63	0.45
LPX fire model, empirical BA	-0.43	0.86	-0.47	0.35	0.63
PFI fire count, empirical BA	(0.06)	0.72	0.29	0.65	(-0.09)

By subdividing the region into continents, as done previously, the temporal performance of each model combination in each region can be assessed. The PFI-based fire counts with empirical BA calculation correlate positively and significantly with the observations everywhere except for Australia, and very strongly in South America, India and S.E. Asia. The negative correlations observed for the LPX models over the whole region stem from Africa. These models produce the strongest positive correlation of all the models and continents (0.86, empirical BA calculation in South America) as well as the only significant negative correlations, and are therefore the least consistent estimates. The burnt area estimates calculated using fire counts from SPITFIRE are the most consistently strong, with only one insignificant

correlation (Australia, with SPITFIRE BA calculation).

By considering the monthly time series correlations per grid cell, it is clear that using the SPITFIRE fire count estimates provides the best temporal estimates of burnt area, regardless of the choice of burnt area calculation. The LPX fire counts show negative correlations in the Sahel, one of the regions with the highest fire activity, but positive correlations in much of Australia (Fig. 4.8). Overall, there are visibly fewer grid cells with significant correlations than for the other models. Burnt area estimate time series that use the PFI-based fire counts are positive and significant in fewer grid cells than when SPITFIRE fire counts are used, and when the empirical BA calculation is chosen, there are more negative correlations, particularly in southern Africa. However, with the exception of Australia, the areas of high fire activity in South America and Africa predominantly show a strong positive correlation with the observations.

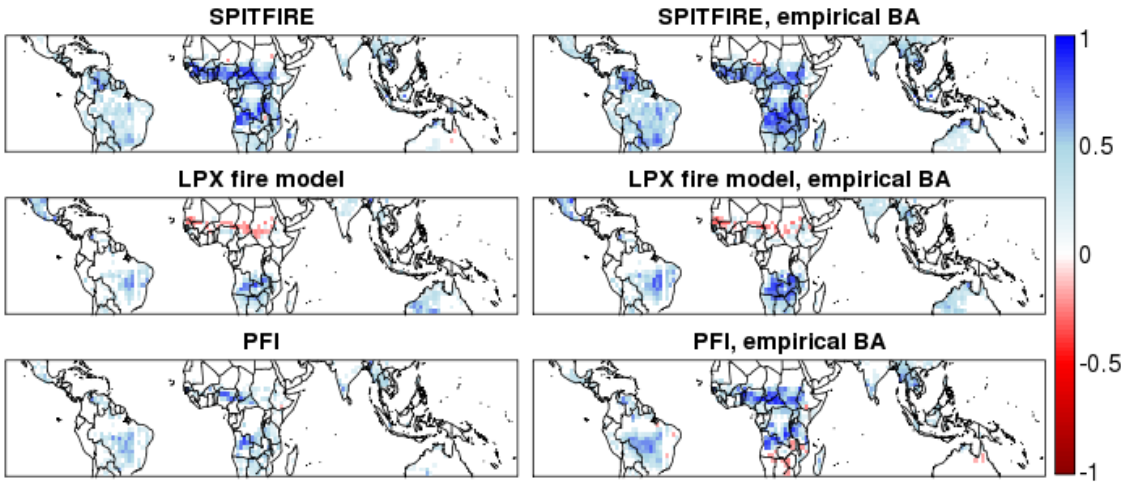

Figure 4.8: Temporal correlations between the monthly time series per grid cell of burnt area estimates from each of the six model combinations and the GFED4 BA product. Only correlations significant at a 5% level are shown.

4.4.5 Ranking the models

In order to better compare the overall performance of each of the combinations of fire count and burnt area models, based on all three of the metrics discussed above – magnitude, and spatial and temporal distribution – the models are ranked for each metric (Table 4.8). The rankings are produced not only for the study region as a whole, but also, where possible, for each continent, since some regions contribute more to the total fire activity than others. In the case of temporal and spatial distributions, non-significant correlations with the observations rank higher than significant negative correlations. Where there is no way of identifying if one set of model estimates is better or worse than another – for instance, if multiple correlations are non-significant – the appropriate rankings are averaged.

Averaging the rankings for each metric for the full study region across every model combination shows that using the PFI-based fire counts with the empirical BA model gives the best estimates of burnt area, if the metrics are given equal importance. This is followed by the SPITFIRE fire counts with the empirical BA model. The SPITFIRE and PFI-based fire counts with the SPITFIRE BA calculation come in the middle, and the estimates that use the LPX fire model fire count calculation consistently give the worst predictions of burnt area.

Table 4.8: Model rankings (for every combination of fire count and burnt area calculation methods) based on the spatial correlations between mean annual BA estimates and observations per grid cell, the temporal correlations between monthly time series of BA estimates and observations, the largest mean annual BA estimate for any grid cell in comparison to the observations, and the mean total annual BA over the study area or continent of interest in comparison to the observations.

	SPITFIRE BA calculation			Empirical BA model		
	SPITFIRE	**LPX**	**PFI**	**SPITFIRE**	**LPX**	**PFI**
			SPATIAL RANKINGS			
Tropics	4	6	3	2	5	1
S. America	5	6	2	3	4	1
Africa	4	5	2	3	6	1
India/S.E.Asia	3	5	2	5	5	1
Australia	1	5	6	3.5	3.5	2
			TEMPORAL RANKINGS			
Tropics	1	6	3	2	5	4
S. America	6	4	2	5	1	3
Africa	1	6	3	2	5	4
India/S.E.Asia	3	6	4	2	5	1
Australia	5	1.5	5	3	1.5	5
			MAGNITUDINAL RANKINGS			
			Maximum			
Tropics	2	6	4	3	5	1
			Total annual			
Tropics	3	6	5	2	4	1
S. America	3	5	4	6	2	1
Africa	3	6	5	2	4	1
India/S.E.Asia	2	5	3	6	1	4
Australia	4	6	5	1	3	2

4.5 DISCUSSION

One of the main points to arise from this chapter is the difficulty in recreating the SPITFIRE and LPX calculations. Various crucial parameters are missing from the literature, and the level of detail required of the input variables, particularly the fuel distribution, is not available in all models. The new models require only precipitation and evapotranspiration from JULES, and land cover type and the PFI-to-fire count conversion parameters as ancillary data.

The LPX fire model can be discounted as a viable option for use in JULES. Whether a result of an incorrect guess of the intended value of the moisture of extinction, inaccurate litter moisture due to the differences between JULES precipitation and LPJ precipitation, or some other factor, fire count and burnt area estimates produced using LPX fire count estimates are consistently inaccurate, both temporally and spatially, and considerably lower than the observations.

The PFI-based fire count estimates have a much more accurate spatial distribution than the SPITFIRE predictions when compared to two separate active fire datasets. The accuracy of the SPITFIRE model has been compromised by the omission of human ignitions and the modifications that were made to ensure compatibility of the model with JULES, as shown in Fig. 4.2. However, these changes to the model were unavoidable, and the spatial correlations with observations are considerably higher when the PFI model is used. Temporally, the PFI-based fire count predictions are slightly worse than the SPITFIRE estimates, though nonetheless good. Suggestions for improving the temporal accuracy of the PFI are given in Chapter 2, and these would directly improve the time series of the resulting burnt area estimates. The

magnitudes of the fire count estimates are impossible to assess at this point, since there is so little agreement between active fire products.

When used with the SPITFIRE burnt area calculation, the PFI-based fire count estimates give burnt area estimates with a better spatial distribution than if the SPITFIRE counts are used, but the temporal estimates are worse. This is consistent with accuracies of the respective fire count predictions from the two models. The low magnitude of burnt area estimates resulting from the PFI-based fire counts is not an indication of problems with the new fire count estimation method, but rather points to a lack of compatibility between this new model and the SPITFIRE BA calculation. This latter was calibrated to higher fire counts, and not scaled down to account for multiple satellite detections of single fire events (Thonicke et al., 2010). Additionally, the SPITFIRE BA calculation was designed to be used at a daily timestep, whereas the PFI is calculated monthly. This may contribute to the lower BA estimates, as a result of the loss of extreme input values to the rate of spread calculations. For instance, wind speed and litter moisture are averaged over the whole month, so very strong winds and exceptionally dry fuel are not necessarily accounted for.

The new, empirical burnt area model generally gives better burnt area estimates than the SPITFIRE BA calculation for each set of fire count predictions. Spatially, although there are some problems with the distribution of burnt area estimates in India and South East Asia, using the fractal BA model results in an overall improvement in the distribution of the predictions. The effect of this model on the temporal accuracy is inconsistent, and varies greatly between continents. The magnitude of the resulting estimates generally increases, as evidenced by the mean total annual BA predictions, although the

range of values may decrease, for instance when used with the SPITFIRE fire count estimates. In the majority of cases, this increase in magnitude represents an improvement in the estimates, since the BA values resulting from the SPITFIRE BA calculations are generally lower than the observations.

The overall best combination of fire count and burnt area models, when spatial, temporal and magnitudinal accuracy are considered together, consists of both of the new models: the PFI-based fire counts and the fractal burnt area model. The BA estimates resulting from the use of these two parameterisations together are consistently the most accurate spatially, and best capture the extent of burning in the tropics. Although the temporal distribution of these predictions are less accurate than those resulting from the SPITFIRE fire counts, regardless of the choice of BA estimation method, this may be due to a potential time lag in the PFI-based fire count predictions, as discussed in Chapter 2. The only region where the temporal correlation with the GFED4 BA product is particularly poor is Australia.

Africa is responsible for approximately 70% of global burnt area (Andela and van der Werf, 2014), and, as such, it is critical that the models work well for this continent, more so than elsewhere. Spatially, the two new models together produce the best BA estimates in this region. They correlate exceptionally strongly with the observations ($r = 0.803$), and the estimated total annual BA is only 4.5% less than the GFED4 product. Temporally, these estimates are not as accurate as they could be, but are adequate until further improvements can be made.

In Chapter 3, the suitability of the new burnt area model in non-forested ecosystems was yet to be tested. The results given here show no evidence of

the model requiring modification to be applicable in such regions, although as more highly-detailed datasets of individual burn sizes become available, this is something that should be investigated further.

5. Discussion and conclusions

This chapter summarises the research presented in this thesis. The key findings are listed, and the limitations of the work, opportunities for further development and the contribution of the work to the research field are discussed.

5.1 SUMMARY OF RESEARCH

The work presented in this thesis consists of novel parameterisations of fire occurrence and spread that are based on known relationships between climate, productivity and fire occurrence, and the often-observed fractal nature of fire size distribution. These parameterisations are simple, and consequently can be used both within a dynamic global vegetation model (DGVM) and as standalone models. They require fewer input variables, parameters and calculations, while simultaneously producing more accurate estimates of fire occurrence and burnt area than their process-based counterparts.

5.2 KEY FINDINGS

The potential fire index described in Chapter 2 (Section 2.1) gives estimates of fire risk that are easy to interpret physically and are spatially more accurate than existing fire danger indices, due to the consideration of the effect of changes in fuel load in different ecosystems. The temporal estimates of fire potential are comparable to those given by existing FDIs. The model suggests that in the most fire-prone ecosystems, changes in wet season moisture and subsequent fuel growth have more impact on fire occurrence than changes in dry season

intensity. Therefore, knowledge of drought severity is not sufficient in itself to predict levels of burning, since a key driver of fire occurrence is omitted.

The method given in Section 2.2 for converting the PFI into fire count estimates further improves the spatial accuracy of the predictions of fire occurrence: they correlate significantly better with observed fire count data than estimates produced by SPITFIRE or the LPX fire model coupled to the same DGVM. Temporally, the performance of the new estimates lies between these two existing fire models. The accuracy of the magnitude of the estimates is difficult to assess, since satellite-derived active fire products are prone to multiple detections of single fires, as well as difficulties in detecting small, understory or daytime fires. The main advantage of this method over existing parameterisations is that it bypasses the need to quantify the relative contributions of lightning and human activity to ignitions, and hence the need to identify and model the main drivers of anthropogenic fire.

The empirical burnt area model developed in Chapter 3 shows that it is possible to predict the parameters of a fractal fire size distribution using fire counts as a sole input, and subsequently predict the spatial and temporal patterns of burnt area in tropical forests. This eliminates the need for data about fuel moisture and quantity, fuel bulk density, wind speed, temperature and the plethora of other variables that are required by traditional process-based fire spread parameterisations.

These parameterisations both work well as standalone models, and when used in conjunction with one another they represent an improvement in the spatial and magnitudinal accuracy of burnt area predictions over existing fire models, with similar temporal precision (Chapter 4). When the new fire count

estimates are used to drive the existing SPITFIRE burnt area calculation, the resulting predictions are well-distributed across the tropics, but considerably too low, since the SPITFIRE parameterisation was calibrated to higher fire counts. Additionally, the PFI is calculated monthly, rather than daily, making it less compatible with the SPITFIRE burnt area calculation. Similarly, the new BA parameterisation is not fully compatible with the SPITFIRE or LPX fire count estimates due to the former being calibrated to lower fire counts. Nonetheless, this new BA calculation generally improves the spatial distribution and magnitude of BA estimates, regardless of the fire count estimation method.

5.3 LIMITATIONS AND OPPORTUNITIES FOR FURTHER DEVELOPMENT

5.3.1 Temporal accuracy

Despite the high spatial accuracy of the new models, they are not particularly effective at capturing the timing of seasonal peaks and dips in fire activity, although they are also not significantly worse than existing models. Since this is the case not only for burnt area estimates, but also for fire count and potential fire predictions, it follows that the majority of this problem can be attributed to the design of the Potential Fire Index.

There are several improvements that could be made to the PFI calculation that may improve the seasonality of the estimates. First, fire is unlikely during a drying season until the fuel has dried sufficiently to become flammable, hence there is probably a time lag between the onset of the drying season and the start of the fire season. It is possible that this time lag can be described using some function of the wet season intensity (WSI) and the local land cover or fuel load, combined with the rate of increase of the dry season

intensity (DSI), since these are the main factors that influence the speed at which fuel reaches a critical dryness that enables burning.

Secondly, Aragão et al. (2008) show that fire activity peaks at the end of each dry season, which is not currently captured by the PFI model: although the PFI increases throughout the dry season, its cumulative nature means that the frequency of predicted fires often tails off at the end of each drying season. The addition of a term to account for this skew would undoubtedly be beneficial.

Finally, the accumulation of fuel conditions over more than just one wet/dry season cycle is likely to have an effect on fire activity (Veblen et al., 2000), particularly if the potential fire is not fulfilled due to a lack of ignition sources: several years of particularly intense wet seasons with little or no fire activity in the corresponding dry seasons is bound to result in an accumulation of fuel which may increase the PFI in fuel-limited fire regions. This issue could potentially be avoided if the PFI model were to be recalibrated with its parameters given as functions of local biomass, rather than constant per PFT, since this would allow fuel loads to accumulate. This would also contribute towards making the model more dynamic, the need for which is discussed next.

5.3.2 Dynamicity

Venevsky et al. (2002) suggest that statistical models are unsuitable for long-term, global use, since they are static and will not take changing climatic and ecological conditions into account. While the models developed in this thesis are not fully static, they could benefit from a few developments to make them more dynamic.

The PFI model is partially dynamic in that climate data is used to drive

the calculations, but the model is calibrated for static land cover types. If the model were to be recalibrated so that the parameters were no longer constant values prescribed for each of the GLC2000 LCTs, but rather functions of biomass, this could potentially improve long-term estimates of fire occurrence. However, this relies heavily on the accuracy of modelled biomass, which in turn is dependent on the reliability of biomass datasets. Houghton et al. (2001) compared seven independent estimates of forest biomass in the Brazilian Amazon and concluded that although there was significant agreement across the methods about the total quantity of stored carbon, there was only as much agreement about the spatial distribution of this biomass as would be expected by chance. Furthermore, estimates are still considerably worse for the tropics than in boreal forests (Houghton, 2005).

The conversion from PFI to fire counts is currently static, but as discussed previously, this is only intended as a temporary solution to ignition modelling. It does not account for changes in human activity and ignition patterns, and although this does not seem to be a major problem during the time period analysed in Chapter 4 (1980 to 2012), it will undoubtedly result in a significant loss of accuracy over longer timeframes. In order to continue avoiding the problem of identifying and modelling the factors that influence human ignition patterns, which has proved unsatisfactory in existing fire models, the use of such parameters is preferable, providing there is some way to update the parameters at regular intervals. This could be done using fire observations as they become available, but would preferably be achieved using some predictable climatic or social variable. Extensive further research would be required to achieve this.

The new burnt area model implicitly accounts for changes in local conditions, since it is driven by fire counts, which are affected by similar variables. However, it may benefit from the inclusion of additional variables in future developments, to allow the distribution parameters to vary as functions of local climate or land cover.

5.3.3 Data availability

The burnt area model developed in Chapter 3 was calibrated to a burn scar dataset that is heavily limited both spatially and temporally, since it covers only the forested regions of Brazilian Amazonia for a single year. Datasets of this kind, with information about not only the frequency but also the size of both canopy and understory fires, are uncommon and unavailable at large scales. If more data of this type were available, this would facilitate the calibration of this model to a range of ecosystems and the identification of which parameter estimation methods would benefit most from additional development.

5.3.4 Combustion, emissions and long-term effects

For the new fire models to fulfill their potential usefulness within a DGVM, new method for converting burnt area to biomass burnt and subsequent trace gas emissions is required. The current calculations in SPITFIRE could not be implemented in JULES as a result of incompatibility between the fuel classes in the DGVM and in the fire model (see Section 4.2.2.10). Even if this issue were solved, the existing fuel combustion equations require the estimated intensity of the fire, which is based on the rate of spread equations, and hence these could not be omitted from the model despite the introduction of the new burnt area

estimation method. A possible solution to this would be to estimate biomass burning using a similar technique to that given in Hao et al. (1994), whereby the fraction of aboveground biomass that is burned is prescribed for each fuel or land cover type. However, this again relies on the accuracy of available biomass estimates. Ideally, fire data such as that available in the Moderate Resolution Imaging Spectroradiometer (MODIS) database or Global Fire Emissions Database (GFED3) should be combined with vegetation type maps in order to quantify affected biomass more accurately, since evergreen rainforests and wooded grassland savannahs contain very different quantities of biomass per unit area (Mouillot et al., 2005). It is also important to treat biomass as dynamic, rather than as static (Houghton et al., 2001).

Emission estimates for a range of trace gas species could be estimated in the same way as in SPITFIRE and the LPX fire model, which consists simply of multiplying the biomass burnt by a PFT-specific emissions factor. If different PFTs are being used to those for which emission factors are given in Thonicke et al. (2010), a highly detailed table of emission factors for a large range of trace gases and PFTs can be found in Akagi et al. (2011). These could be grouped together as required. A more concise table of emission factors is given in van der Werf et al., (2010), based on estimates drawn from several other studies (Andreae & Merlet, 2001; Christian et al., 2003). However, there is some dispute over the accuracy of such methods. Van Leeuwen & van der Werf (2011) argue that constant emission factors may be too simplistic an approach to adequately model reality, and that they are influenced by a range of ambient conditions, including precipitation, temperature, dry season length, vegetation greenness as given by the Normalize Difference Vegetation Index (NDVI), and

fractional tree cover. Whether a model based on variable rather than constant EFs would significantly improve emission estimates is a question that requires further analysis.

Similarly, long-term mortality and decomposition should ideally be included in any fire model. There are some calculations for this within SPITFIRE, but these again use the rate of spread estimates, and hence are not ideal for use with the new fire count and burnt area models. As with other aspects of fire modelling, there are studies that have investigated post-fire mortality in specific regions or vegetation types (e.g. Brando et al., 2011). However, this is a complex process and development of a pan-tropical or global model of post-fire mortality would require extensive further research.

5.4 CONTRIBUTION TO THE RESEARCH FIELD

The models developed in this thesis bridge the gap between the two main types of contemporary fire research: small-scale observational studies, and large-scale model development. Paradoxically, the former deals with broad patterns in fire behaviour in specific study areas and time periods, whereas the latter attempts to quantify the behaviour of individual fires in order to predict global, long-term fire activity. There has previously been very little crossover between these two fields. The models developed here make use of the knowledge obtained by the first type of fire study in order to improve the second. They therefore make practical use of theories that are well-documented and supported by the literature.

The results show that empirical modelling is a valid alternative to large-scale, process-based fire models. The new models produce estimates of fire

occurrence and spread in the tropics that correlate more strongly with observed fire data than existing fire models, which have been shown in the literature to poorly represent tropical fires. A substantial amount of further work is required to produce a fully dynamic, comprehensive fire model that provides the same functionality as existing fire models and that can be fully coupled, with feedback, to a vegetation model. However, the parameterisations presented here are a solid starting point.

Even if such models prove to have finite limits to their potential use for long-term fire prediction, their simplicity makes them useful for benchmarking of existing or future fire models. Unlike current models, they can be easily implemented within any DGVM for comparison to current fire parameterisations, as shown in Chapter 4. New process-based models should be able to produce estimates of fire activity that are at least as accurate as those given by the new fire count and burnt area models developed in this thesis to prove that the additional complexity is warranted.

Bibliography

Alencar, A.A.C., Solórzano, L.A. & Nepstad, D.C. (2004) Modeling forest understory fires in an eastern Amazonian landscape. Ecological Applications, **14(4)** Supplement, S139-S149, doi: 10.1890/01-6029.

Alencar, A., Nepstad, D. & Vera Diaz, M. del C. (2006) Forest Understory Fire in the Brazilian Amazon in ENSO and Non-ENSO Years: Area Burned and Committed Carbon Emissions. Earth Interactions, **10(6)**, 1-17, doi: 10.1175/EI150.1.

Alencar, A., Asner, G.P., Knapp, D. & Nepstad, D. (2011) Temporal variability of forest fires in eastern Amazonia. Ecological Applications, **21(7)**, 2397-2412, doi: 10.2307/41416666.

Andela, N. & van der Werf, G.R. (2014) Recent trends in African fires driven by cropland expansion and El Niño to La Niña transition. Nature Climate Change, **4**, 791-795, doi:10.1038/nclimate2313.

Anderson, A.N., Cook, G.D. & Williams, R.J. (eds.) (2003) Fire in tropical savannas: the Kapalga experiment. Ecological Studies, **169**, Springer.

Andreae, M.O. (1991) Biomass burning: Its history, use and distribution and its impact on environmental quality and global climate. Global Biomass Burning: Atmospheric, Climatic and Biospheric Implications, J.S. Levine (ed.), 3-21, MIT Press, Cambridge, Mass.

Andreae, M.O. & Merlet, P. (2001) Emission of trace gases and aerosols from biomass burning. Global Biogeochemical Cycles, **15(4)**, 955-966, doi: 10.1029/2000GB001382.

Aragão, L.E.O.C., Malhi, Y., Roman-Cuesta, R.M., Saatchi, S., Anderson, L.O. & Shimabukuro, Y.E. (2007) Spatial patterns and fire response of recent Amazonian droughts. Geophysical Research Letters, **34**, L07701, doi:10.1029/2006GL028946.

Aragão, L.E.O.C., Malhi, Y., Barbier, N., Lima, A., Shimabukuro, Y.E., Anderson, L. & Saatchi S. (2008) Interactions between rainfall, deforestation and fires during recent years in the Brazilian Amazonia. Philosophical Transactions of the Royal Society B, **363**, 1779-1785, doi: 10.1098/rstb.2007.0026.

Aragão, L.E.O.C. & Shimabukuro, Y.E. (2010) The Incidence of Fire in Amazonian Forests with Implications for REDD. Science, **328**, doi: 10.1126/science.1186925.

Archibald, S., Roy, D.P., Van Wilgen, B.W. & Scholes, R.J. (2009) What limits fire? An examination of drivers of burnt area in Southern Africa. Global Change Biology, **15**, 613-630, doi: 10.1111/j.1365-2486.2008.01754.x

Archibald, S., Lehmann, C.E.R., Gómez-Dans, J.L. & Bradstock, R.A. (2013) Defining pyromes and global syndromes of fire regimes. PNAS, **110(16)**, 6442-6447, doi: 10.1073/pnas.1211466110.

Arino, O., Simon, M., Piccolini, I. & Rosaz, J.-M. (2001) The ERS-2 ATSR-2 world fire atlas and the ERS-2 ATSR-2 world burnt surface atlas project. Eighth ISPRS Conference on Physical Measurements and Signatures in Remote Sensing, Aussois, France.

Arino, O., Casadio, S. & Serpe, D. (2012) Global night-time fire season timing and fire count trends using the ATSR instrument series. Remote Sensing of Environment, **116**, 226-238, doi: 10.1016/j.rse.2011.05.025.

Arora, V.K. & Boer, G.J. (2005) Fire as an interactive component of dynamic vegetation models. Journal of Geophysical Research, **110**, G02008, doi: 10.1029/2005JG000042.

Akagi, S.K., Yokelson, R.J., Wiedinmyer, C., Alvarado, M.J., Reid, J.S., Karl, T., Crounse, J.D. & Wennberg, P.O. (2011) Emission factors for open and domestic biomass burning for use in atmospheric models. Atmospheric Chemistry and Physics, **11**, 4039-4072, doi: 10.5194/acp-11-4039-2011.

Bachelet, D., Lenihan, J.M., Daly, C., Neilson, R.P., Ojima, D.S. & Parton, W.J. (2000) MC1: A Dynamic Vegetation Model for Estimating the Distribution of Vegetation and Associated Ecosystem Fluxes of Carbon, Nutrients, and Water. USDA General Technical Report PNW-GTR-508, 95.

Bailey, P. (1995), SADIST-2 v100 products, Tech. Note ER-TN-RAL-AT- 2164, Space Sci. Dep., Rutherford Appleton Lab., Oxfordshire, IUK. (Available at http://www.atsr.rl.ac.uk/documentation/docs/sadist/sadist2/sadist2_products_v100.pdf)

Balch, J.K., Nepstad, D.C., Brando, P.M., Curran, L.M., Portela, O., de Carvalho Jr., O. & Lefebvre, P. (2008) Negative fire feedback in a transitional forest of southeastern Amazonia. Global Change Biology, **14**, 2276-2287, doi: 10.1111/j.1365-2486.2008.01655.x.

Ball, G.H. & Hall, D.J. (1965) ISODATA, a novel method of data analysis and pattern classification. Stanford Research Institute, Menlo Park, California, 1965.

Barlow, J., Peres, C.A., Lagan, B.O. & Haugaasen, T. (2003) Large tree mortality and the decline of forest biomass following Amazonian wildfires. Ecology Letters, **6**, 6-8, doi: 10.1046/j.1461-0248.2003.00394.x.

Bartholomé, E. & Belward, A.S. (2005) GLC2000: a new approach to global land cover mapping from Earth observation data. International Journal of Remote Sensing, **26**, 1959-1977.

Best, M.J., Pryor, M., Clark, D.B., Rooney, G.G., Essery, R.L.H., Ménard, C.B., Edwards, J.M., Hendry, M.A., Porson, A., Gedney, N., Mercado, L.M., Sitch, S., Blyth, E., Boucher, O., Cox, P.M., Grimmond, C.S.B. & Harding, R.J. (2011) The Joint UK Land Environment Simulator (JULES), model description – Part 1: Energy and water fluxes. Geoscientific Model Development, **4**, 677-699, doi: 10.5194/gmd-4-677-2011.

Bistinas, I., Oom, D., Sá, A.C.L., Harrison, S.P., Prentice, I.C. & Pereira, J.M.C. (2013) Relationships between Human Population Density and Burned Area at Continental and Global Scales. PLoS ONE, **8(12)**, e81188, doi: 10.1371/journal.pone.0081188.

Bistinas, I., Harrison, S.P., Prentice, I.C. & Pereira, J.M.C. (2014) Causal relationships versus emergent patterns in the global controls of fire frequency. Biogeosciences, **11**, 5087-5101, doi: 10.5194/bg-11-5087-2014.

Blate, G.M. (2005) Modest trade-offs between timber management and fire susceptibility of a Bolivian semi-deciduous forest. Ecological Applications, **15(5)**, 1649-1663, doi: 10.1890/04-0385.

Boden, T., Marland, G. & Andres, R. (2011) Global CO_2 emissions from fossil-fuel burning, cement manufacture, and gas flaring: 1751–2008. Available at: http://cdiac.ornl.gov/trends/emis/overview_2008.html. Accessed on 15/09/2014. Oak Ridge National Laboratory, U. S. Department of Energy, Carbon Dioxide Information Analysis Center, Oak Ridge, TN, U.S.A., doi: 10.3334/CDIAC/00001_V2011.

Bofetta, G., Carbone, V., Giuliani, P., Veltri, P. & Vulpiani, A. (1999) Power

Laws in Solar Flares: Self-Organized Criticality or Turbulence? Physical Review Letters, **83(22)**, 4662-4665, doi: 10.1103/PhysRevLett.83.4662.

Bond, W.J., & Keeley, J.E. (2005) Fire as a global 'herbivore': the ecology and evolution of flammable ecosystems. Trends in Ecology and Evolution, **21(7)**, 387 – 394, doi: 10.1016/j.tree.2005.04.025.

Bond, W.J., Woodward, F.I. & Midgley, G.F. (2005) The global distribution of ecosystems in a world without fire. New Phytologist, **165**, 525-538, doi: 10.1111/j.1469-8137.2004.01252.x.

Booth, B.B.B, Dunstone, N.J., Halloran, P.R., Andrews, T. & Bellouin, N. (2012) Aerosols implicated as a prime driver of twentieth-century North Atlantic climate variability. Nature, 484, 228-232, doi: 10.1038/nature10946.

Bowman, D.M.J.S., Balch, J.K., Artaxo, P., Bond, W.J., Carlson, J.M., Cochrane, M.A., D'Antonio, C.M., DeFries, R.S., Doyle, J.C., Harrison, S.P., Johnston, F.H., Keeley, J.E., Krawchuk, M.A., Kull, C.A., Marston, J.B., Moritz, M.A., Prentice, I.C., Roos, C.I., Scott, A.C., Swetnam, T.W., van der Werf, G.R. & Pyne, S.J. (2009) Fire in the Earth System. Science, **324**, 481-484, doi: 10.1126/science.1163886.

Bowman, D.M.J.S., Murphy, B.P., Williamson, G.J. & Cochrane, M.A. (2014) Pyrogeographic models, feedbacks and the future of global fire regimes. Global Ecology and Biogeography, **23**, 821-824, doi: 10.1111/geb.12180.

Bradstock, R.A. (2010) A biogeographic model of fire regimes in Australia: current and future implications. Global Ecology and Biogeography, **19**, 145-158, doi: 10.1111/j.1466-8238.2009.00512.x.

Brando, P.M., Nepstad, D.C., Balch, J.K., Bolker, B., Christman, M.C., Coe, M.

& Putz, F.E. (2011) Fire-induced tree mortality in a neotropical forest: the roles of bark traits, tree size, wood density and fire behavior. Global Change Biology, **18(2)**, 630-641, doi: 10.1111/j.1365-246.2011.02533.x.

Brown, J.K. (1981) Bulk Densities of Nonuniform Surface Fuels and Their Application to Fire Modeling. Forest Science, **27(4)**, 667-683.

Cecil, D.J., Beuchler, D.E. & Blakeslee, R.J. (2014) Gridded lightning climatology from TRMM-LIX and OTD: Dataset description. Atmospheric Research, **135-136**, 404-414, doi: 10.1016/j/atmosres.2012.06.028.

Chen, F. & Dudhia, J. (2001) Coupling an Advance Land Surface-Hydrology Model with the Penn State-NCAR MM5 Modeling System. Part I: Model Implementation and Sensitivity. Monthly Weather Review, **129(4)**, 569-585, doi: 10.1175/1520-0493(2001)129<0569:CAALSH>2.0.CO;2.

Chen, Y., Randerson, J.T., Morton, D.C., DeFries, R.S., Collatz, G.J., Kasibhatla, P.S., Giglio, L., Jin, Y. & Marlier, M.E. (2011) Forecasting Fire Season Severity in South America Using Sea Surface Temperature Anomalies. Science, **344**, 787-791, doi: 10.1126/science.1209472.

Chen, Y., Velicogna, I., Famiglietti, J.S. & Randerson, J.T. (2013) Satellite observations of terrestrial water storage provide early warning information about drought and fire season severity in the Amazon. Journal of Geophysical Research: Biogeosciences, **118(2)**, 495-594, doi: 10.1002/jgrg.20046.

Christian, T.J., Kleiss, B., Yokelson, R.J., Holzinger, R., Crutzen, P.J., Hao, W.M., Saharjo, B.H. & Ward, D.E. (2003) Comprehensive laboratory measurements of biomass-burning emissions: 1. Emissions from Indonesian, African, and other fuels. Journal of Geophysical Research: Atmospheres (1984-2012), **108(D23)**, 4719, doi:10.1029/2003JD003704.

Ciais, P., Sabine, C., Bala, G., Bopp, L., Brovkin, V., Canadell, J., Chhabra, A., DeFries, R., Galloway, J., Heimann, M., Jones, C., Le Quéré, C., Myneni, R.B., Piao, S. & Thornton, P. (2013) Carbon and Other Biogeochemical Cycles. In: Climate Change 2013: The Physical Science Basis. Contribution of Working Group I to the Fifth Assessment Report of the Intergovernmental Panel on Climate Change. Stocker, T.F., Qin, D., Plattner, G.-K., Tignor, M., Allen, S.K., Boschung, J., Nauels, A., Xia, Y., Bex, V. & Midgley, P.M. (eds.). Cambridge University Press, Cambridge, United Kingdom and New York, NY, USA.

Clark, D.B., Mercado, L.M., Sitch, S., Jones, C.D., Gedney, N., Best, M.J., Pryor, M., Rooney, G.G., Essery, R.L.H., Blyth, E., Boucher, O., Harding, R.J., Huntingford, C. & Cox, P.M. (2011) The Joint UK Land Environment Simulator (JULES), model description – Part 2: Carbon fluxes and vegetation dynamics. Geoscientific Model Development, **4**, 701-722, doi: 10.5194/gmd-4-701-2011.

Cochrane, M.A., Alencar, A.A., Schulze, M.D., Souza Jr., C.M., Nepstad, D.C., Lefebvre, P. & Davidson, E.A. (1999) Positive Feedbacks in the Fire Dynamic of Closed Canopy Tropical Forests. Science, **248**, 1832-1835, doi: 10.1126/science.284.5421.1832.

Cochrane, M.A. (2001) Synergistic Interactions between Habitat Fragmentation and Fire in Evergreen Tropical Forests. Conservation Biology, **15(6)**, 1515-1521, doi: 10.1046/j.1523-1739.2001.01091.x.

Cochrane, M.A. (2003) Fire science for rainforests. Nature, **421**, 913 – 919, doi: 10.1038/nature01437.

Cox, P.M., Harris, P.P., Huntingford, C., Betts, R.A., Collins, M., Jones, C.D., Jupp, T.E., Marengo, J.A. & Nobre, C.A. (2008) Increasing risk of Amazonian drought due to decreasing aerosol pollution. Nature, **453**, 212-215, doi:

10.1038/nature06960.

Cui, W. & Perera, A.H. (2008) What do we know about forest fire size distribution, and why is this knowledge useful for forest management? International Journal of Wildland Fire, **17(2)**, 234–244, doi: 10.1071/WF06145.

Cumming, S.G. (2001) A parametric model of the fire-size distribution. Canadian Journal of Forest Research, **31(8)**, 1297–1303, doi: 10.1139/x01-032.

D'Antonio, C.M. & Vitousek, P.M. (1992) Biological invasions by exotic grasses, the grass/fire cycle, and global change. Annual Review of Ecology and Systematics, **23**, 63-87, doi: 10.1146/annurev.es.23.110192.000431.

Daniau, A.-L., Bartlein, P.J., Harrison, S.P., Prentice, I.C., Brewer, S., Friedlingstein, P., Harrison-Prentice, T.I., Inoue, J., Izumi, K., Marlon, J.R., Mooney, S., Power, M.J., Stevenson, J., Tinner, W., Andrič, M., Atanassova, J., Behling, H., Black, M., Blarquez, O., Brown, K.J., Carcailler, C., Colhoun, E.A., Colombaroli, D., Davis, B.A.S., D'Costa, D., Dodson, J., Dupont, L., Eshetu, Z., Gavin, D.G., Genries, A., Haberle, S., Hallett, D.J., Hope, G., Horn, S.P., Kassa, T.G., Katamura, F., Kennedy, L.M., Kershaw, P., Krivonogov, S., Long, C., Magri, D., Marinova, E., McKenzie, G.M., Moreno, P.I., Moss, P., Neumann, F.H., Norström, E., Paitre, C., Ruis, D., Roberts, N., Robinson, G.S., Sasaki, N., Scott, L., Takahara, H., Terwilliger, V., Thevenon, F., Turner, R., Valsecchi, V.G., Vannière, B., Walsh, M., Williams, N. & Zhang, Y (2012) Predictability of biomass burning in response to climate changes. Global Biogeochemical Cycles, **26(4)**, GB4007, doi: 10.1029/2011GB004249.

Deeming, J.E., Burgan, R.E. & Cohen, J.D. (1977) The National Fire-Danger Rating System – 1978. USDA Forest Service General Technical Report INT-

39.

Del Grosso, S., Parton, W., Stohlgren, T., Zheng, D., Bachelet, D., Prince, S., Hibbard, K. & Olsen, R. (2008) Global potential net primary production predicted from vegetation class, precipitation, and temperature. Ecology, **89(8)**, 2117-2126, doi: 10.1890/07-0850.1.

Dowdy, A.J., Mills, G.A., Finkele, K. & de Groot, W. (2009) Australian fire weather as represented by the McArthur Forest Fire Danger Index and the Canadian Forest Fire Weather Index. CAWCR Technical Report, **10**.

Dwyer, E., Pereira, J.M.C., Grégoire, J.-M. & DaCamara, C.C. (2000) Characterization of the spatio-temporal patterns of global fire activity using satellite imagery for the period April 1992 to March 1993. Journal of Biogeography, **27(1)**, 57-69, doi: 10.1046/j.1365-2699.2000.00339.x.

Eastwood, J. A., Plummer, S. E., Wyatt, B. K. & Stocks, B. J. (1998) The potential of SPOT-Vegetation data for fire scar detection in boreal forests. International Journal of Remote Sensing, **19**, 3681–3687, doi: 10.1080/01411698213894.

Ek, M.B., Mitchell, K.E., Lin, Y., Rogers, E., Grunmann, P., Koren, V., Gayno, G. & Tarpley, J.D. (2003) Implementation of Noah land surface model advances in the National Centres for Environmental Prediction operational mesoscale Eta model. Journal of Geophysical Research: Atmospheres (1984-2012), **108**, D22, doi:10.1029/2002JD003296.

Flannigan, M.D., Stocks, B.J. & Wotton, B.M. (2000) Climate change and forest fires. Science of The Total Environment, **262(3)**, 221-229, doi: 10.1016/S0048-9697(00)00524-6.

Flannigan, M.D., Krawchuk, M.A., de Groot, W.J., Wotton, B.M. & Gowman, L.M. (2009) Implications of changing climate for global wildland fire. International Journal of Wildland Fire, **18**, 483-507, doi: 10.1071/WF08187.

Flato, G., Marotzke, J., Abiodun, B., Braconnot, P., Chou, S.C., Collins, W., Cox, P., Driouech, F., Emori, S., Eyring, V., Forest, C., Gleckler, P., Guilyardi, E., Jakob, C., Kattsov, V., Reason, C. & Rummukainen, M. (2013) Evaluation of Climate Models. In: Climate Change 2013: The Physical Science Basis. Contribution of Working Group I to the Fifth Assessment Report of the Intergovernmental Panel on Climate Change. Stocker, T.F., D. Qin, G.-K. Plattner, M. Tignor, S.K. Allen, J. Boschung, A. Nauels, Y. Xia, V. Bex and P.M. Midgley (eds.). Cambridge University Press, Cambridge, United Kingdom and New York, NY, USA.

Fletcher, I.N., Aragão, L.E.O.C., Lima, A., Shimabukuro, Y. & Friedlingstein, P. (2014) Fractal properties of forest fires in Amazonia as a basis for modelling pan-tropical burnt area. Biogeosciences, **11**, 1449 – 1459, doi: 10.5194/bg-11-1449-2014.

Fletcher, I.N., Friedlingstein, P., Murray-Tortarolo, G., Gilham, R.J.J., Sitch, S. & Aragão, L.E.O.C (submitted) A novel index of potential fire incidence based on the productivity-aridity gradient. Earth System Dynamics.

Fraser, R.H. & Li, Z. (2002) Estimating fire-related parameters in boreal forest using SPOT VEGETATION. Remote Sensing of Environment, **82(1)**, 95–110, doi: 10.1016/S0034-4257(02)00027-5.

Friedl, M.A., McIver, D.K., Hodges, J.C.F., Zhang, X.Y., Muchoney, D., Strahler, A.H., Woodcock, C.E., Gopal, S., Schneider, A., Cooper, A., Baccini, A., Gao, F. & Schaaf, C. (2002) Global land cover mapping from MODIS: algorithms and early results. Remote Sensing of Environment, **83**, 287–302, doi: 10.1016/S0034-4257(02)00078-0.

Frost, P.G.H. (1999) Fire in southern African woodlands: Origins, impacts, effects, and control. Proceedings of an FAO Meeting on Public Policies Affecting Forest Fires. 1999 Food and Agricultural Organization of the United Nations Forestry Paper 138, pp 181–205.

Fu, R., Yin, L., Li, W., Arias, P.A., Dickinson, R.E., Huang, L., Chakraborty, S., Fernandes, K., Liebmann, B., Fisher, R. & Myneni, R.B. (2013) Increased dry-season length over southern Amazonia in recent decades and its implication for future climate projections. PNAS, **110(45)**, 18110-18115, doi: 10.1073/pnas.1302584110.

Gerten, D., Schaphoff, S., Haberlandt, U., Lucht, W. & Sitch, S. (2004) Terrestrial vegetation and water balance – hydrological evaluation of a dynamic global vegetation model. Journal of Hydrology, **286**, 249-270, doi: 10.1016/j.jhydrol.2003.09.029.

Giglio, L., van der Werf, G.R., Randerson, J.T., Collatz, G.J. & Kasibhatla, P. (2006) Global estimation of burned area using MODIS active fire observations. Atmospheric Chemistry and Physics, **6**, 957-974, doi: 10.5194/acp-6-957-2006.

Giglio, L. (2010) MODIS Collection 5 Active Fire Product User's Guide Version 2.4, Science Systems and Applications, Inc., University of Maryland, Department of Geography.

Giglio L., Randerson J.T., van der Werf G.R., Kasibhatla P.S., Collatz G.J., Morton D.C. & DeFries, R.S. (2010) Assessing variability and long-term trends in burned area by merging multiple satellite fire products. Biogeosciences, **7**, 1171–1186, doi: 10.5194/bg-7-1171-2010.

Giglio, L., Randerson, J.T. & van der Werf, G.R. (2013) Analysis of daily, monthly, and annual burned area using the fourth-generation global fire emissions database (GFED4). Journal of Geophysical Research, **118(1)**, 317-328, doi: 10.1002/jgrg.20042.

Global Land Cover 2000 database. European Commission, Joint Research Centre, (2003). Available at: http://bioval.jrc.ec.europa.eu/products/glc2000/glc2000.php, last accessed: 17 November 2012).

Glover, D. & Jessup, T. (eds.) (2006). Indonesia's Fires and Haze: The Cost of a Catastrophe. Singapore: Institute of Southeast Asian Studies.

Golding, N. & Betts, R. (2008) Fire risk in Amazonia due to climate change in the HadCM3 climate model: Potential interactions with deforestation. Global Biogeochemical Cycles, **22**, GB4007, doi: 10.1029/2007GB003166.

Grégoire, J.-M., Tansey, K. & Silva, J. M. N. (2003) The GBA2000 initiative: Developing a global burned area database from SPOT-VEGETATION imagery. International Journal of Remote Sensing, **24**, 1369–1376, doi: 10.1080/0143116021000044850.

Guyette, R.P., Muzika, R.M. & Dey, D.C. (2002) Dynamics of an Anthropogenic Fire Regime. Ecosystems, **5(5)**, 472-486, doi: 10.1007/s10021-002-0115-7.

Han, X., Franssen, H.-J.H., Montzka, C. & Vereecken, H. (2014) Soil moisture and soil properties estimation in the Community Land Model with synthetic brightness temperature observations. Water Resources Research, **50(7)**, 6081-6105, doi: 10.1002/2013WR014586.

Hao, W.M. & Liu, M.H. (1994) Spatial and temporal distribution of tropical biomass burning. Global Biogeochemical Cycles, **8(4)**, 495-503, doi:

10.1029/94GB02086.

Haugaasen, T., Barlow, J. & Peres, C.A. (2003) Surface wildfire in central Amazonia: short-term impact on forest structure and carbon loss. Forest Ecology and Management, **179**, 321-331, doi: 10.1016/S0378-1127(02)00548-0.

Hijmans, R.J. (2013) raster: raster: Geographic data analysis and modeling. R package version 2.1-66, available at: http://CRAN.R-project.org/package=raster, last access: 17 November 2012.

Hirota, M., Holmgren, M., Van New, E.H. & Scheffer, M. (2011) Global resilience of tropical forest and savanna to critical transitions. Science, **334**, 232-235, doi: 10.1126/science.1210657.

Hoelzemann, J.J., Schultz, M.G., Brasseur, G.P. & Granier, C. (2004) Global Wildland Fire Emission Model (GWEM): Evaluation the use of global area burnt satellite data. Journal of Geophysical Research, **109**, D14S04, doi: 10.1029/2003JD003666.

Hoffmann, W.A., Orthen, B. & do Nascimento, P.K.V. (2003) Comparative fire ecology of tropical savanna and forest trees. Functional Ecology, **17**, 720-726, doi: 10.1111/j.1365-2435.2003.00796.x.

Hoffman, W.A., Geiger, E.L., Gotsch, S.G., Rossatto, R., Silva, L.C.R., Lau, O.L., Haridasan, M. & Franco, A.C. (2012) Ecological thresholds at the savannah-forest boundary: how plant traits, resources and fire govern the distribution of tropical biomes. Ecology Letters, **15(7)**, 759-768, doi: 10.1111/j.1461-0248.2012.01789.x.

Holmes, T.P., Prestemon, J.P., Pye, J.M., Butry, D.T., Mercer, D.E. & Abt, K.L.

(2004) Using size-frequency distributions to analyze fire regimes in Florida. (RT Engstrom, KEM Galley, WJ de Groot (eds.)) In: Proceedings of the 22nd Tall Timbers Fire Ecology Conference: Fire in Temperate, Boreal, and Montane Ecosystems. Tall Timbers Research Station, Tallahassee, FL., pp. 88–94.

Houghton, R.A., Skole, D.L., Nobre, C.A., Hackler, J.L., Lawrence, K.T. & Chomentowski, W.H. (2000a) Annual fluxes of carbon from deforestation and regrowth in the Brazilian Amazon. Nature, **403**, 301-304, doi: 10.1038/35002062.

Houghton, R.A., Hackler, J.L. & Lawrence, K.T. (2000b) Changes in terrestrial carbon storage in the United States. 2: The role of fire and fire management. Global Ecology & Biogeography, **9**, 145-170, doi: 10.1046/j.1365-2699.2000.00164.x.

Houghton, R.A., Lawrence, K.T., Hackler, J.L. & Brown, S. (2001) The spatial distribution of forest biomass in the Brazilian Amazon: a comparison of estimates. Global Change Biology, **7**, 731-746, doi: 10.1111/j.1365-2486.2001.00426.x.

Houghton, R.A. (2005) Aboveground Forest Biomass and the Global Carbon Balance. Global Change Biology, **11**, 945-958, doi: 10.1111/j.1365-2486.2005.00955.x.

INPE (National Institute for Space Research) PRODES: Assessment of Deforestation in Brazilian Amazonia project, available at: www.obt.inpe.br/prodes/index.html, last access: March 2013.

IPCC (2006) IPCC 2006 Guidelines for National Greenhouse Gas Inventories Volume 4: Agriculture, Forestry, and Other Landuse. OECD, Paris.

Ito, A. & Penner, J.E. (2004) Global estimates of biomass burning emissions based on satellite imagery for the year 2000. Journal of Geophysical Research, **109**, D14S05, doi: 10.1029/2003JD004423.

Joint Research Centre (2008) Forest fires in Europe 2007. JRC Scientific and Technical Reports, Report No. 8, Luxembourg: Institute for Environment and Sustainability, European Commission, Office for Official Publications of the European Communities.

Johnston, F.H., Henderson, S.B., Chen, Y., Randerson, J.T., Marlier, M., DeFries, R.S., Kinney, P., Bowman, D.M.J.S. & Brauer, M. (2012) Estimates Global Mortality Attributable to Smoke from Landscape Fires. Environmental Health Perspectives, **120(5)**, 695-701, doi: 10.1289/ehp.1104422.

Justice, C.O., Giglio, L., Korontzi, S., Owens, J., Morisette, J., Roy D., Descloitres, J., Alleaume, S., Petitcolin, F. & Kaufman, Y. (2002) The MODIS fire products. Remote Sensing of Environment, **83(1-2)**, 244-262, doi: 10.1016/S0034-4257(02)00076-7.

Kantzas, E., Lomas, M. & Quegan, S. (2013) Fire at high latitutde: Data-model comparisons and their consequences. Global Biogeochemical Cycles, **27(3)**, 677-691, doi: 10.1002/gbc.20059.

Kasischke, E.S., Christensen Jr., N.L. & Stocks, B.J. (1995) Fire, global warming, and the carbon balance of boreal forests. Ecological Applications, **5(2)**, 437-451, doi: 10.2307/1942034.

Kawakubo, F.S., Morato, R.G. & Luchiari, A. (2013) Use of fraction imagery, segmentation and masking techniques to classify land-use and land-cover types in the Brazilian Amazon. International Journal of Remote Sensing, **34**, 5452-5467, doi: 10.1080/01431161.2013.791758.

Keeley, J.E. & Bond, W.J. (2001) On Incorporating Fire into Our Thinking about Natural Ecosystems: A Response to Saha and Howe. The American Naturalist, **158(6)**, 664-670, doi: 10.1086/323594.

Kelley, D.I., Harrison, S.P. & Prentice, I.C. (2014) Improved simulation of fire-vegetation interactions in the Land surface Processes and eXchanges dynamic global vegetation model (LPX-Mv1)**.** Geoscientific Model Development Discussion, **7**, 931–1000, doi: 10.5194/gmdd-7-931-2014.

Kempeneers, P., Swinnen, E. & Fierens, F. (2002) GLOBSCAR Final Report. VITO TAP/N7904/FF/FR-001 version 1.2, Eur. Space Ag., Paris.

Kloster, S., Mahowald, N.M., Randerson, J.T., Thornton, P.E., Hoffman, F.M., Levis, S., Lawrence, P.J., Feddema, J.J., Oleson, K.W. & Lawrence, D.M. (2010) Fire dynamics during the 20th century simulated by the Community Land Model. Biogeosciences, **7**, 1877-1902, doi: 10.5194/bg-7-1877-2010.

Kochi, I., Donovan, G.H., Champ, P.A. & Loomis, J.B. (2010) The economic cost of adverse health effects from wildfire-smoke exposure: a review. International Journal of Wildland Fire, **19**, 803-817, doi: 10.1071/WF09077.

Krawchuk, M.A., Moritz, M.A., Parisien, M.-A., Van Dorn, J. & Hayhoe, K. (2009) Global Pyrogeography: the Current and Future Distribution of Wildfire. PLoS ONE, **4(4)**, e5102, doi: 10.1371/journal.pone.0005102.

Krawchuk, M.A. & Moritz, M.A. (2011) Constraints on global fire activity vary across a resource gradient. Ecology, **92(1)**, 121-132, doi: 10.1890/09-1843.1.

Latrubesse, E.M., Stevaux, J.C. & Sinha, R. (2005) Tropical rivers. Geomorphology, **70(3-4)**, 187- 206, doi: 10.1016/j.geomorph.2005.02.005.

Lavorel, S., Flannigan, M.D., Lambin, E.F. & Scholes, M.C. (2007) Vulnerability of land systems to fire: Interactions among humans, climate, the atmosphere, and ecosystems. Mitigation and Adaptation Strategies for Global Change, **12**, 33-53, doi: 10.1007/s11027-006-9046-5.

Le Quéré, C., Raupach, M.R., Canadell, J.G., Marland, G. *et al.* (2009) Trends in the sources and sinks of carbon dioxide. Nature Geoscience, **2**, 831–836, doi: 10.1038/ngeo689.

Lehmann, C.E., Anderson, T.M., Sankaran, M., Higgins, S.I., Archibald, S., Hoffmann, W.A., Hanan, N.P., Williams, R.J., Rensham, R.J., Felfili, J., Hutley, L.B., Ratnam, J., San Jose, J., Montes, R., Franklin, D., Russel-Smith, J., Ryan, C.M., Durigan, G., Hiernaux, P., Haidar, R., Bowman, D.M.J.S. & Bond, W.D. (2014) Savanna Vegetation-Fire-Climate Relationships Differ Among Continents. Science, **343**, 548-552, doi: 10.1126/science.1247355.

Lenihan, J.M., Daly, C., Bachelet, D. & Neilson, R.P. (1998) Simulating Broad-Scale Fire Severity in a Dynamic Global Vegetation Model. Northwest Science, **72**, 91-103.

Lewis, S.L., Lloyd, J., Sitch, S., Mitchard, E.T.A & Laurance, W.F. (2009) Changing Ecology of Tropical Forests: Evidence and Drivers. Annual Review of Ecology, Evolution, and Systematics, **40**, 529-549, doi: 10.1146/annurev.ecolsys.39.110707.173345.

Li, F., Zeng, X.D. & Levis, S. (2012a) A process-based fire parameterization of intermediate complexity in a Dynamic Global Vegetation Model. Biogeosciences, **9**, 2761-2780, doi: 10.5194/bg-9-2761-2012.

Li, F., Zeng, X.D. & Levis, S. (2012b) Corrigendum to “A process-based fire parameterization of intermediate complexity in a Dynamic Global Vegetation

Model". Biogeosciences, **9**, 4771-4772, doi: 10.5194/bg-9-4771-2012.

Li, F., Levis, S. & Ward, D.S. (2013) Quantifying the role of fire in the Earth system – Part 1: Improved global fire modeling in the Community Earth System Model (CESM1). Biogeosciences, **10**, 2293-2314, doi: 10.5194/bg-10-2293-2013.

Lima A., Shimabukuro Y.E., Adami M., Freitas R.M., Aragão L.E., Formaggio A.R. et al. (2009) Mapeamento de cicatrizes de queimadas na amazônia brasileira a partir de aplicação do modelo linear de mistura espectral em imagens do sensor MODIS. In: *Anais do XIV Simpósio Brasileiro de Sensoriamento Remoto*, Natal, pp. 5925–5932. (Portuguese)

Lu, D. (2006) The potential and challenge of remote sensing-based biomass estimation. International Journal of Remote Sensing, **27(7)**, 1297-1328, doi: 10.1080/01431160500486732.

Malhi, Y., Wood, D., Baker, T.R., Wright, J., Phillips, O.L., Cochrane, T., Meir, P., Chave, J., Almeida, S., Arroyo, L., Higuchi, N., Killeen, T.J., Laurance, S.G., Laurance, W.F., Lewis, S.L., Monteagudo, A., Neill, D.A., Vargas, P.N., Pitman, N.C.A., Quesada, C.A., Salomão, R., Silva, J.N.M., Lezama, A.T., Terborgh, J., Martínez, R.V. & Vinceti, B. (2006) The regional variation of aboveground live biomass in old-growth Amazonian forests. Global Change Biology, **12**, 1107-1138, doi: 10.1111/j.1365-2486.2006.01120.x.

Malhi, Y., Aragão, L.E.O.C., Galbraith, D., Huntingford, C., Fisher, R., Zelazowski, P., Sitch, S., McSweeney, C. & Meir, P. (2009) Exploring the likelihood and mechanism of a climate-change-induced dieback of the Amazon rainforest. PNAS, **106(49)**, 20610-20615, doi: 10.1073/pnas.0804619106.

Malamud, B.D., Morein, G. & Turcotte, D.L. (1998) Forest Fires: An Example of

Self-Organized Critical Behavior. *Science*, **281(5384)**, 1840–1842, doi: 10.1126/science.281.5384.1840.

Marlon, J.R., Bartlein, P.J., Carcaillet, C., Gavin, D.G., Harrison, S.P., Higuera, P.E., Joos, F., Power, M.J. & Prentice, I.C. (2008) Climate and human influences on global biomass burning over the past two millennia. Nature Geoscience, **1**, 697-702, doi: 10.1038/ngeo313.

McArthur, A.G. (1967) Fire Behaviour in Eucalyptus Forests. Leaflet 107. Department of National Development, Forest and Timber Bureau, Canberra.

McKenzie, D., Peterson, D.L. & Ernesto, A. (1996) Extrapolation problems in modelling fire effects at large scales. International Journal of Wildland Fire, **6(4)**, 165-176, doi: 10.1071/WF9960165.

Meyn, A., White, P.S., Buhk, C. & Jentsch, A. (2007) Environmental drivers of large, infrequent wildfires: the emerging conceptual model. Progress in Physical Geography, **31(3)**, 287-312, doi: 10.1177/0309133307079365.

Middleton, B.A., Sanchez-Rojas, E., Suedmeyer, B. & Michels, A. (1997) Fire in a Tropical Dry Forest of Central America: A Natural Part of the Disturbance Regime? Biotropica, **29(4)**, 515-517, doi: 10.1111/j.1744-7429.1997.tb00045.x.

Moreno, M.V., Malamud, B.D. & Chuvieco, E. (2011) Wildfire Frequency-Area Statistics in Spain. Procedia Environmental Sciences, **7**, 182–187, doi: 10.1016/j.proenv.2011.07.032.

Morton, D.C., DeFries, R.S., Randerson, J.T., Giglio, L., Schroeder, W. & van der Werf, G.R. (2008) Agricultural intensification increases deforestation fire activity in Amazonia. Global Change Biology, **14**, 2262-2275, doi:

10.1111/j.1365-2486.2008.01652.x.

Mouillot, F. & Field, C.B. (2005) Fire history and the global carbon budget: a 1ºx1º fire history reconstruction for the 20th century. Global Change Biology, **11(3)**, 398–420, doi: 10.1111/j.1365-2486.2005.00920.x.

Murray-Tortarolo, G., Friedlingstein, P., Sitch, S., Seneviratne, S., Fletcher, I., Mueller, B., Greve, P., Anav, A. & Liu, Y. (submitted) Changes in dry season intensity are the main driver of global NPP trends. Nature Geoscience.

Myneni, R.B., Dong, J., Tucker, C.J., Kaufmann, R.K., Kauppi, P.E., Liski, J., Zhou, L., Alexeyev, V. & Hughes, M.K. (2001) A large carbon sink in the woody biomass of northern forests. PNAS, **98(26)**, 14784 – 14789, doi: 10.1073/pnas.261555198.

Nikolov, N. & Helmisaari, H. (1993) Silvics of the circumpolar boreal forest tree species. P13-84 in Shugart, Leemans & Bonan (eds.): A systems analysis of the global boreal forest. Cambridge University Press, Cambridge, England.

Noble, I.R., Gill, A.M., Bary, G.A.V. (1980) McArthur's fire-danger meters expressed as equations. Austral Ecology, **5(2)**, 201-203, doi: 10.1111/j.1442-9993.1980.tb01243.x.

Oleson, K.W., Bonan, G.B., Feddema, J., Vertenstein, M., & Grimmong, C.S.B. (2008) An urban paramterization for a global climate model. Part 1: Formulation and evaluation of two cities. Journal of Applied Meteorology and Climatology, **47**, 1038–1060, doi: 10.1175/2007JAMC1587.1.

Pacifico, F., Harrison, S.P., Jones, C.D., Arneth, A., Sitch, S., Weedon, G.P., Barkley, M.P., Palmer, P.I., Serça, D., Potosnak, M., Fu, T.-M., Goldstein, A., Bai, J. & Schurgers, G. (2011) Evaluation of a photosynthesis-based biogenic

isoprene emission scheme in JULES and simulation of isoprene emissions under present-day climate conditions. Atmospheric Chemistry and Physics, **11**, 4371-4389, doi: 10.5194/acp-11-4371-2011.

Page, S.E., Siegert, F., Rieley, J.O., Boehm, H.-D.V., Jaya, A. & Limin, S. (2002) The amount of carbon released from peat and forest fires in Indonesia during 1997. Nature, **420**, 61-53, doi: 10.1038/nature01131.

Pausas, J.G. & Bradstock, R.A. (2007) Fire persistence traits of plants along a productivity and disturbance gradient in Mediterranean shrublands of south-east Autralia. Global Ecology and Biogeography, **16(3)**, 330-340, doi: 10.1111/j.1466-8238.2006.00283.x.

Pausas, J.G. & Keeley, J.E. (2009) A Burning Story: The Role of Fire in the History of Life. BioScience, **59(7)**, 593-601, doi: 10.1525/bio.2009.59.7.10.

Pausas, J.G. & Paula, S. (2012) Fuel shapes the fire-climate relationship: evidence from Mediterranean ecosystems. Global Ecology and Biogeography, **21**, 1074-1082, doi: 10.1111/j.1466-8238.2012.00769.x.

Pausas, J.G. & Ribeiro, E. (2013) The global fire-productivity relationship. Global Ecology and Biogeography, **22(6)**, 728-736, doi: 10.1111/geb.12043.

Peylin, P., Bousquet, P., Le Quéré, C., Sitch, S., Friedlingstein, P., McKinley, G., Gruber, N., Rayner, P. & Ciais, P. (2005) Multiple constraints on regional CO_2 flux variations over land and oceans. Global Biogeochemical Cycles, **19**, GB1011, doi: 10.1029/2003GB002214.

Phillips, O.L., Aragão, L.E.O.C., Lewis, S.L., Fisher, J.B., Lloyd, J., López-González, G., Malhi, Y., Monteagudo, A., Peacock, J., *et al.* (2009) Drought Sensitivity of the Amazon Rainforest. Science, **323**, 1344-1347, doi:

10.1126/science.1164033.

Piao, S., Friedlingstein, P., Ciais, P., Viovy, N. & Demarty, J. (2007) Growing season extension and its impact on terrestrial carbon cycle in the Northern Hemisphere over the past 2 decades. Global Biogeochemical Cycles, **21**, GB3018, doi: 10.1029/2006GB002888.

Piao, S., Sitch, S., Ciais, P., Friedlingstein, P., Peylin, P., Wang, X., Ahlström, A., Anav, A., Canadell, J.G., Cong, N., Huntingford, C., Jung, M., Levis, S., Levy, P.E., Li, J., Lin, X., Lomas, M.R., Lu, M., Luo, Y., Ma, Y., Myneni, R.B., Poulter, B., Sun, Z., Wang, T., Viovy, N, Zaehle, S & Zeng, N. (2013) Evaluation of terrestrial carbon cycle models for their response to climate variability and to CO_2 trends. Global Change Biology, doi: 10.1111/gcb.12187.

Planas, E. & Pastor, E. (2013) Wildfire Behaviour and Danger Ratings. In: Fire Phenomena and the Earth System: An Interdisciplinary Guide to Fire Science (ed. C. M. Belcher), John Wiley & Sons, Oxford. doi: 10.1002/9781118529539.ch4.

Potter, C.S., Brooks-Genovese, V., Klooster, S.A., Bobo, M. & Torregrosa, A. (2001) Biomass burning losses of carbon estimated from ecosystem modeling and satellite data analysis for the Brazilian Amazon region. Atmospheric Environment, **35(10)**, 1773 – 1781, doi: 10.1016/S1352-2310(00)00459-3.

Prentice, I.C., Kelley, D.I., Foster, P.N., Friedlingstein, P., Harrison, S.P. & Bartlein, P.J. (2011) Modeling fire and the terrestrial carbon balance. Global Biogeochemical Cycles, **25(3)**, doi: 10.1029/2010GB003906.

Pueyo, S. (2007) Self-organised criticality and the response of wildland fires to climate change. Climatic Change, **82**, 131-161, doi: 10.1007/s10584-006-

9134-2.

Pueyo, S., Graça, P.M.L.D.A., Barbosa, R.I., Cots, R., Cardona, E. & Fearnside, P.M. (2010) Testing for criticality in ecosystem dynamics: the case of Amazonian rainforest and savanna fire. Ecology Letters, **13(7)**, 793–802, doi: 10.1111/j.1461-0248.2010.01497.x.

R Core Team. R: A language and environment for statistical computing. R Foundation for Statistical Computing, Vienna, Austalia, available at: http://www.R-project.org/, last access: September 2013.

Ramos-Neto, M.B. & Pivello, V.R. (2000) Lightning Fires in a Brazilian Savanna National Park: Rethinking Management Strategies. Environmental Management, **26(6)**, 675-684, doi: 10.1007/s002670010124.

Randerson, J.T., Hoffman, F.M., Thornton, P.E., Mahowald, N.M., Lindsay, K., Lee, Y.-H., Nevison, C.D., Doney, S.C., Bonan, G., Stoeckli, R., Covey, C., Running, S.W. & Fung, I.Y.(2009) Systematic assessment of terrestial biogeochemistry in coupled climate-carbon models. Global Change Biology, **15**, 2462–2484, doi: 10.1111/j.1365-2486.2009.01912.x.

Randerson, J.T., Chen, Y., van der Werf, G.R., Rogers, B.M. & Morton, D.C. (2012) Global burned area and biomass burning emissions from small fires. Journal of Geophysical Research, **117**, G04012, doi: 10.1029/2012JG002128.

Raupach, M.R., Marland, G., Ciais, P., Le Quéré, C., Canadell, J.G., Klepper, G. & Field, C.B. (2007) Global and regional drivers of accelerating CO_2 emissions. PNAS, **104**, 10288–10293, doi: 10.1073/PNAS.0700609104.

Reed, W.J. & McKelvey, K.S. (2002) Power-law behaviour and parametric

models for the size-distribution of forest fires. Ecological Modelling, **150(3)**, 239–254, doi: 10.1016/S0304-3800(01)00483-5.

Ricotta C., Avena G. & Marchetti M. (1999) The flaming sandpile: self-organized criticality and wildfires. Ecological Modelling, **119(1)**, 73–77, doi: 10.1016/S0304-3800(99)00057-5.

Rothermel, R.C. (1972) A mathematical model for predicting fire spread in wildland fuels. Research Paper INT-115, Ogden, UT: U.S. Department of Agriculture, Intermountain Forest and Range Experiment Station.

Rowe, J.S. & Scotter, G.W. (1973) Fire in the boreal forest. Quaternary Research, **3**, 444-464.

Roy, D.P., Jin, Y., Lewis, P.E. & Justice, C.O. (2005) Prototyping a global algorithm for systematic fire affected area mapping using MODIS time series data. Remote Sensing of Environment, **97**, 137−162, doi: 10.1016/j.rse.2005.04.007.

Roy, D.P., Boschetti, L, Justice, C.O. & Ju. J. (2008) The collection 5 MODIS burned area product – Global evaluation by comparison with the MODIS active fire product. Remote Sensing of Environment, **112**, 3690-3707, doi: 10.1016/j.rse.2008.05.013.

Russell-Smith, J., Yates, C.P., Whitehead, P.J., Smith, R., Craig, R., Allan, G.E., Thackway, R., Frakes, I., Cridland, S., Meyer, M.C.P. & Gill, A.M. (2007) Bushfires ‘down under’: patterns and implications of contemporary Australian landscape burning. International Journal of Wildland Fire, **16(4)**, 361-377, doi: 10.1071/WF07018.

Saatchi, S.S., Harris, N.L., Brown, S., Lefsky, M., Mitchard, E.T.A., Salas, W.,

Zutta, B.R., Buermann, W., Lewis, S.L., Hagn, S., Petrova, S., White, L., Silman, M. & Morel, A. (2011) Benchmark map of forest carbon stocks in tropical regions across three continents. PNAS, **108(24)**, 9899-9904, doi: 10.1073/pnas.1019576108.

Sastry, N. (2002) Forest fires, air pollution, and mortality in Southeast Asia. Demography, **39(1)**, 1-23, doi: 10.1353/dem.2002.0009.

Schimel, D. & Baker, D. (2002) Carbon cycle: the wildfire factor. Nature, **420**, 29-30, doi: 10.1038/420029a.

Schoenberg F.P., Peng R. & Woods J. (2003) On the distribution of wildfire sizes. Environmetrics, **14(6)**, 583–592, doi: 10.1002/env.605.

Scholze, M., Knorr., W, Arnell, N.W. & Prentice, I.C. (2006) A climate-change risk analysis for world ecosystems. PNAS, **103(35)**, 13116-13120, doi: 10.1073/pnas.0601816103.

Schultz, M.G., Heil, A., Hoelzemann, J.J., Spessa, A., Thonicke, K., Goldammer, J.G., Held, A.C., Pereira, J.M.C. & van het Bolscher, M. (2008) Global wildland fire emissions from 1960 to 2000. Global Biogeochemical Cycles, **22**, BG2002, doi: 10.1029/2007GB003031.

Shimabukuro Y.E. & Smith J.A. (1991) The least-square mixing models to generate fraction images derived from remote sensing multispectral data. IEEE Transactions on Geoscience and Remote Sensing, **29(1)**, 16–20, doi: 10.1009/36.103288.

Shimabukuro, Y.E., Duarte, V., Arai, E., de Freitas, R.M., Lima, A., Valeriano, D.M., Brown, I.F. & Maldonado, M.L.R. (2009) Fraction images derived from Terra Modis data for mapping burnt areas in Brazilian Amazonia.

International Journal of Remote Sensing, **30(6)**, 1537–1546, doi: 10.1080/01431160802509058.

Simon, M. (2002) GLOBSCAR products qualification report. Technical Note, European Space Agency, Paris.

Simon, M., Plummer, S., Fierens, F., Hoelzemann, J.J. & Arino, O. (2004) Burnt area detection at a global scale using ATSR-2: The GLOBSCAR products and their qualifications. Journal of Geophysical Research, **109**, D14S02, doi: 10.1029/2003JD003622.

Sinnott, R.W. (1984) Virtues of the Haversine. Sky and Telescope, **68**(2), 158-159.

Sitch. S., Smith, B., Prentice, I.C., Arneth, A., Bondeau, A., Cramer, W., Kaplan, J.O., Levis, S., Lucht, W., Sykes, M.T., Thonicke, K. & Venevsky, S. (2003) Evaluation of ecosystem dynamics, plant geography and terrestrial carbon cycling in the LPJ dynamic global vegetation model. Global Change Biology, **9(2)**, 161-185, doi: 10.1046/j.1365-2486.2003.00569.x

Sitch, S., Huntingford, C., Gedney, N., Levy, P.E., Lomas, M., Piao, S.L., Betts, R., Ciais, P., Cox, P., Friedlingstein, P., Jones, C.D., Prentice, I.C. & Woodward, F.I. (2008) Evaluation of the terrestrial carbon cycle, future plant geography and climate-carbon cycle feedbacks using fire Dynamic Global Vegetation Models (DGVMs). Global Change Biology, **14**, 2015-2039, doi: 10.1111/j.1365-2486.2008.01626.x.

Sitch, S., Friedlingstein, P., Gruber, N., Jones, S.D., Murray-Tortarolo, G., Ahlström, A., Doney, S.G., Graven, H., Heinze, C., Huntingford, C., Levis, S., Levy, P.E., Lomas, M., Poulter, B., Viovy, N., Zaehle, S., Zeng, N., Arneth, A., Bonan, G., Bopp, L., Canadell, J.G., Chevallier, F., Ciais, P., Ellis, R., Gloor, M., Peylin, P., Piao, S., Le Quéré, C., Smith, B., Zhu, Z., & Myneni, R.

(2013) Trends and drivers of regional sources and sinks of carbon dioxide over the past two decades. Biogeosciences Discussion, **10**, 20113-20177, doi: 10.5194/bgd-10-20113-2013.

Solé, R.V. & Manrubia, S.C. (1996) Extinction and self-organized criticality in a model of large-scale evolution. Physical Review E, **54(1)**, 42-45, doi: 10.1103/PhysRevE.54.R42.

Sornette, A. & Sornette, D. (1989) Self-Organized Criticality and Earthquakes. Europhysics Letters, **9(3)**, 197-202, doi: 10.1209/0295-5075/9/3/002.

Spessa, A., McBeth, B. & Prentice, C. (2005) Relationships among fire frequency, rainfall and vegetation patterns in the wet-dry tropics of northern Australia: an analysis based on NOAA-AVHRR data. Global Ecology and Biogeography, **14(5)**, 439-454, doi: 10.1111/j.1466-822x.2005.00174.x

Staver, A.C., Archibald, S. & Levin, S.A. (2011) The global extent and determinants of savannah and forest as alternative biome states. Science, **334**, 230-232, doi: 10.1126/science.1210465.

Stoeckli, R., Lawrence, D.M., Niu, G.-Y., Oleson, K.W., Thornton, P.E., Yang, Z.-L., Bonan, G.B., Denning, A.S. & Running, S.W. (2008) The use of FLUXNET in the Community Land Model development. Journal of Geophysical Research: Biogeosciences, **113(G1)**, G01025, doi: 10.1029/2007JG000562.

Tansey, K. (2002) Implementation of regional burnt area algorithms for the GBA-2000 initiative. Rep. EUR 20532 EN, Joint Research Centre, European Commission, Ispra, Italy.

Tansey, K., Grégoire, J.-M., Stroppiana, D., Sousa, A., Silva, J., Pereira, J.M.C.,

Boschetti, L., Maggi, M., Brivio, P.A., Fraser, R., Flasse, S., Ershov, D., Binaghi, E., Graetz, D. & Peduzzi, P. (2004) Vegetation burning in the year 2000: Global burnt area estimates from SPOT VEGETATION data. Journal of Geophysical Research, **109**, D14S03, doi: 10.1029/2003JD003598.

Teague, B., McClead, R. & Pascoe, S. (2009) 2009 Victorian Bushfire Royal Commission Interim Report. Australia: Government Printer for the State of Victoria.

Thomey, M.L., Collins, S.L., Vargas, R., Johnson, J.E., Brown, R.F., Natvig, D.O. & Friggens, M.T. (2011) Effect of precipitation variability on net primary production and soil respiration in a Chihuahuan Desert grassland. Global Change Biology, **17**, 1505-1515, doi:10.1111/j.1365-2486.2010.02363.x.

Thonicke, K., Venevsky, S., Sitch, S. & Cramer, C. (2001) The role of fire disturbance for global vegetation dynamics: coupling fire into a Dynamic Global Vegetation Model. Global Ecology and Biogeography, **10(6)**, 661-677, doi: 10.1046/j.1466-822X.2001.00175.x.

Thonicke, K., Spessa, A., Prentice, I.C., Harrison, S.P., Dong, L. & Carmona-Moreno, C. (2010) The influence of vegetation, fire spread and fire behaviour on biomass burning and trace gas emissions: results from a process-based model. Biogeosciences, **7**, 1991–2011, doi: 10.5194/bg-7-1991-2010.

Thornton, P.E., Lamarque, J.F., Rosenbloom, N.A. & Mahowald, N.M. (2007) Influence of carbon-nitrogen cycle coupling on land model response to CO_2 fertilization and climate variability. Global Biogeochemical Cycles, **21**, GB4018, doi: 1029/2006GB002868.

Thornton, P.E., Doney, S.C., Lindsay, K., Moore, J.K., Mahowald, N., Randerson, J.T., Fung, I., Lamarque, J.-F., Feddema, J.J. & Lee, Y.-H. (2009) Carbon-nitrogen interactions regulate climate-carbon cycle feedbacks:

results from an atmosphere-ocean general circulation model. Biogeosciences, **6**, 2099–2120, doi: 10.5194/bg-6-2099-2009.

Tutin, C.E.G., White, L.J.T. & Mackanga-Missandzou, A. (1996) Lightning strike burns large forest tree in the Lopé Reserve, Gabon. Global Ecology and Biogeography Letters, **5(1)**, 36-41.

University of East Anglia Climatic Research Unit (CRU) [Phil Jones, Ian Harris] (2013) CRU TS3.21: Climatic Research Unit (CRU) Time-Series (TS) Version 3.21 of High Resolution Gridded Data of Month-by-month Variation in Climate (Jan. 1901 – Dec. 2012), [Internet]. NCAS British Atmospheric Data Centre. Available from http://badc.nerc.ac.uk/view/badc.nerc.ac.uk__ATOM__ ACTIVITY_0c08abfc-f2d5-11e2-a948-00163e251233, last accessed: 24/07/2013. doi: 10.5285/D0E1585D-3417-485F-87AE-4FCECF10A992.

Van der Werf, G.R., Randerson, J.T., Collatz, G.J. & Giglio, L. (2003) Carbon emissions from fires in tropical and subtropical ecosystems. Global Change Biology, **9**, 547 – 562, doi: 10.1046/j.1365-2486.2003.00604.x.

Van der Werf, G.R., Randerson, J.T., Collatz, G.J., Giglio, L., Kasibhatla, P.S., Arellano Jr., A.F., Olsen, S.C. & Kasischke, E.S. (2004) Continental-Scale Partitioning of Fire Emissions During the 1997 to 2001 El Niño/La Niña Period. Science, **303**, 73 – 76, doi: 10.1126/science.1090753.

Van der Werf, G.R., Randerson, J.T., Giglio, L., Collatz, G.J., Kasibhatla, P.S. & Arellano, Jr., A.F. (2006) Interannual variability in global biomass burning emissions from 1997 to 2004. Atmospheric Chemistry and Physics, **6**, 3423-3441, doi: 10.5194/acp-6-3423-2006.

Van der Werf, G.R., Randerson, J.T., Giglio, L., Gobron, N. & Dolman, A.J. (2008) Climate controls on the variability of fires in the tropics and subtropics. Global Biogeochemical Cycles, **22(3)**, GB2038, doi: 10.1029/2007GB003122.

Van der Werf, G.R., Randerson J.T., Giglio L., Collatz G.J., Mu M., Kasibhatla P.S., Morton, D.C., DeFries, R.S., Jin, Y. & van Leeuwen, T.T. (2010) Global fire emissions and the contribution of deforestation, savanna, forest, agricultural, and peat fires (1977–2009). Atmospheric Chemistry and Physics, **10**, 11707–11735, doi: 10.5194/acp-10-11707-2010.

Van Leeuwen, T.T. & van der Werf, G.R. (2011) Spatial and temporal variability in the ratio of trace gases emitted from biomass burning. Atmospheric Chemistry and Physics, **11**, 3611-3629, doi: 10.5194/acp-11-3611-2011.

Van Wagner, C.E. & Pickett, T.L. (1985) Equations and FORTRAN Program for the Canadian Forest Fire Weather Index System. Technical Report 33, Canadian Forest Service, Ottawa, Ontario.

Van Wagner, C.E. (1993) Prediction of crown fire behavior in two stands of jack pine. Canadian Journal of Forest Research, **23(3)**, 442-449, doi: 10.1139/x93-062.

Veblen, T.T., Kitzberger, T. & Donnegan, J. (2000) Climatic and human influences on fire regimes in ponderosa pine forests in the Colorado Front Range. Ecological Applications, **10(4)**, 1178-1195, doi: 10.1890/1051-0761(2000)010[1178:CAHIOF]2.0CO;2.

Venevsky, S., Thonicke, K., Sitch, S. & Cramer, W. (2002) Simulating fire regimes in human-dominated ecosystems: Iberian Peninsula case study. Global Change Biology, **8(10)**, 984-998, doi: 10.1046/j.1365-2486.2002.00528.

Vermote, E.F., Saleous, N.Z.E. & Justice, C.O. (2002) Operational atmospheric correction of the MODIS data in the visible to middle infrared: first results. Remote Sensing of Environment, **83**, 97–111, doi: 10.1016/S0034-4257(02)00089-5.

Ward, D.S., Kloster, S., Mahowald, N.M., Rogers, B.M., Randerson, J.T. & Hess, P.G. (2012) The changing radiative forcing of fires: global model estimates for past, present and future. Atmospheric Chemistry and Physics, **12**, 10857-10866, doi: 10.5194/acp-12-10857-2012.

Weedon, G.P., Balsamo, G., Bellouin, N., Gomes, S., Best, M.J. & Viterbo, P. (2014) The WFDEI meteorological forcing dataset: WATCH Forcing Data methodology applied to ERA-Interim reanalysis data. Water Resources Research, doi: 10.1002/2014WR015638.

Westerling, A.L., Hidalgo, H.G., Cayan, D.R. & Swetnam, T.W. (2006) Warming and Earlier Spring Increase Western U.S. Forest Wildfire Activity. Science, 313, 940-943, doi: 10.1126/science.1128834.

Yocom, L.L. & Fulé, P.Z. (2012) Human and climate influences on frequent fire in a high-elevation tropical forest. Journal of Applied Ecology, **49**, 1356-1364, doi: 10.1111/j.1365-2664.2012.02216.x.

Zeng, N., Yoon, J.H., Marengo, J.A., Subramaniam, A., Nobre, C.A., Mariotti, A. & Neelin, J.D. (2008) Causes and impacts of the 2005 Amazon drought. Environmental Research Letters, **3(1)**, doi: 10.1088/1748-9326/3/1/014002.